DOTTORATO DI RICERCA IN
INFORMATICA, SISTEMI E TELECOMUNICAZIONI

CICLO XXVII

COORDINATORE Prof. Luigi Chisci

Real-Time Control Reconfiguration for Active Disturbance Attenuation

Settore Scientifico Disciplinare ING-INF/04

Dottoranda
Dott. Daniela Selvi

_____

Tutori
Prof. Giorgio Battistelli

_____

Prof. Alberto Tesi

_____

Coordinatore
Prof. Luigi Chisci

_____

Anni 2012/2014

Acknowledgements

While getting close to the end of this journey, I would like to express my gratitude to all those who have been on my route and have contributed in determining the final destination. I hope that I will be able to gain experience from each single victory, but also from each difficulty, that I have experienced in these years, as well as from the advices and support that I have felt and that have helped me growing from all points of view.

With this respect, first of all, thanks to my Tutors. Thanks to Prof. Giorgio Battistelli, for the very useful discussions about (and not limited to) the topics developed in this work, for your encouragement and advices, as well as for the conversations about the past, the future and, mainly, the present moment. Thanks to Prof. Alberto Tesi, for your constant presence and encouragement, for the technical discussions and, above all, for the example that you provide, not only as a Professor.

Thanks also to all the other people from my Department, and, more in general, from the School of Engineering of Florence, to every single person who has addressed me with advices or simply with a joke or a "good morning" accompanied by a smile, or has contributed in inspiring my interest in research. With this respect, special thanks to Proff.

Benedetto Allotta, Michele Basso, Luigi Chisci, Duccio Fanelli, Roberto Genesio, Giacomo Innocenti, Russel Allan Johnson, Edoardo Mosca, Stefano Ruffo, Fabio Schoen, Marco Sciandrone.

Thanks to the guys that I have met as (not only) colleagues, Giovanni Mugnai, Stefano Gherardini, Nicola Forti, Claudio Fantacci; special thanks to my friend Daniele Mari, for your support and encouragement. Thanks to Pietro Tesi for several technical and less technical discussions...and also for giving me the opportunity to strengthen my character..! Thanks also to the guys from the "Operations Research" lab, for your friendship and several lunches together.

With respect to my work related to adaptive optics, special thanks to Guido Agapito from the Arcetri Astrophysical Observatory, for having provided me with information, advices, and having performed several tests by using the equipment available at Arcetri.

I am also indebted to all the LA lab of the Échole Polythechnique Fédérale de Lausanne for the friendly atmosphere that I could enjoy while staying with them; it has been an important experience for me from many points of view. Special thanks to Prof. Alireza Karimi for the technical discussions and for having introduced me to the lab, and to Zlatko Emedi for your help and advices.

I am deeply grateful to all my family, for your love, support, encouragement, for always being on my side. Thanks for helping me growing up, by providing me with your example and, above all, by believing in me.

Contents

Abstract

In this work, the problem of active attenuation of disturbances with uncertain and possibly time-varying characteristics is addressed. The focus is on situations in which the uncertainty set is large, that is, the possible operating conditions of the system subject to disturbances can be different so that a single robust controller cannot ensure satisfactory performance levels. These situations underline the importance of control solutions able to *reconfigure* their action in *real-time*.

The first part of this work is focused on the description of two different case studies, namely an active suspension system and an adaptive optics system, as well as on an overview of relevant contributions within the literature related to this subject. The solution that we propose is described in the second part; this method relies on the Adaptive Switching Control (ASC) paradigm, which has emerged as an alternative to classical Adaptive Control. In ASC, a finite family of candidate controllers is pre-synthesized off-line, and a supervisory logic has to select the potentially best one to be put in feedback with the plant. Particular attention is devoted to both performance and stability of the overall switching system. Finally, as an extension of the solution based on ASC, in the third part of this work an algorithm is proposed which combines both switching and tuning, aiming at preserving the beneficial features of the two different approaches, while possibly overcoming their drawbacks.

The effectiveness of the proposed solutions is validated by means of simulation tests performed in the context of the two considered case studies.

Introduction

A disturbance is an element that affects the normal behavior of a system. These few words roughly explain the importance of solutions able to counteract the effects of disturbances, that is, aiming at leading the system to act, as closely as possible, as if the disturbances do not affect it. Disturbance attenuation is a common goal in several diversified contexts of application, such as: active noise control [58]; noise cancellation in an acoustic duct [10]; vibration attenuation for helicopter rotors [12]; biomass productivity in a fed-batch reactor [89]; eccentricity compensation [26]; disturbance torque compensation in electric machines [81]; laser systems [52]; active suspension systems [64]; disturbance attenuation for adaptive optics applications for ground-based telescopes [2]. In this work, two case studies are considered, namely an active suspension system and an adaptive optics system. In particular, the former case refers to a quarter-car model with the aim of attenuating the effects of the road unevenness, while in the latter case the problem is that of attenuating the effects of wavefront distortion, caused by atmospheric turbulence and structural vibrations, in order to recover a satisfactory resolution.

In several situations, a non-negligible uncertainty affects the a priori available disturbance model. If the possible uncertainty set is sufficiently small, that is, the possible operating conditions of the system subject to the disturbances are quite close one another, a single robust controller can in general achieve a satisfactory performance level. On the contrary, if the uncertainty set is large, it becomes difficult to achieve desirable attenuation capabilities by means of a unique control action. The concept of robustness is thus naturally extended to the concept of *real-time control reconfiguration*.

Specifically, the reconfiguration of the control action in real-time arises in both *learning* and *adaptation* problems. In particular, a learning problem refers to the case in which the disturbance characteristics are almost stationary, thus the aim is that of finding

the controller, within a family of candidate controllers, able to ensure the best possible level of attenuation. On the other hand, an adaptation problem arises when the disturbance characteristics vary with time, then the control action must be adjusted to fit the current operating condition.

Much interest to adaptive solutions for the problem of disturbance attenuation has been raised with respect to narrow-band disturbances. In this context, the proposed techniques follow in general the classical Adaptive Control paradigm, involving either direct approaches (providing algorithms inherently designed for disturbance attenuation objectives) or indirect approaches (exploiting the separation principle and resorting to disturbance frequency estimation).

The control solution that we propose in this work is based on a different paradigm, that is, the Adaptive Switching Control (ASC) approach. ASC has emerged as an alternative to classical Adaptive Control, and has been largely studied and adopted in the context of plant model uncertainty. In ASC, a finite family of candidate controllers is pre-synthesized off-line, and a supervisory logic has to select the potentially best one to be put in feedback with the plant. Among the possible advantages of ASC, discussed for example in [46], we can mention the modularity, that is, the independence between the synthesis of the controllers and the design of the switching logic. This feature can be useful either when existing control solutions should be used, or when advanced control strategies are required for specific problems. Further, it is worth noting that the ASC approach is also more suitable to quickly achieve satisfactory performance and to deal with abrupt changes in the uncertain disturbance characteristics, provided that the supervisor is able to select in a short time the potentially best controller; however, the attenuation level achievable by the pre-synthesized controllers in the finite set determines the performance that can be achieved by the overall control scheme. On the other hand, classical adaptive techniques based on parameter tuning can usually achieve better performance levels in the long run, but it is possible that the tuning procedure requires a non-negligible time interval before achieving a satisfactory behavior. With this respect, as an extension of the proposed solution to the problem of active disturbance attenuation based on the ASC paradigm, we propose an algorithm combining both switching and tuning, aiming at preserving the beneficial features of the two different approaches, while possibly overcoming the mentioned drawbacks.

Within the control strategies that have been briefly outlined above, the problem of stability of the overall closed-loop switching system is analyzed, and specifically two different solutions are proposed. One of them addresses the stability requirement directly within the synthesis of the set of controllers; this makes the complexity of the multi-controller architecture independent of the plant order, but, on the other hand, affects the modularity which is typical of the ASC paradigm. The other solution relies on the *Youla* parametrization of the stabilizing controllers, and on a specific implementation of the multi-controller based on a switching mechanism between the Youla parameters; with respect to this solution, the modularity of the ASC approach is preserved, but the complexity of the adopted architecture is unavoidably influenced by the plant order.

This work presents results and solutions that we propose for the problem of disturbance attenuation; part of its contents has been published or submitted in [2, 3, 21, 19, 20, 18]. The organization of the work is as follows.

Part I aims at providing a presentation of the topic by describing in some detail both the considered case studies and relevant solutions for the problem of active disturbance attenuation that have been proposed in the literature. In particular, Chapter 1 illustrates the problem of control design for adaptive optics systems, while Chapter 2 introduces the challenges related to active suspension systems. Finally, Chapter 3 provides an overview of significant contributions proposed in the literature in the context of active disturbance attenuation.

The solution based on the ASC paradigm is introduced in Part II. Details on the selection of the potentially best controller by the supervisory unit are provided in Chapter 4, with particular emphasis on the properties of test functionals which are computed to evaluate the potential behavior of each candidate controller. Then, Chapter 5 and Chapter 6 focus on the proposed solutions for the problem of ensuring stability of the feedback loop under arbitrary switching. Further, the simulation results shown in Chapter 6 underline the validity of the ASC approach in the presence of different classes of disturbances.

Part III is devoted to the presentation of the algorithm combining switching and tuning. In particular, it is shown that, under appropriate assumptions, the proposed scheme is able to achieve an arbitrary attenuation level. The theoretical findings are validated by means of simulation tests.

Finally, concluding remarks and future perspectives are indicated.

PART I
Problem overview and applications

Chapter 1

Control Design for Adaptive Optics

A central problem when dealing with ground-based telescopes arises from deformations of the light wavefront caused by the atmosphere. It is well known that the maximum resolution of any optical device depends on diffraction; in order to recover diffraction limited-resolution, modern ground-based telescopes are equipped with adaptive optics (AO) devices, which aim at reducing, thanks to the use of deformable mirrors, the aforementioned effects of wavefront distortion. In addition to the atmospheric turbulence [84], telescopes also suffer from structural vibrations due to situations such as telescope orientation, telescope tracking errors, and wind shaking. In view of their potential impact, considerable attention has been devoted over the last decades to the analysis and design of AO systems. Together with developments of physics, mathematics and technology, contributions to the subject have been recently proposed also from a control engineering perspective, as witnessed by [57, 78, 39, 80, 48, 2, 3] and the special issue on AO for ground-based telescopes organized by the European Journal of Control [29].

We focus on the control architecture installed on the Large Binocular Telescope (LBT, located on Mt. Graham, Arizona, USA) [2, 5, 1, 4, 3], and one of the two Magellan Telescopes (Las Campanas Observatory, Chile) [28]. A similar architecture will be also adopted for the upgrading of one of the four Very Large Telescopes (Cerro Paranal, Chile) [66] and the Giant Magellan Telescope (Las Campanas, Chile), which is expected to be operative by the end of 2024 [37]. The considered AO unit comprises a wavefront sensor (WFS) - specifically, we consider a pyramid one - an adaptive secondary mirror (ASM), and a real-time computer (RTC). Roughly speaking, the pyramid WFS delivers a signal

that is proportional, by a first-order approximation, to the first derivative of the incoming wavefront. The RTC, which implements the AO controller, computes the command vector driving the actuators of the ASM. Through the use of hundreds of voice-coil (electromagnetic force) actuators, distributed on the mirror shell, the ASM corrects the wavefront distortion according to the RTC command vector. The correction is realized in such a way that the shape of the shell of the ASM becomes, as closely as possible, opposite to that of the wavefront distortion [84, 25].

As pointed out in [29], AO systems are becoming bigger and also more complex, with the aim of achieving higher performance levels. This obviously raises increasingly challenging issues for the design and implementation of appropriate control techniques, which have to ensure satisfactory performance while requiring low computational burden.

Classical approaches to AO control can be subdivided into two main groups: those which do not employ any form of identification of turbulence and vibrations models [31, 42]; and those which employ models of turbulence and/or vibrations in combination with model-based control design techniques, such as H_2, H_∞ and LQG control [78, 79, 5, 30, 57]. Model-based approaches have the intuitive advantage of including a notion of *optimality* in the sense of performance ideally achievable for the identified process model. However, it is to be noticed that it is practically impossible to achieve exact models for the disturbances, and it is therefore important that the models used to synthesize the controller are sufficiently accurate at the frequencies of concern. This basically means that model-based approaches provide controllers whose order is essentially determined by the order of the underlying models. High-order turbulence/vibrations models, in addition to requiring non-negligible identification effort, will therefore lead to high-order controllers, which may be infeasible (or simply not desired) from an implementation viewpoint. On the other hand, models with reduced complexity may fail to capture well the behavior of turbulence and/or vibrations at the frequencies of concern.

The previous considerations suggest that techniques not relying on identified models of the disturbances could represent an appealing strategy for the reduction of wavefront distortion. Specifically, in Appendix 6.B we will describe a design method [2], which allows to optimize the parameters of a modal controller of given order with respect to a relevant AO performance criterion which is defined on a "sampled" frequency-domain; this means that the optimization procedure involves samples of turbulence and vibrations frequency pro-

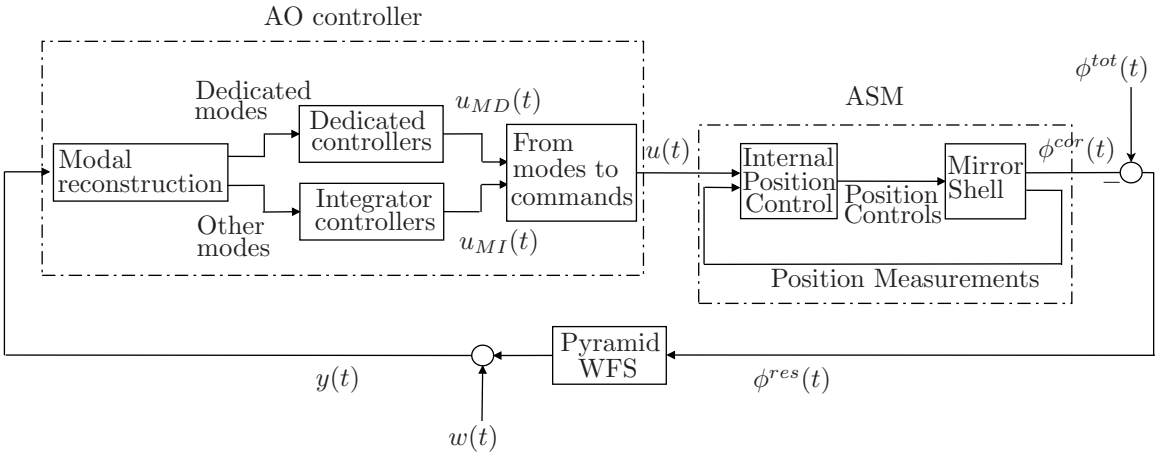

Figure 1.1: AO control scheme.

files, rather than their analytical models (as happens in classical H_2, H_∞ and LQG control design). This makes it possible to use turbulence/vibration profiles of arbitrary complexity, even empirical power spectral densities (PSDs) from data, while keeping the controller order at a manageable value. As it will appear clearly from Appendix 6.B, the proposed technique allows to deal also with the contribution of the measurement noise by employing directly its frequency profile, or empirical PSD from data, within the above-mentioned sampled frequency-domain framework.

Finally, it is worth noting that the frequency profiles of the aforementioned disturbances, that is turbulence, vibration and measurement noise, vary in accordance with the operating conditions of the telescope (*e.g.*, different wind speed, different cloudiness during the exposure time). Situations of this type can be managed for example by accounting for robustness in the frequency-based control synthesis approach outlined above [3], or, alternatively, by resorting to an adaptive switching control approach as described in next chapters (simulation results related to the latter case will be shown in Section 6.3).

1.1 AO control system architecture

The architecture of the AO control system that we consider is depicted in Fig. 1.1, and is composed of an *external* AO control system (working at the AO sampling time $T_s = 1\,ms$), whose task is to determine the commands to the ASM, and an *internal* ASM control

system (with sampling time $T_{ASM} \approx 10^{-2}\, T_s$). The main devices characterizing the control loop are the AO controller, the Pyramid WFS, and the ASM. The AO controller receives at time tT_s (where $t \in \mathbb{Z}_+$, $\mathbb{Z}_+ := \{0, 1, \cdots\}$) the measurement vector $y(t) \in \mathbb{R}^q$, with q the number of measurements, from the Pyramid WFS and computes the command vector $u(t) \in \mathbb{R}^p$, with p the number of actuators, so as to pilot the actuators acting on the ASM shell. The command vector provides the information about the shape to be reproduced by the shell in order to compensate for the wavefront distortions. Due to the non-negligible dynamics of the shell, a dedicate control loop is needed to get the desired shape within T_s. Such a control loop is realized through the use of p capacitive sensors co-located with the actuators and placed at the back of the shell. Specifically, the control law piloting each actuator has a decentralized component obtained by a Proportional-Derivative feedback action which depends on the measurement of the co-located sensor, and a centralized component implemented through a feed-forward action which equals the force needed to statically deform the shell as indicated by the command vector $u(t)$; this latter action is obtained by multiplying $u(t)$ with an estimate of the shell stiffness matrix of dimensions $p \times p$, which is a-priori calibrated. For more details about the ASM internal position control, the interested reader is referred to [1, 83].

In Fig. 1.1 the phase aberration of the light wavefront due to turbulence and vibrations is denoted by $\phi^{tot}(t)$. Such a distortion has to be corrected by the shell deformations which provide the so called correction phase $\phi^{cor}(t)$. The difference $\phi^{res}(t) = \phi^{tot}(t) - \phi^{cor}(t)$ is the residual phase after the ASM correction. The objective of the external control loop therefore consists in regulating the residual phase $\phi^{res}(t)$ about 0.

The control architecture of Fig. 1.1 refers to a modal control scheme where the phase aberrations are expressed through a modal basis. Common choices in this regard are *Zernike* and *Karhunen-Loève* basis [25, 84], the latter being considered in our framework. The residual phase is translated into the measurement vector $y(t)$ from the Pyramid WFS as described by

$$y(t) = \mathcal{D}\, \phi^{res}(t-1) \,+\, w(t)\,, \tag{1.1}$$

where $w(t) \in \mathbb{R}^q$ is the measurement noise vector, which is assumed to be a zero-mean white noise. The matrix $\mathcal{D}$ characterizes the WFS and describes the geometric relationship between the modal space and the measurement space. Notice that the modal space depends

on the selected modal basis and all the phase variables represent coefficient vectors belonging to $\mathbb{R}^p$, where p denotes the dimension of the modal space.

The ASM correction phase is obtained as

$$\phi^{cor}(t) = \mathcal{N}\, u(t-1), \tag{1.2}$$

where $\mathcal{N}$ is the so-called *Commands-to-Modes* matrix, which describes the geometric relationship between the command space and the modal space. An estimate of $\mathcal{N}$ can be obtained via finite elements analysis of the mirror shell, once chosen the modal basis to be used.

The command vector provided to the ASM is computed by the AO controller as follows [1]

$$u(t) = \mathcal{M}\, \mathcal{K}_M(d)\, \mathcal{R}\, y(t)\,, \tag{1.4}$$

where $\mathcal{M}$ is the *Modes-to-Commands* (or *Projection*) matrix, represented by the *From modes to commands* block in Fig. 1.1, and $\mathcal{R}$ is the *Reconstruction* matrix, which yields the geometric relationship between the WFS measurements and the deformations of the ASM (*Modal reconstruction* block in Fig. 1.1). The transfer matrix $\mathcal{K}_M(d)$ has dimension $p \times p$ and has to be designed in order to satisfy the control requirements. In the proposed setting, $\mathcal{K}_M(d)$ is chosen as a diagonal matrix, $\mathcal{K}_M(d) = \mathrm{diag}\{C_1(d), \cdots, C_p(d)\}$, as the ideal goal is to control the $i-$th mode by means of controller $C_i(d)$.

In fact, the residual phase satisfies the relationship

$$\phi^{res}(t) = \phi^{tot}(t) - \mathcal{N}\, d\, u(t) = \phi^{tot}(t) - d\mathcal{N}\, \mathcal{M}\, \mathcal{K}_M(d)\, \mathcal{R}\, y(t) \tag{1.5}$$

which can be rewritten as

$$\Delta(d)\, \phi^{res}(t) = \phi^{tot}(t) - \Xi(d)\, w(t) \tag{1.6}$$

[1] Given an LTI dynamic system with input u and output y, by the notation $y(t) = W(d)u(t)$ we mean that the signal y is computed by means of the difference equation

$$\sum_{k=0}^{n_G} G_k\; y(t-k) = \sum_{k=0}^{n_H} H_k\; u(t-k) \tag{1.3}$$

where $W(d) = [G(d)]^{-1}H(d)$ is the system I/O operator in the unit backward shift operator d, where $H(d) = \sum_{k=0}^{n_H} H_k d^k$ and $G(d) = \sum_{k=0}^{n_G} G_k d^k$ are polynomial matrices having maximum degree n_G and n_H, respectively; further, $G(0) = I$.

where $\Delta(d) := (I + d^2 \mathcal{N}\,\mathcal{M}\,\mathcal{K}_M(d)\,\mathcal{R}\,\mathcal{D})$ and $\Xi(d) := d\,\mathcal{N}\,\mathcal{M}\,\mathcal{K}_M(d)\,\mathcal{R}$. The matrix $\mathcal{R}$ is then selected as the Moore-Penrose inverse of $\mathcal{D}$, *i.e.* $\mathcal{R} := (\mathcal{D}^\top\mathcal{D})^{-1}\mathcal{D}^\top$. Accordingly, $\Delta(d)$ simplifies to $\Delta(d) = (I + d^2 \mathcal{N}\,\mathcal{M}\,\mathcal{K}_M(d))$. The matrices $\mathcal{N}$ and $\mathcal{M}$ are instead calibrated so as to yield $\mathcal{N}\,\mathcal{M} \approx I$ (more precisely for the LBT, $\mathcal{N}\,\mathcal{M}$ is a matrix with elements on the diagonal equal to 1 and extra-diagonal elements with absolute values $\approx 2^{-15}$). Thus, by neglecting the measurement noise, we can therefore select a diagonal controller $\mathcal{K}_M(d)$ and achieve modal decoupling, *i.e.* $\phi^{res}(t) \approx (I + d^2\mathcal{K}_M(d))^{-1}\,\phi^{tot}(t)$.

In principle, one could synthesize a dedicated controller $C_i(d)$ for each mode. However, in practice, it is convenient to consider advanced control design techniques only for those modes having more influence on the value of $\phi^{res}(t)$. Within the addressed framework, dedicated controllers $C_D(d)$ are synthesized only for tip and tilt modes [5, 4, 39], which consist in the image displacements in the two orthogonal directions of the focal plane, while the remaining modes are regulated by simple integrator controllers $C_I(d) = g/(1-d)$, where g is a gain to be set. In fact, it has been observed by means of experimental studies on LBT that turbulence and vibrations affect mainly tip/tilt modes. In turn, according to the Kolmogorov theory, in the considered operating setting tip/tilt modes yield more than 80% of the overall atmospheric turbulence variance [77]. The choice of considering only two dedicated controllers is mainly motivated by the memory constraints of the RTC which, as detailed in [5], has been designed to work with a modal integrator, so that the maximum state dimension allowed for the AO controller $\mathcal{K}_M(d)$ is 672.

Let $u_M(t) \in \mathbb{R}^p$ be the command vector in the modal space, such that $u(t) = \mathcal{M}\,u_M(t)$, and suppose that tip and tilt correspond to the first two entries of the vector $u_M(t)$, then $\mathcal{K}_M(d) = diag\{C_D(d), C_D(d), C_I(d), \cdots, C_I(d)\}$, where for simplicity the same controller is used for tip and tilt modes.

To conclude this presentation and to introduce the framework which will be considered for the simulation results of Section 6.3, we point out that we will refer to the modal control scheme related to tip and depicted in Fig. 1.2; accordingly, the subscript *tip* is adopted to indicate variables related to tip mode. The blocks $M(d)$ and $H(d)$ represent the dynamics of the ASM and WFS, respectively; the cascade of these two blocks represents the plant to be controlled in the presence of the disturbances $\phi^{tot}_{tip}(t)$ and $w_{tip}(t)$. In particular, within the considered setting, both $M(d)$ and $H(d)$ can be assumed to behave as a unit delay, since their tasks are supposed to be executed within one sampling time of

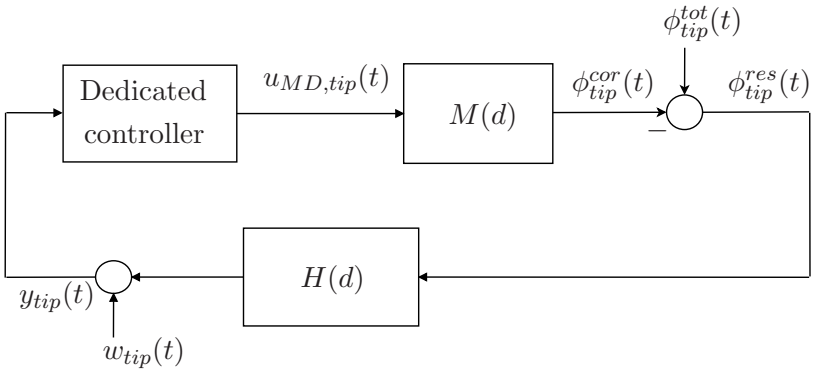

Figure 1.2: Modal control scheme.

the external loop. In fact, the internal position control acting on the mirror shell, see Fig. 1.1, works with a sampling time much lower than the one of the external AO loop (in LBT, for example, it is about $0.01\,ms$), and thus it allows the mirror shell to achieve the desired shape within one AO loop sampling time.

Chapter 2

Active suspension systems

The interest in the study and improvement of suspension systems for ground vehicles arises from the fact that road unevenness causes vibrations which are detrimental both for comfort and for the durability of the vehicle. With this respect, a suspension system aims at guaranteeing ride comfort and road holding for different road conditions and maneuvers, thus ensuring the vehicle stability and safety [38]. As pointed out in [86], a suspension comprises three main elements: a) an elastic element (typically a coil spring); b) a damping element (typically a hydraulic shock absorber); c) mechanical elements which link the suspended body to the unsprung mass. Specifically, while the spring and the damper have to be considered from the dynamic point of view, the mechanical elements are mainly related to the suspension kinematics.

The goal of a suspension system is to provide comfortable ride and good road-holding, which, however, turn out to be conflicting requirements; thus, as underlined in [86], it is not surprising that, at a certain point, the interest of suspension designers focused on possible solutions to overcome the problem of *a-priori* compromising between these opposite goals. With this respect, the possibility of easily modifying part of a suspension became a topic of major concern, opening the way to the idea of "on-line" electronic adaptation.

The suspension systems can be subdivided into three main classes: passive, semi-active, and active. Roughly speaking, a passive suspension comprises a spring and a damper, where both components are fixed; energy is stored in the spring and dissipated through the damper. In semi-active suspensions, on the other hand, a controllable shock absorber with adjustable damping replaces the passive damper with fixed damping. Finally, active

suspensions are composed of the passive components, augmented by actuators that provide additional forces [11]; this type of suspensions can ideally achieve the best performance (even if the technological and economical burden associated to them has to be taken into account).

In the next section, we will give insight into the mathematical description of the passive and active suspensions, mainly referring to [86].

2.1 Suspension system models

A possible model used for the design of suspension systems is the so-called *quarter-car* model. Basically, this model "aims at describing the interactions between the suspension system, the tire and the chassis in a single corner of a vehicle" [86].

With reference to a passive suspension system, a general description for the passive quarter-car model can be provided in terms of the following equations:

$$\begin{aligned} m_1\ddot{z}_1(t) &= F_k(t) + F_d(t) + F_L(t) - m_1 g \\ m_2\ddot{z}_2(t) &= -F_k(t) - F_d(t) + F_{kt}(t) + F_{dt}(t) - m_2 g\,, \end{aligned} \tag{2.1}$$

where, with abuse of notation, we use the letter t to indicate continuous time; further, g denotes the gravitational constant, m_1 is the suspended mass representing the chassis, and m_2 is the tire mass (accounting for the wheel, multiple links from the chassis to the road, etc.). We denote by z_1 and z_2 the vertical chassis and wheel bounce absolute displacements, respectively. The functions F_k and F_d represent the suspension spring and damper vertical forces, respectively; F_{kt} and F_{dt} express the tire stiffness and damping vertical forces, respectively. Finally, $n(t)$ denotes the road vertical excitation, while F_L is the vertical load disturbance.

Following [86], some assumptions are introduced in order to simplify the model (2.1). Specifically, $F_L(t)$ is assumed to be identically equal to zero, since it comprises effects produced by steering and braking maneuvers which are not accounted for in this work. Further, the tire spring force is described by the linear function

$$F_{kt}(t) = -\kappa_2(z_2(t) - n(t) - R_t)\,, \tag{2.2}$$

with κ_2 and R_t the linearized stiffness and nominal length of the tire spring, respectively. With respect to the tire damping factor, it is assumed that $F_{dt}(t) = 0$, that is, the tire damp-

ing coefficient is assumed to be negligible if compared to the tire stiffness. The suspension spring force is described in terms of the linear function

$$F_k(t) = -\kappa_1(z_1(t) - z_2(t) - L)\,, \tag{2.3}$$

with κ_1 and L the linearized stiffness and nominal length of the suspension spring, respectively. Finally, the suspension damper force is described in terms of the linear function

$$F_d(t) = -c(\dot{z}_1(t) - \dot{z}_2(t))\,. \tag{2.4}$$

Thanks to the assumptions that have been introduced (further details can be found in [86]), the quarter-car model can be simplified as follows:

$$\begin{aligned} m_1\ddot{z}_1(t) &= -\kappa_1(z_1(t) - z_2(t) - L) - c(\dot{z}_1(t) - \dot{z}_2(t)) - m_1 g \\ m_2\ddot{z}_2(t) &= \kappa_1(z_1(t) - z_2(t) - L) + c(\dot{z}_1(t) - \dot{z}_2(t)) - \kappa_2(z_2(t) - n(t) - R_t) - m_2 g\,, \end{aligned} \tag{2.5}$$

which can be considered valid provided that the deflections of the suspension are small around the nominal load compression, and the wheel is always linked to the ground [86]. Further, as shown in [86], by computing the system equilibrium point from model (2.5), the linear time-invariant (LTI) passive quarter-car model can be finally expressed as

$$\begin{aligned} m_1\ddot{y}_1(t) &= -\kappa_1(y_1(t) - y_2(t)) - c(\dot{y}_1(t) - \dot{y}_2(t)) \\ m_2\ddot{y}_2(t) &= \kappa_1(y_1(t) - y_2(t)) + c(\dot{y}_1(t) - \dot{y}_2(t)) - \kappa_2(y_2(t) - n(t))\,, \end{aligned} \tag{2.6}$$

where y_1 and y_2 denote the displacement of m_1 and m_2, respectively, around the corresponding equilibrium point. Accordingly, the graphical representation in Fig. 2.1 is considered.

Further, if we denote by $F(t)$ the external force which is introduced into the system (representing the control input), the LTI quarter-car model with active suspension system can be derived from (2.6) as:

$$\begin{aligned} m_1\ddot{y}_1(t) &= -\kappa_1(y_1(t) - y_2(t)) - c(\dot{y}_1(t) - \dot{y}_2(t)) + F(t) \\ m_2\ddot{y}_2(t) &= \kappa_1(y_1(t) - y_2(t)) + c(\dot{y}_1(t) - \dot{y}_2(t)) - \kappa_2(y_2(t) - n(t)) - F(t)\,. \end{aligned} \tag{2.7}$$

The corresponding graphical representation is provided in Fig. 2.2.

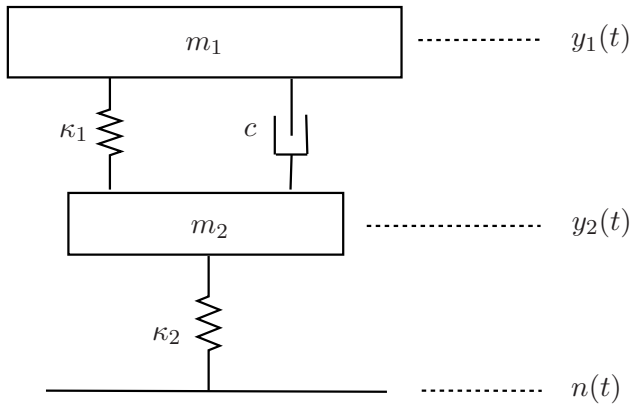

Figure 2.1: Quarter-car model scheme with passive suspension system.

By applying the Laplace Transform to model (2.7), we can derive the transfer function from the disturbance n to the displacement y_1 of the suspended mass (with respect to its equilibrium point) as:

$$F_p(s) = \frac{(c\kappa_2)s + (\kappa_1\kappa_2)}{(m_1m_2)s^4 + (cm_2 + cm_1)s^3 + (m_1\kappa_1 + m_2\kappa_1 + m_1\kappa_2)s^2 + (c\kappa_2)s + (\kappa_1\kappa_2)}\,, \quad (2.8)$$

where s is the Laplace variable. Further, the transfer function from the force F to the displacement y_1 can be derived as:

$$P(s) = \frac{m_2s^2 + \kappa_2}{(m_1m_2)s^4 + (cm_2 + cm_1)s^3 + (m_1\kappa_1 + m_2\kappa_1 + m_1\kappa_2)s^2 + (c\kappa_2)s + (\kappa_1\kappa_2)}\,. \quad (2.9)$$

We refer to the transfer function $F_p(s)$ in (2.8) as the *primary path*, and to $P(s)$ in (2.9) as the *secondary path* (or, simply, the *plant*). Notice that $P(s)$ and $F_p(s)$ have the same denominator.

By discretizing $F_p(s)$ and $P(s)$, we obtain the following transfer functions

$$F_p(d) = \frac{E(d)}{A(d)}\,, \qquad P(d) = \frac{B(d)}{A(d)}\,,$$

from which the difference equation

$$A(d)y(t) = B(d)u(t) + E(d)n(t) \quad (2.10)$$

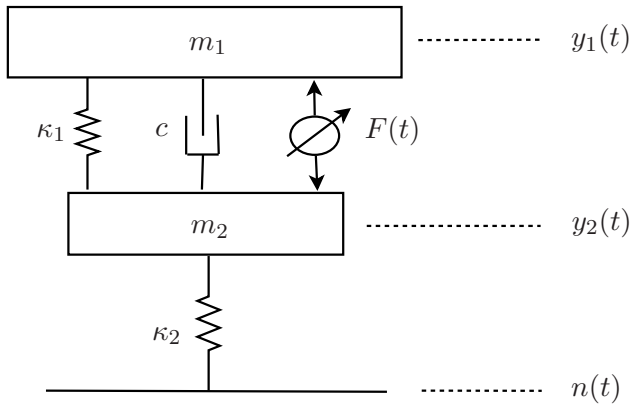

Figure 2.2: Quarter-car model scheme with active suspension system.

suspended mass	m_1	117 kg
tire mass	m_2	30 kg
suspension damping	c	3000 Ns/m
suspension stiffness	κ_1	30000 N/m
tire stiffness	κ_2	200000 N/m

Table 2.1: Parameter set used in the simulation tests.

is derived, where y and u correspond to the displacement y_1 and to the force F, respectively; further, in this case $t \in \mathbb{Z}_+$, $\mathbb{Z}_+ := \{0, 1, \cdots\}$, denotes discrete-time instants, and d is the unit backward shift operator. In the following, for the sake of brevity, we will consider $\nu(t) = E(d)n(t)$, thus we will consider the following difference equation

$$A(d)y(t) = B(d)u(t) + \nu(t)\,. \tag{2.11}$$

In particular, in the simulation tests that will be shown in Chapters 6 and 7, the sampling time T_s is set to $10^{-3}\,s$ in the discretization procedure, and the considered parameters refer to the motorcycle model of [86] and are summarized in Table 2.1.

A general control scheme involving an active suspension system for the quarter-car model is shown in Fig. 2.3, where we denote by $\overline{n}$ the signal produced as

$$\overline{n}(t) = F_p(d)n(t)\,. \tag{2.12}$$

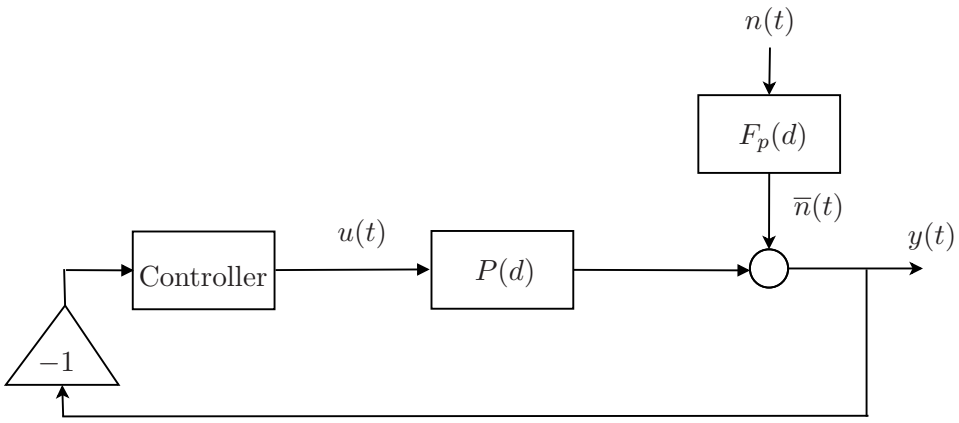

Figure 2.3: General control scheme involving an active suspension system.

Remark 2.1.1. For the sake of completeness, we show in Fig. 2.4 the quarter-car model with semi-active suspension system; as briefly described in the beginning of this chapter, with respect to the passive model, in this type of suspension systems the damping c is adjustable and hence represents the control input.

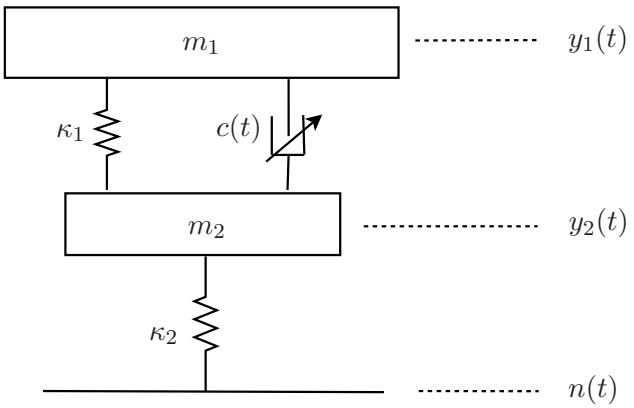

Figure 2.4: Quarter-car model scheme with semi-active suspension system.

Chapter 3

Literature overview

The design of control architectures able to deal with the problem of adaptive disturbance attenuation is a topic of great interest within the control community, as witnessed by the wide range of contexts of application including (but not limited to) acoustics [10], active suspension systems [60], adaptive optics for ground-based telescopes [2], laser systems [52]; the aim of this chapter is that of providing a brief overview of some of the most relevant solutions which have been proposed in the literature related to this subject.

When a measurement correlated with the disturbance (called *image* of the disturbance) is available thanks to the use of an additional transducer, a possible approach for addressing the problem is based on a *feedforward compensation*. Specifically, a control input is generated by filtering such a measurement via an adaptive filter whose parameters are adjusted with the aim of minimizing the effects of the disturbance on the output. A brief introduction to solutions based on the feedforward approach is provided in [63], which refers to [23, 34, 35, 40] and especially indicates the technique described in [91] in the context of adaptive noise cancellation as the one inspiring this type of approaches. Some drawbacks of the feedforward approach are the need of the additional transducer and the difficulty in the choice of its location. Other interesting works on this subject are [59, 61, 8, 62], which point out the presence in many systems of a "positive feedback coupling" between the compensator system and the measurement of the image of the disturbance which can lead the system to instability; an outline of previous solutions to this problem is also provided.

In the following, the focus will be on solutions based on feedback control for the attenuation of disturbances with uncertain and possibly time-varying characteristics. Much

interest in adaptive solutions for the problem of disturbance attenuation has been raised with respect to narrow-band disturbances; the proposed techniques involve either indirect approaches (exploiting the separation principle and resorting to disturbance frequency estimation), or direct approaches (proposing algorithms inherently designed for disturbance attenuation objectives). Following the review proposed in [63], some approaches that have been proposed as solutions to the problem of attenuating disturbances having uncertain characteristics and affecting a known plant could be mentioned:

- solutions based on the internal model principle (see for example [64, 9, 10, 89]);
- solutions based on adaptive observers (see for example [32, 67]);
- solutions based on the *phase-locked loop* structure used in communication systems (see for example [24]).

Specifically, strategies relying on the internal model principle adopt a control structure which incorporates the model of the disturbance; since this model is unknown/uncertain, this part of the controller should be adapted and re-designed in real-time. Indirect solutions of this class estimate the disturbance model and re-compute the controller by including in its transfer function the estimated model. As an alternative, by adopting the *Youla-Kucera* parametrization (also known as Q-parametrization) of the controller and adjusting the parameters of the Q polynomial, it is possible to adapt the internal model in the controller within a direct scheme.
The second class of solutions employ adaptive observers of the disturbance which are incorporated in the controller. These strategies rely on the idea of integrating in the control structure a device able to provide an estimate of the disturbance, so that it can be employed to generate an appropriate control signal.
Finally, the method proposed in [24] is a direct approach for the rejection of sinusoidal disturbances based on a phase-locked loop structure for adaptive feedback control, wherein a single error signal is employed to simultaneously accomplish frequency estimation and disturbance cancellation. Rough initial estimates of the disturbance frequency are required, which are provided by means of an initialization scheme.

In order to give better insight into the problem of active disturbance attenuation and the relevance of this issue within the control community, in the remaining of this chapter we will describe in some detail some of the most relevant contributions that can be found in

the literature, with particular reference to solutions based on internal model principle and adaptive observers.

3.1 Direct adaptive scheme for the rejection of narrow band disturbances

The solution proposed in [64], and later refined in [63, 27], consists in a direct adaptive scheme for the asymptotic rejection of narrow band disturbances. The approach has been developed as a solution within a benchmark for the rejection of unknown multiple narrow band disturbances affecting an active suspension system. The plant model is obtained by identification, and thus it is assumed to be known. The disturbance is expressed as a Dirac impulse filtered through the *model of the disturbance*, whose order n_{D_p} is assumed to be known (for narrow band or sinusoidal disturbances, it can be directly deduced in terms of the number of peaks in the power spectral density of the output signal); however, the parameters of the disturbance model are unknown. The idea of this approach relies on the well known *Internal Model Principle*, thus the rejection of unknown disturbances implies the adaptation and re-design in real-time of the internal model of the controller. The controller is expressed in terms of the Youla-Kucera parametrization of the stabilizing controllers; specifically, the polynomial $Q(d)$ has the form

$$Q(d) = q_0 + q_1 d + \cdots + q_{n_Q} d^{n_Q} , \tag{3.1}$$

where d is the unit backward shift operator and n_Q is the order of $Q(d)$, such that $n_Q = n_{D_p} - 1$. Thanks to the adopted Q-parametrization, the internal model is incorporated and adjusted in the controller by means of the parameters $q_0, q_1, \cdots, q_{n_Q}$. Further, variations of the Q polynomial in (3.1) do not affect the closed-loop poles.

A parameter adaptation algorithm is performed directly on the parameters of the Q polynomial, with the aim of iteratively tuning such parameters and thus adjusting the internal model in the controller. The adaptation is carried out at each time instant if an adaptive operation is considered; otherwise, the procedure can be activated either on demand or when the performance becomes unsatisfactory. A stability analysis proving the parametric convergence of the procedure is provided in [64], under the following hypotheses: the considered model for the plant is identical to the true plant model; the disturbance model has poles on the unit circle; the denominator of the disturbance model has a known order.

3.2 Indirect adaptive scheme for the attenuation of narrow band disturbances

In [6], an indirect adaptive regulation strategy is presented for the attenuation of narrow-band disturbances (see also [7]). The controller design relies on an output-sensitivity shaping which is achieved by the use of band-stop filters (BSFs) with transfer functions of the form

$$\frac{S_{BSF_i}(d)}{P_{BSF_i}(d)} = \frac{1+\beta_1^i d+\beta_2^i d^2}{1+\alpha_1^i d+\alpha_2^i d^2}\,,\; i\in\{1,2,\cdots,n\}\,, \tag{3.2}$$

with n the known number of spikes in the spectral characteristics of the disturbance. The transfer functions in (3.2) are a discretized version of the continuous filters

$$F_i(s) = \frac{s^2+2\zeta_{n_i}\omega_i s+\omega_i^2}{s^2+2\zeta_{d_i}\omega_i s+\omega_i^2}\,,\; i\in\{1,2,\cdots,n\}\,, \tag{3.3}$$

each one introducing an attenuation of

$$M_i = -20\,log_{10}\left(\frac{\zeta_{n_i}}{\zeta_{d_i}}\right) \tag{3.4}$$

at the frequency ω_i. To take into account n narrow-band disturbances, n BSFs can be combined as

$$H_{BSF}(d) = \frac{S_{BSF}(d)}{P_{BSF}(d)} = \frac{\prod_{i=1}^n S_{BSF_i}(d)}{\prod_{i=1}^n P_{BSF_i}(d)}\,. \tag{3.5}$$

The number n of the BSFs, that is, the number of narrow-band disturbances that can be compensated, can in principle be as large as necessary; however, it has to be underlined that there is a trade off between the value of n and the attenuation level that can be achieved. As mentioned above, the BSFs are used to shape the output sensitivity function; specifically, the poles of the BSFs are desired poles of the closed loop system, while their zeros are implemented in the controller. With this respect, it is shown that the computation of the numerator and denominator polynomials of the controller turns out to require a reduced complexity if the Youla-Kucera parametrization is adopted.

The control scheme described above can be applied to attenuate unknown and possibly time-varying narrow-band disturbances if an estimation in real-time of the frequencies corresponding to the peaks in the disturbance spectrum is available. It is assumed that a reliable estimate $\hat{p}$ of the disturbance is available and that the number n of narrow band disturbances is known; then a technique based on adaptive notch filters (ANFs) can be used

to estimate the frequencies of the sinusoidal signals in the disturbance[1]. An ANF has the following general form:

$$H_f(d) = \frac{A_f(d)}{A_f(\rho d)}\,, \tag{3.6}$$

where $A_f(d)$ has its roots on the unit circle, and $A_f(\rho d)$ has its roots on a circle of radius $1/\rho$ (on the same radial lines as the roots of $A_f(d)$). The cascade of n second-order ANF is considered of the form

$$H_f(d) = \prod_{i=1}^{n} H_f^i(d) = \prod_{i=1}^{n} \frac{1 + a^{f_i} d + d^2}{1 + \rho a^{f_i} d + \rho^2 d^2}\,. \tag{3.7}$$

The estimation of the frequency corresponding to one peak is performed assuming convergence of the other $n-1$, which in practice can be filtered out of the estimated disturbance signal $\hat{p}$. The parametric adaptation algorithm is thus performed with respect to the coefficients a^{f_i} for each i. Once the frequencies corresponding to the spikes have been estimated, they can be employed within the design method described above. Further details regarding the described technique can be found in [6] and [7]. Specifically, [7] provides a stability analysis of the overall adaptive scheme.

3.3 Adaptive internal models for disturbance cancellation

The approach proposed recently in [71] extends the results of [69, 68, 70], by addressing the problem of designing an adaptive regulator in the presence of disturbances and/or reference signals generated by a linear unknown exosystem (both its parameters and its order are unknown). Specifically, the linear system

$$\dot{x} = Ax + bu + Pw\,, \qquad x(0) = x_0 \tag{3.8}$$

$$e = cx + qw \tag{3.9}$$

is considered, with $x \in \mathbb{R}^n$ the state vector (n is a positive integer), $u \in \mathbb{R}$ the scalar input, $e \in \mathbb{R}$ the scalar output to be regulated around zero; it is assumed that the output e is the only measured signal. Both the disturbances and the possible references are generated by a linear exosystem, described by the differential equation

$$\dot{w} = Rw, \qquad w(0) = w_0, \qquad w \in \mathbb{R}^{2r+1}\,, \tag{3.10}$$

[1] In the context of narrow-band disturbance rejection it a common assumption that the disturbances are sinusoidal signals with variable frequencies [6].

where r is the number of frequencies $\{\omega_1, \cdots, \omega_r\}$ which characterize the disturbance Pw to be rejected and/or the reference qw to be tracked. While the triple (A, b, c) is assumed to be known, P, R, q and the order of the exosystem are not. The proposed technique is based on the following assumptions: (H1) (A, b) is stabilizable; (H2) (A, c) is detectable; (H3) $\text{rank} \begin{bmatrix} A - \lambda I & b \\ c & 0 \end{bmatrix} = n+1$, for any eigenvalue λ of R; (H4) the spectrum of the exosystem matrix R can be bounded from below by a known value ω_{min}, that is, it can be expressed as $\{0, \pm j\omega_i,\ 1 \leq i \leq r\}$ with $\omega_i \geq \omega_{min}$. It is underlined that there is no requirement that the system (A, b, c) is minimum-phase; by virtue of (H3), the zeros of the system are only required not to coincide with the eigenvalues of the matrix R.
The regulator employs two different observers and includes an adaptive internal model which tunes m parameters on the basis of the output regulation error. A stability analysis is provided which shows that, if $m \geq r$, the regulation error tends exponentially to zero; in fact, in this case the adaptive internal model is able to reproduce the exogenous signal to be rejected or tracked. On the other hand, if $m < r$, the adaptive internal model can only approximate the exogenous signal with an approximation error ϵ; in this case it is shown that, under appropriate assumptions on the value of ϵ, the regulation error tends exponentially into a closed ball whose radius is proportional to ϵ.

3.4 Gain-scheduled H_∞ synthesis method

The approach proposed in [54] within the benchmark on adaptive regulation for the rejection of narrow-band disturbances presented in [60] relies on a synthesis method of gain-scheduled H_∞ controllers. This technique hinges upon the approach originally proposed in [55] for the synthesis of a single robust fixed-order controller for SISO plants represented by nonparametric models. With reference to [55], the transfer function $K(d)$ of the controller is an affine function of a parameter vector ρ:

$$K(d) = K(d, \rho) = \phi^\top(d)\rho\,. \tag{3.11}$$

The performance requirement

$$||W_1\, S||_\infty < 1\,, \tag{3.12}$$

where $W_1(d)$ is the transfer function of a performance weighting filter for the output-sensitivity having transfer function $S(d, \rho)$, is considered and linearized around a known

desired open-loop transfer function $L_d(d)$. This leads to the following linear approximation of (3.12) in the frequency domain:

$$\left|W_1(e^{-j\omega})[1+L_d(e^{-j\omega})]\right| - Re\{[1+L_d(e^{j\omega})]\,[1+P(e^{-j\omega})\phi_i^\top(e^{-j\omega})\rho]\} < 0 \;\; \forall\omega\,, \quad (3.13)$$

where we denote by $Re\{x\}$ the real part of the complex number x. In fact, by recalling that $Re\{x\} \leq |x|$, where $|x|$ is the modulus of x, inequality (3.13) leads to

$$\left|W_1(e^{-j\omega})[1+L_d(e^{-j\omega})]\right| - \left|[1+L_d(e^{j\omega})]\right| \left|[1+P(e^{-j\omega})\phi_i^\top(e^{-j\omega})\rho]\right| < 0 \;\; \forall\omega\,, \quad (3.14)$$

and thus to

$$\left|W_1(e^{-j\omega})\right| < \left|[1+P(e^{-j\omega})\phi^\top(e^{-j\omega})\rho]\right| \;\; \forall\omega\,, \quad (3.15)$$

from which (3.12) follows. The performance criterion expressed by (3.12) can be improved by taking into account an upper bound γ on the H_∞ norm, thus leading to the following optimization problem to be solved:

$$\min_{\gamma,\rho} \gamma \quad (3.16)$$

s.t.

$$\left|\frac{1}{\gamma}W_1(e^{-j\omega})[1+L_d(e^{-j\omega})]\right| - Re\{[1+L_d(e^{j\omega})][1+P(e^{-j\omega})\phi_i^\top(e^{-j\omega})\rho]\} < 0 \;\; \forall\omega\,. \quad (3.17)$$

By adopting the bisection algorithm, thus fixing the value of γ at each step, the problem can be recast as a linear programming problem.

Within the gain-scheduling scheme of [54], each element of the vector ρ is an affine or polynomial function of a scheduling parameter θ. Further, the desired open-loop transfer function $L_d(d)$ can be a function of θ as well. The approximation (3.13) of the performance criterion (3.12) can thus be expressed as

$$\left|W_1(e^{-j\omega})[1+L_d(e^{-j\omega},\theta)]\right| - Re\{[1+L_d(e^{j\omega},\theta)]\,[1+P(e^{-j\omega})\phi_i^\top(e^{-j\omega})\rho(\theta)]\} < 0 \;\; \forall\omega\,,\forall\theta\,. \quad (3.18)$$

Obviously, considering the infinite number of constraints in (3.18) is intractable; a possibility to overcome this problem is that of choosing finite grids for both ω and θ. The authors considered the first two levels of the benchmark of [60], namely the rejection of one sinusoidal disturbance having frequency in a certain range Ω, and the rejection of two sinusoidal disturbances having frequency in the same range Ω. For the first level, a controller $K(d,\rho)$ of the following form is considered:

$$K(d,\theta) = [K_0(d) + \theta K_1(d)]M(d,\theta)\,, \quad (3.19)$$

where K_0 and K_1 are Finite Impulse Response filters and

$$M(d,\theta) = \frac{1}{1+\theta d+d^2} \tag{3.20}$$

the disturbance model (in accordance with the internal model principle). The optimization problem to be solved accounts also for the particular specifications imposed within the benchmark (*e.g.*, it is required that the maximum of the modulus of the output-sensitivity does not exceed a specified upper bound). The scheduling parameter θ which appears in the internal model of the disturbance is estimated by means of a recursive parameter adaptation algorithm. For the second level of the benchmark, the controller transfer function has the form

$$K(d,\theta_1,\theta_2) = [K_0(d) + \theta_1 K_1(d) + \theta_2 K_2(d)]M(d,\theta_1,\theta_2)\,, \tag{3.21}$$

where K_0, K_1 and K_2 are Finite Impulse Response filters and

$$M(d,\theta_1,\theta_2) = \frac{1}{1+\theta_1 d+\theta_2 d^2+\theta_1 d^3+d^4}\,. \tag{3.22}$$

The same parameter adaptation algorithm is used for this level, taking into account that the scheduling parameter θ in this case is replaced by the vector $[\theta_1,\ \theta_2]$.

3.5 Adaptive control design for the suppression of laser beam jitter

Finally, in [52] a robust adaptive scheme for the suppression of laser beam jitter in the presence of unmodeled dynamics is presented. It is pointed out that much of the jitter is caused by periodic disturbances with unknown and possibly time-varying frequencies and amplitudes. In such applications, it is usually assumed that the system has already been stabilized (*e.g.*, by means of an integrator). The problem is formulated in continuous time. The considered disturbance is composed of a bounded noise disturbance and of the combination of sinusoidal signals with unknown frequency, amplitude and phase. The controller transfer function is affine in a n-dimensional parameter vector θ.

A first analysis is carried out by assuming that all the sinusoidal components of the disturbance are known; it is shown in this case that, if the number of parameters in the controller transfer function is large enough, under appropriate assumptions the sinusoidal part can be completely rejected and the output signal will be limited by a value depending on the

amplitude of the bounded additive noise. In the absence of noise, the output signal will converge to zero exponentially fast.
The analysis is then extended to the case of unknown disturbance. The aim is that of designing an adaptively tuned filter to minimize the output variance. The robust least-square algorithm [51, 50] is adopted to estimate the parameter vector θ. An upper bound on the norm of the estimate $\hat{\theta}$ is imposed by defining a compact set $\mathbb{S}$ as

$$\mathbb{S} = \{\hat{\theta} \in \mathbb{R}^n \quad \text{s.t.} \quad \hat{\theta}^\top \hat{\theta} - \theta_{max}^2 \leq 0\}\,, \tag{3.23}$$

with $\theta_{max} > 0$ large enough to ensure that the optimal (unknown) parameter vector (achieving perfect rejection of the sinusoidal components of the disturbance) belongs to $\mathbb{S}$. Then, projection can be used within the adaptation algorithm in order to have $\hat{\theta} \in \mathbb{S}$. It is shown that, by adopting the proposed adaptive law, the average energy of the output signal is of the order of the modeling error and the noise amplitude; thus, in the absence of modeling error and noise, the output signal converges to zero.

PART II
A Switching Control approach

Chapter 4

Adaptive disturbance attenuation: a Switching Control approach

In Chapter 3, an outline of some solutions to the problem of the attenuation of disturbances having uncertain and possibly time-varying characteristics has been provided; the described methods rely in general on control structures which aim at adaptively changing their action in order to be able to deal with the uncertainty and to react to changes in the operating conditions of the system to be controlled.

The objective of controlling a system subject to uncertainty, either in the plant model or in the model of the disturbances acting on it, has been a topic of major concern over the past decades, and there is still a strong interest with respect to this subject. It is to be noted that, if the uncertainty set is sufficiently small, a single robust controller can in general achieve satisfactory performance with respect to all the possible operating conditions (see [92] and the references therein). However, the need for control reconfiguration becomes important especially when the uncertainty set is large (in the sense that the possible operating conditions of the system could be very different from one another), so that the action of a single robust controller cannot ensure a satisfactory performance level in all the possible situations. Further, when the uncertain characteristics are also time-varying, the ability of adapting can in general provide a more appropriate action (at least in the long run) with respect to the specific operating condition.

With this respect, several techniques have been proposed, following either the *Adaptive Control* paradigm (see for example [51, 74, 13, 63]), or, more recently, the *Adaptive*

Switching Control (ASC) paradigm (see [73, 75, 45, 15, 53, 17, 16, 19]). Despite the common goal of providing a control structure which is able to adaptively change its action, the two approaches have their own distinguishing, and in some measure, complementary features. A comparison between the two paradigms is provided for example in [46]. Specifically, within the ASC paradigm, a finite family of controllers is pre-synthesized off-line, each one suitable for a specific operating condition. Then the choice, at each time instant, of which controller should be put in feedback with the plant is made by a high-level supervisory unit. An important feature of this control approach is modularity: the control strategy and the adaptation mechanism are designed independently from one another. Specifically, each controller can be synthesized according to any technique, since the design procedure is carried out off-line. The absence of any connection with the switching rule can be useful either when existing control structures should be used, or when advanced control strategies are required for specific problems.

It is worth underlining that the ASC scheme has been largely adopted and studied in the context of plant model uncertainty, as witnessed by most of the bibliographical references which have been mentioned above. We propose to employ the ASC paradigm to deal with the problem of the attenuation of disturbances with uncertain and possibly time-varying characteristics [19, 21, 20]. In fact, by relying on a family of controllers, each one synthesized so that it enjoys satisfactory performance with respect to a subregion of the uncertainty set, and on a logic able to select the (potentially) best one at each time instant, it is possible to obtain very good attenuation capabilities even with respect to large uncertainty sets. Further, the modularity which characterizes the ASC approach makes the technique well-suited to being applied in different contexts (such as, for example, active vibration control, eccentricity compensation, adaptive optics applications, as well as noise cancellation in acoustic ducts) since the switching mechanism does not depend on the disturbance model, which has to be taken into account only within the controller family design.

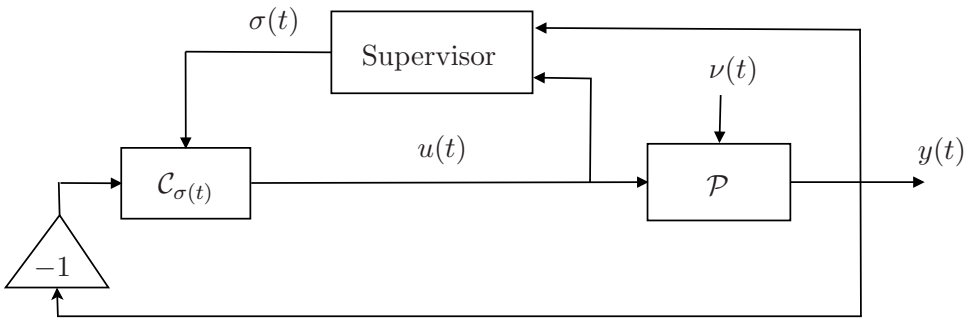

Figure 4.1: Overall control scheme.

4.1 Problem setting

Consider a single-input single-output (SISO) linear time-invariant (LTI) dynamical system whose input-output behavior can be described by the difference equation

$$A(d)y(t) = B(d)u(t) + \nu(t)\,, \tag{4.1}$$

where $y(t)$ is the system output, $u(t)$ the control input, and $\nu(t)$ an unknown bounded disturbance acting on the system. The polynomials $A(d) = 1 + a_1\,d + \cdots + a_{n_a}\,d^{n_a}$ and $B(d) = b_1\,d + \cdots + b_{n_b}\,d^{n_b}$ in the unit backward shift operator d are known and have strictly Schur greatest common divisor (g.c.d.).

Remark 4.1.1. We underline that the model provided in (4.1) can be used without loss of generality. In fact, a general LTI model of the form

$$\overline{A}(d)y(t) = \frac{B(d)}{F(d)}u(t) + \frac{H(d)}{R(d)}e(t)\,, \tag{4.2}$$

where $e(t)$ is a zero mean white noise with variance σ_e^2, and $B(d)$ and $F(d)$ are coprime polynomials, can be written as in (4.1) by defining

$$A(d) := \overline{A}(d)F(d)\ , \qquad \nu(t) := \frac{H(d)F(d)}{R(d)}\,e(t)\,.$$

In the simulation setup presented in Chapter 6, for example, we will resort to the model in (4.1) with the disturbance $\nu(t)$ obtained as the output of a suitable filter.

We denote by $\mathcal{P}$ the plant in (4.1) having transfer function $P(d) = B(d)/A(d)$. The problem of interest is that of attenuating the disturbance $\nu(t)$ by regulating the plant

output $y(t)$ around zero. We suppose that a non-negligible uncertainty affects the a priori available disturbance model, so that a single robust LTI controller cannot achieve satisfactory performance within the whole uncertainty set.

The solution that we propose for the problem of disturbance attenuation relies on the ASC paradigm; in fact, the control architecture is composed of a finite family of pre-designed controllers supervised by a high-level switching logic. The controllers are supposed to have been synthesized off-line, according to any design technique, so that: each of the pre-synthesized controllers stabilize the plant; and, for any possible operating conditions, at least one of the controllers is able to achieve a certain prescribed performance level (for example, in terms of disturbance-to-output energy gain). Then, at each time instant, the supervisory unit infers the potential behavior of each candidate controller and selects the one providing the best potential performance, which is quantified in terms of test functionals defined on the basis of the plant input/output data.

Let $\mathscr{C} := \{\mathcal{C}_i,\, i \in \overleftarrow{N}\}$ denote the family of pre-designed candidate controllers, where $\overleftarrow{N} := \{1, 2, \cdots, N\}$. The transfer function of the i-th controller is $C_i(d) = S_i(d)/R_i(d)$ with the polynomials $R_i(d) = 1 + r_{i1}d + \cdots + r_{in_{r_i}}d^{n_{r_i}}$ and $S_i(d) = s_{i0} + s_{i1}d + \cdots + s_{in_{s_i}}d^{n_{s_i}}$ having strictly Schur g.c.d. At each time instant, the selected controller belonging to $\mathscr{C}$ is identified by means of the switching signal $\sigma(\cdot) : \mathbb{Z}_+ \to \overleftarrow{N}$. Accordingly, we denote by $\mathcal{C}_{\sigma(t)}$ the switching controller (or multi-controller), with the understanding that, on all the time intervals on which $\sigma(t)$ is constant and equal to a certain i, the multi-controller takes the form of a LTI system having transfer function equal to $C_i(d)$. We defer any discussion on the internal structure of the multi-controller to Section 6.1, where it will be shown how a suitable implementation of such a block always preserves stability under arbitrary switching. The overall control scheme is depicted in Fig. 4.1.

4.1.1 Controller selection

In this section, a criterion is proposed for selecting, among the controllers belonging to $\mathscr{C}$, the one to be put in feedback to the plant. To this end, at any time t, a set of test functionals $\Pi(t) := \left\{\Pi_i(t),\, i \in \overleftarrow{N}\right\}$ is computed, each one quantifying the performance achievable by the use of the related candidate controller $\mathcal{C}_i$. Each test functional is computed only on the grounds of the plant input/output data without the necessity of inserting the corresponding controller in the feedback loop.

Let

$$\varepsilon(t) := A(d)\, y(t) - B(d)\, u(t) \tag{4.3}$$

denote the prediction error, where $y(t)$ and $u(t)$ are the output and input data produced by the switching system $(\mathcal{P}/\mathcal{C}_{\sigma(t)})$ composed of the feedback interconnection of $\mathcal{P}$ and $\mathcal{C}_{\sigma(t)}$. We underline that, for any $t \geq n = \max\{n_a, n_b\}$, the prediction error $\varepsilon(t)$ coincides with the disturbance $\nu(t)$. Hence, the potential performance achievable by a certain candidate controller $\mathcal{C}_i$ can be evaluated by filtering the prediction error $\varepsilon(t)$ with a suitable transfer matrix $\Sigma_i(d)$ related to the potential loop $(\mathcal{P}/\mathcal{C}_i)$, defined as the feedback interconnection of the plant $\mathcal{P}$ with the controller $\mathcal{C}_i$.

In particular, we consider the weighted mixed-sensitivity $\Sigma_i(d)$ related to the loop $(\mathcal{P}/\mathcal{C}_i)$ and defined as

$$\Sigma_i(d) := \frac{1}{\chi_i(d)}\, L_i(d) \tag{4.4}$$

where

$$L_i(d) = \begin{bmatrix} R_i(d) \\ -\eta\, S_i(d) \end{bmatrix}$$

and $\chi_i(d) = A(d)\, R_i(d) + B(d)\, S_i(d)$ is the characteristic polynomial of $(\mathcal{P}/\mathcal{C}_i)$. It can be seen that the two elements of $\Sigma_i(d)$ represent the disturbance-to-output and, respectively, disturbance-to-control transfer functions of $(\mathcal{P}/\mathcal{C}_i)$. The latter one is weighted by a non-negative scalar η which can be tuned to give more or less importance to the contribution of the control input in the performance evaluation.

Then, in order to compute, for each $i \in \overleftarrow{N}$, the hypothetical weighted response

$$z_i = \begin{bmatrix} y_i & \eta\, u_i \end{bmatrix}^\top \tag{4.5}$$

of the potential loop $(\mathcal{P}/\mathcal{C}_i)$ to the disturbance ν, we solve, at each time instant, the difference equation

$$\chi_i(d) z_i(t) = L_i(d)\varepsilon(t)\,. \tag{4.6}$$

The computation of the signals $z_i(t)$ by means of (4.6) is started at a time $t_0 \geq n$ with zero initial conditions.

On the basis of the foregoing definitions, the performance of each potential loop can be evaluated in terms of the test functional

$$\Pi_i(t) := \begin{cases} \frac{\| z_i|_{t-M(t)}^{t} \|}{\| \varepsilon|_{t-M(t)}^{t} \|}\,, & \text{if } \| \varepsilon|_{t-M(t)}^{t} \| > 0 \\ \\ 0\,, & \text{if } \| \varepsilon|_{t-M(t)}^{t} \| = 0\,, \end{cases} \tag{4.7}$$

where $\| \varepsilon|_{\underline{t}}^{\bar{t}} \| := \sqrt{\sum_{k=\underline{t}}^{\bar{t}} |\varepsilon(k)|^2}$, with $\underline{t}$ and $\bar{t}$ two generic time instants such that $\underline{t} \leq \bar{t}$; $|\cdot|$ is the Euclidean norm and $\varepsilon|_{\underline{t}}^{\bar{t}} := \text{col}[\varepsilon(\underline{t}), \ldots, \varepsilon(\bar{t})]$. The *memory* $M(t)$ of the test functionals, that is the size of the time window on which the test functionals are computed, is a design parameter. In practice, the choice of $M(t)$ is related to the disturbance characteristics which are expected within the specific context. In particular, we can distinguish between two different situations. When the disturbance can be assumed to be almost stationary, albeit with an unknown frequency profile, we can use a *persistent memory* and set $M(t) = t - t_0$. In fact, the switching logic is activated at the time instant t_0 from which the computation of the signals $z_i(t)$ (and thus of the test functionals $\Pi_i(t)$) starts. On the contrary, if it is expected that the disturbance characteristics vary with time, a *finite memory* is more appropriate so as to make the test functionals able to promptly reflect any change in the environmental conditions. Then, in this case, we set

$$M(t) = \begin{cases} t - t_0\,, & \text{if } t < t_0 + M_* \\ M_*\,, & \text{otherwise}\,, \end{cases} \tag{4.8}$$

where M_* is a positive integer. Specific values for M_* are related to the properties that the test functionals satisfy under certain assumptions on the nature of the disturbance, as will be shown in Section 4.2. We can notice that, if the disturbance can be assumed to be almost stationary, the problem to be solved is a learning problem; otherwise, if the disturbance is supposed to change in time, the aim is that of solving an adaptation problem.

Remark 4.1.2. It is interesting to underline that the choice of M_* does not affect the closed-loop stability. As a matter of fact, the choice of M_* only affects the closed-loop performance in the sense that for smaller M_*, the more prompt the control scheme to react to changes in the disturbance characteristics, but also the more prone to spurious switching, as will be clear from Section 4.2.2. An alternative to the finite memory is a *fading* memory, which can be achieved for instance by introducing a forgetting factor in the Euclidean norm.

This choice also ensures that the effect of old data vanishes as time advances. In this case, however, no simple characterization of the switching behavior exists to our knowledge. The simplest and most effective way for improving performance consists perhaps in an *adaptive* memory. This basically means replacing M_* with $M(t)$, where the latter is chosen on-line depending on the exhibited process behavior. Specifically, the idea is that, based on the values taken on by $\Pi_i(t)$, old data can be retained ($M(t)$ increases) so as to facilitate "learning" or discarded ($M(t)$ decreases) if they contain information which is irrelevant for taking switching decisions. A detailed analysis and discussion of logics of this kind can be found in [22].

With respect to the switching rule, we assume that the sequence σ is determined according to the Hysteresis Switching Logic (HSL) (see [73])

$$\begin{aligned} &\sigma(t+1) = l(\sigma(t), \Pi(t)), \qquad \sigma(t_0) = i_0 \in \overleftarrow{N} \\ &l(i, \Pi(t)) = \begin{cases} i, & \text{if} \quad \Pi_i(t) < \Pi_{i_*(t)}(t) + h \\ i_*(t), & \text{if} \quad \Pi_i(t) \geq \Pi_{i_*(t)}(t) + h \end{cases} \end{aligned} \tag{4.9}$$

where $i_*(t)$ is the smallest index in $\overleftarrow{N}$ such that $\Pi_{i_*(t)}(t) \leq \Pi_i(t)$, $\forall i \in \overleftarrow{N}$, and $h > 0$ is the hysteresis constant. For $t \leq t_0$, $\sigma(t)$ is kept constant and equal to an arbitrary initial value $i_0 \in \overleftarrow{N}$.

4.2 Properties of the test functionals

In this section, the properties of the test functionals will be analyzed for both the cases of persistent and finite memory. In the following we assume that $\| \varepsilon|_{t-M(t)}^{t} \| > 0$, for any $t \geq t_0$, so that $\Pi_i(t)$ is defined as in the first case of (4.7).

4.2.1 Persistent memory

Consider first the case of a learning problem wherein a persistent memory $M(t) = t - t_0$ is adopted. Then, the following result can be readily stated.

Theorem 4.2.1. *Let the test functionals $\Pi_i(t)$, $i \in \overleftarrow{N}$, be defined as in (4.7) with $M(t) = t - t_0$. Then, for any $i \in \overleftarrow{N}$ and $t \geq t_0$*

$$\Pi_i(t) \leq \|\Sigma_i\|_\infty \,. \tag{4.10}$$

If, in addition, the disturbance $\nu(t)$ is supposed to be quasi-stationary and ergodic, the following facts hold.

i) For any $i \in \overleftarrow{N}$, the test functional $\Pi_i(t)$ converges to the gain of the system $\Sigma_i(d)$ in response to ν

$$\overline{\Pi}_i := \left(\frac{\int_{-\pi}^{\pi} |\Sigma_i(e^{-j\omega})|^2 \, \Phi_\nu(\omega) \, d\,\omega}{\int_{-\pi}^{\pi} \Phi_\nu(\omega) \, d\,\omega} \right)^{1/2} \tag{4.11}$$

as $t \to \infty$, where $\Phi_\nu(\omega)$ denotes the power spectral density of the signal $\nu(t)$;

ii) when the HSL (4.9) is adopted, there is a finite time $t_f \in \mathbb{Z}_+$, after which no more switching occurs and the final controller, say $\mathcal{C}_f$, ensures the best achievable performance apart from the hysteresis constant, i.e.,

$$\overline{\Pi}_f < \min_{i \in \overleftarrow{N}} \overline{\Pi}_i + h \, . \tag{4.12}$$

□

The bound in (4.10) as well as the asymptotic result of fact i) are straightforward consequences of the stability of $\Sigma_i(d)$. Further, fact ii) descends from the well-known *HSL Lemma* of [73].

Remark 4.2.1. A case of special interest arises when the disturbance $\nu(t)$ is narrow-band and can be well modeled by a sinusoidal signal of frequency ω_0. In this case, the asymptotic value $\overline{\Pi}_i$ turns out to be equal to $\overline{\Pi}_i = |\Sigma_i(e^{-j\omega_0})|$. Then, if the disturbance frequency ω_0 is known to belong to a given interval $[\omega_{\min}, \omega_{\max}]$ and the family $\mathscr{C}$ is designed so as to ensure a desired level of attenuation γ in the whole frequency interval of interest so that

$$\max_{\omega_0 \in [\omega_{\min}, \omega_{\max}]} \min_{i \in \overleftarrow{N}} |\Sigma_i(e^{-j\omega_0})| \leq \gamma \, ,$$

the proposed switching control scheme ensures a disturbance attenuation level smaller than $\gamma + h$.

We conclude this section dedicated to the case of persistent memory by noting that, whenever the disturbance $\nu(t)$ is periodic, it is possible to analyze in some detail the behavior of the test functionals and of the overall switching scheme during the transient. First of all, we establish an upper bound on the difference $|\Pi_i(t) - \overline{\Pi}_i|$ that holds for any $t \geq t_0$.

Lemma 4.2.1. *Let the test functionals* $\Pi_i(t)$, $i \in \overleftarrow{N}$, *be defined as in (4.7) with* $M(t) = t - t_0$. *Further, let the disturbance* ν *be periodic with period* $T > 0$. *Then there exist suitable nonnegative constants* λ_i *such that, for any* $t \geq t_0$ *and* $i \in \overleftarrow{N}$,

$$|\Pi_i(t) - \overline{\Pi}_i| \leq \frac{\lambda_i T C_\nu}{\| \nu|_{t_0}^t \|} \tag{4.13}$$

with C_ν *the magnitude of the disturbance* ν.

Proof: see the Appendix. □

The result given in Lemma 4.2.1 is useful to derive the following theorem.

Theorem 4.2.2. *Let the same assumptions as in Lemma 4.2.1 hold, and let* $\overline{\lambda} := \max_{i \in \overleftarrow{N}} \lambda_i$. *Finally, let the HSL (4.9) be adopted. Then no switching can occur after* $\tilde{t}$, *namely the first switching time such that condition*

$$\| \nu|_{t_0}^{\tilde{t}} \| > \frac{4\overline{\lambda} T C_\nu}{h} \tag{4.14}$$

holds.

Proof: see the Appendix. □

Notice that condition (4.14) is always attained in finite time for any non-null periodic disturbance sequence. By comparing (4.14) with (4.12), it can be seen that the choice of the hysteresis constant h leads to a trade off between attenuation performance (the right-hand side of (4.12)) and learning time (the right-hand side of (4.14)).

4.2.2 Finite memory

In this section, we take into account an adaptation problem wherein a finite memory $M(t)$ defined as in (4.8) is used. The following results hold in this case.

Proposition 4.2.1. *Let the test functionals* $\Pi_i(t)$, $i \in \overleftarrow{N}$, *be defined as in (4.7) with* $M(t)$ *defined as in* (4.8). *Then, for any* $i \in \overleftarrow{N}$ *and* $t \geq t_0$,

$$\Pi_i(t) \leq \begin{cases} \|\Sigma_i\|_\infty \,, & \text{if} \quad t < t_0 + M_* \\ \|\Sigma_i\|_\infty + \frac{\delta_i C_\nu}{\| \nu|_{t-M_*}^t \|} \,, & \text{if} \quad t \geq t_0 + M_* \end{cases} \tag{4.15}$$

holds, with δ_i *a suitable nonnegative constant.*

Proof: see the Appendix. □

Proposition 4.2.1 provides an upper bound on the test functionals $\Pi_i(t)$ defined in (4.7) when a finite memory is adopted. Notice that, for $t \geq t_0 + M_*$, the non-zero initial conditions of (4.6) at time $t - M_*$ are taken into account by means of the additional term $\delta_i C_\nu / \| \nu|_{t-M_*}^{t} \|$, where δ_i is a constant which is independent of the disturbance ν and is such that $\delta_i C_\nu$ provides a bound on the norm of the free-response of the system $\Sigma_i(d)$ to the initial conditions at time $t - M_*$.

With the aim of proving some properties that the test functionals $\Pi_i(t)$, $i \in \overleftarrow{N}$, satisfy when a finite memory is adopted within an adaptation problem, we consider a periodic signal $s(t)$ with period $T > 0$, and denote the gain of the system $\Sigma_i(d)$ in response to s as

$$\overline{\Pi}_i := \left[\frac{\sum_{\ell=1}^{T} \left| \Sigma_i(e^{-j\frac{2\pi}{T}\ell}) \hat{s}_T\left(\frac{2\pi\ell}{T}\right) \right|^2}{\sum_{\ell=1}^{T} \left| \hat{s}_T\left(\frac{2\pi\ell}{T}\right) \right|^2} \right]^{1/2}, \tag{4.16}$$

where $\hat{s}_T\,(2\pi\ell/T)$ are the coefficients of the Discrete Fourier Transform of the sequence $s|_1^T$. This definition coincides with the one given in (4.27) within the Proof of Lemma 4.2.1. However, differently from the case of persistent memory, here $\overline{\Pi}_i$ cannot be interpreted as the asymptotic limit of $\Pi_i(t)$, in that the asymptotic limit need not exist.

If the disturbance $\nu(t)$ coincides with the periodic signal $s(t)$, at least in a sufficiently large time interval, we can provide the following results.

Lemma 4.2.2. *Let the test functionals $\Pi_i(t)$, $i \in \overleftarrow{N}$, be defined as in (4.7) with $M(t)$ defined as in* (4.8)*. Further, let the disturbance $\nu(t)$ coincide with the periodic signal $s(t)$ for any $t \in [t_1\,,\, t_2]$ such that $t_2 \geq t_1 + M_*$. Then, for any $t \in [t_1 + M_*\,,\, t_2]$ and $i \in \overleftarrow{N}$, there exist suitable nonnegative constants λ_i, δ_i such that*

$$|\Pi_i(t) - \overline{\Pi}_i| \leq \frac{[\lambda_i\, T + \delta_i]\, C_\nu}{\| \nu|_{t-M_*}^{t} \|}\,. \tag{4.17}$$

Proof: see the Appendix. □

Notice that the larger the interval spanned by the finite memory, the lower the bound on the difference $|\Pi_i(t) - \overline{\Pi}_i|$. In fact, for a generic time instant $t \in [t_1 + M_*\,,\, t_2]$, we can assert that

$$\| \nu|_{t-M_*}^{t} \| \geq \left\lfloor \frac{M_*}{T} \right\rfloor \| s|_1^T \|\,, \tag{4.18}$$

where $\lfloor M_*/T \rfloor$ denotes the largest integer ξ such that $\xi \leq M_*/T$; the equality in (4.18) holds if $M_* = \mu T$, with μ a positive integer. We point out that, if $t_1 \equiv t_0$, then (4.17) reduces to

$$|\Pi_i(t) - \overline{\Pi}_i| \leq \frac{\lambda_i \, T \, C_\nu}{\| \, \nu|_{t-M_*}^{t} \, \|} \, . \tag{4.19}$$

Thanks to Lemma 4.2.2 it is possible to derive the following theorem.

Theorem 4.2.3. *Let the same assumptions as in Lemma 4.2.2 hold. Further, let* $\overline{\lambda}$ *be defined as in Theorem 4.2.2 and* $\overline{\delta} := \max_{i \in \underline{N}} \delta_i$. *Finally, assume that the HSL (4.9) is adopted. Then, if*

$$\left\lfloor \frac{M_*}{T} \right\rfloor > 4 \, \frac{\overline{\lambda} T + \overline{\delta}}{h \, \| \, s|_1^T \, \|} \, C_\nu \tag{4.20}$$

holds, there can be at most one switch in the interval $[t_1 + M_* \, , \, t_2]$.

Proof: see the Appendix. □

The previous theorem shows that at most one switch can occur in the interval $[t_1 + M_* \, , \, t_2]$ if the size M_* of the finite memory is sufficiently large, given a certain h, or, equivalently, if the value of the hysteresis constant h is sufficiently large, given a certain M_*. This means that the smaller the value of M_*, the more prompt the control scheme to react to changes in the disturbance characteristics, but also the more prone to spurious switching. If the disturbance characteristics vary in time, this result holds for each pair $(t_1 \, , \, t_2)$ such that the hypotheses of the theorem are satisfied; a special case of interest is when the disturbance is piecewise periodic. We point out that, if $t_1 \equiv t_0$, (4.20) reduces to

$$\left\lfloor \frac{M_*}{T} \right\rfloor > \frac{4 \overline{\lambda} T C_\nu}{h \, \| \, \nu|_1^T \, \|} \, . \tag{4.21}$$

Remark 4.2.2. The extension of the performance analysis of Theorems 4.2.2 and 4.2.3 to more general classes of disturbances (*e.g.*, bounded quasi stationary signals) is quite challenging and appears to be a more difficult task. From a technical point of view, such a difficulty is essentially dictated by the fact that Theorems 4.2.2 and 4.2.3 hinge upon Lemmas 4.2.1 and 4.2.2, which provide an explicit characterization of the distance between $\Pi_i(t)$ and $\overline{\Pi}_i$ (see (4.13) and (4.17)). However, for general quasi-stationary signals, only *asymptotic* (rather than *finite-time*) bounds are available. The simulation tests presented in Chapter 6, nonetheless, illustrate the effectiveness of the considered approach even in more general situations than those captured by Theorems 4.2.2 and 4.2.3.

4.3 Stability under arbitrary switching

A critical issue related to solutions involving switching is that of guaranteeing the stability of the overall closed-loop system; in fact, as well known, even if each of the subsystems is stable (*i.e.*, each of the synthesized controllers is stabilizing), the stability of the system as a whole is not ensured under arbitrary switching sequences. In classical approaches (see for example [43, 65]), the stability of the switching system is verified *a-posteriori*, and it is in general guaranteed by increasing either the dwell-time or the hysteresis constant. In the former case, this means increasing the minimum time interval between two switching instants; in the latter one, this means increasing the minimum difference between performance functionals related to the controllers that allows the replacement of the controller which is currently in feedback with the plant by a potentially better one. It is clear, however, that such mechanisms can be detrimental for the performance of the system, since they slow down the switching and hence make the system less prompt to reconfigure the control action when needed.

In this chapter, it has been shown that, under appropriate assumptions, the switching can be ensured to stop in finite time, and this is enough to guarantee the stability of the overall feedback scheme, since the final controller is stabilizing by assumption. This is the case, for example, of a disturbance with almost stationary characteristics when a persistent memory is adopted. However, in more general situations, as it could happen when the disturbance characteristics vary persistently with time, the switching need not stop in finite time, and this raises the problem of ensuring the stability of the overall feedback loop under arbitrary switching sequences.

A possible solution is that of addressing the stability requirement directly within the synthesis of the controller family. As will be shown in detail in Chapter 5, this allows the complexity of the multi-controller architecture to be independent of the plant order; on the other hand, the inclusion in the synthesis step of a constraint related to the switching mechanism affects the modularity which is typical of the ASC paradigm.

Another solution in order to ensure the stability of the overall feedback loop is that of considering the *Youla* parametrization of all the stabilizing controllers and adopting a specific implementation of the multi-controller based on a switching mechanism between the Youla parameters. This solution completely preserves the modularity of the switching con-

trol approach; on the other hand, the complexity of the adopted architecture is unavoidably influenced by the plant order. Details will be provided in Chapter 6.

4.A Appendix: Proofs

Proof of Lemma 4.2.1

Since the disturbance $\nu(t)$ is a periodic signal with period T, we can express the generic time instant $t \geq t_0$ as $t = t_0 + KT + \theta$, with $K, \theta \in \mathbb{Z}_+$. Further, recall that, for any $t \geq t_0$, $\varepsilon(t)$ coincides with $\nu(t)$.

With respect to $z_i|_{t_0}^t$, we can distinguish between two different contributions:

$$z_i|_{t_0}^t = z_{i,\Sigma_i}|_{t_0}^t + z_{i,\nu}|_{t_0}^t \,, \tag{4.22}$$

with $z_{i,\Sigma_i}|_{t_0}^t$ conveying the effects of the poles of $\Sigma_i(d)$ and $z_{i,\nu}|_{t_0}^t$ conveying the effects of the eigenvalues of the system generating ν. It can be noticed that $z_{i,\Sigma_i}|_{t_0}^t$ depends on C_ν and T (the magnitude and the period of $\nu(t)$, respectively), as well as on the dynamics of $\Sigma_i(d)$, and is such that

$$\| \, z_{i,\Sigma_i}|_{t_0}^t \, \| \leq \alpha_i T C_\nu, \tag{4.23}$$

for some nonnegative constant α_i.

For all $K > 0$, both

$$\| \, \nu|_{t_0}^{t_0+KT-1} \, \|^2 = K \sum_{\ell=1}^{T} \left| \hat{\nu}_T \left(\frac{2\pi\ell}{T} \right) \right|^2 \tag{4.24}$$

and

$$\| \, z_{i,\nu}|_{t_0}^{t_0+KT-1} \, \|^2 = K \sum_{\ell=1}^{T} \left| \hat{z}_{i,\nu,T} \left(\frac{2\pi\ell}{T} \right) \right|^2 \tag{4.25}$$

hold, where $\hat{\nu}_T \left(2\pi\ell/T\right)$ and $\hat{z}_{i,\nu,T} \left(2\pi\ell/T\right)$ are the coefficients of the Discrete Fourier Transform of the sequences $\nu|_1^T$ and $z_{i,\nu}|_1^T$, respectively. For the sake of brevity, we make (4.24) and (4.25) hold also for $K = 0$ by letting $\| \, \nu|_{t_0}^{t_0-1} \, \| = \| \, z_{i,\nu}|_{t_0}^{t_0-1} \, \| = 0$.

In turn, we can compute $\hat{z}_{i,\nu,T} \left(2\pi\ell/T\right)$ as

$$\hat{z}_{i,\nu,T} \left(\frac{2\pi\ell}{T} \right) = \Sigma_i(e^{-j\frac{2\pi}{T}\ell}) \hat{\nu}_T \left(\frac{2\pi\ell}{T} \right). \tag{4.26}$$

We denote $\overline{\Pi}_i$ as the gain of the system $\Sigma_i(d)$ in response to ν:

$$\overline{\Pi}_i := \left[\frac{\sum_{\ell=1}^{T} \left| \Sigma_i(e^{-j\frac{2\pi}{T}\ell}) \hat{\nu}_T \left(\frac{2\pi\ell}{T} \right) \right|^2}{\sum_{\ell=1}^{T} \left| \hat{\nu}_T \left(\frac{2\pi\ell}{T} \right) \right|^2} \right]^{1/2} . \tag{4.27}$$

Appendix: Proofs

We point out that, for a periodic disturbance ν and in the case of persistent memory, $\overline{\Pi}_i$ coincides with the asymptotic limit of the test functional $\Pi_i(t)$ in (4.11).
From (4.7), (4.22) and (4.23) we can assert that

$$\frac{\| z_{i,\nu}|_{t_0}^{t} \|}{\| \nu|_{t_0}^{t} \|} - \frac{\alpha_i TC_\nu}{\| \nu|_{t_0}^{t} \|} \leq \Pi_i(t) \leq \frac{\| z_{i,\nu}|_{t_0}^{t} \|}{\| \nu|_{t_0}^{t} \|} + \frac{\alpha_i TC_\nu}{\| \nu|_{t_0}^{t} \|}. \tag{4.28}$$

Then

$$\begin{aligned} \Pi_i(t) &\leq \frac{\| z_{i,\nu}|_{t_0}^{t_0+KT-1} \| + \| z_{i,\nu}|_{t_0+KT}^{t} \|}{\| \nu|_{t_0}^{t} \|} + \frac{\alpha_i TC_\nu}{\| \nu|_{t_0}^{t} \|} \\ &\leq \frac{\| z_{i,\nu}|_{t_0}^{t_0+KT-1} \|}{\| \nu|_{t_0}^{t_0+KT-1} \|} + \frac{\| z_{i,\nu}|_{t_0+KT}^{t} \|}{\| \nu|_{t_0}^{t} \|} + \frac{\alpha_i TC_\nu}{\| \nu|_{t_0}^{t} \|} \\ &\leq \overline{\Pi}_i + \frac{\alpha_i TC_\nu}{\| \nu|_{t_0}^{t} \|} + \frac{\beta_i TC_\nu}{\| \nu|_{t_0}^{t} \|}, \end{aligned} \tag{4.29}$$

where the last inequality (4.29) follows from the fact that $\| z_{i,\nu}|_{t_0+KT}^{t} \|$ can be upper-bounded as in

$$\| z_{i,\nu}|_{t_0+KT}^{t} \| \leq \beta_i TC_\nu \tag{4.30}$$

for some nonnegative constant β_i.
Similarly,

$$\begin{aligned} \Pi_i(t) &\geq \frac{\| z_{i,\nu}|_{t_0}^{t_0+(K+1)T-1} \| - \| z_{i,\nu}|_{t+1}^{t_0+(K+1)T-1} \|}{\| \nu|_{t_0}^{t} \|} - \frac{\alpha_i TC_\nu}{\| \nu|_{t_0}^{t} \|} \\ &\geq \frac{\| z_{i,\nu}|_{t_0}^{t_0+(K+1)T-1} \|}{\| \nu|_{t_0}^{t_0+(K+1)T-1} \|} - \frac{\| z_{i,\nu}|_{t+1}^{t_0+(K+1)T-1} \|}{\| \nu|_{t_0}^{t} \|} - \frac{\alpha_i TC_\nu}{\| \nu|_{t_0}^{t} \|} \\ &\geq \overline{\Pi}_i - \frac{\alpha_i TC_\nu}{\| \nu|_{t_0}^{t} \|} - \frac{\beta_i TC_\nu}{\| \nu|_{t_0}^{t} \|}. \end{aligned} \tag{4.31}$$

The last inequality (4.31) follows from the fact that β_i can be chosen such that

$$\| z_{i,\nu}|_{t+1}^{t_0+(K+1)T-1} \| \leq \beta_i TC_\nu \tag{4.32}$$

holds.
Consequently,

$$|\Pi_i(t) - \overline{\Pi}_i| \leq \frac{(\alpha_i + \beta_i)TC_\nu}{\| \nu|_{t_0}^{t} \|}. \tag{4.33}$$

Eq. (4.13) then follows by defining $\lambda_i := (\alpha_i + \beta_i)$. □

Appendix: Proofs

Proof of Theorem 4.2.2

Let $\tilde{t}$ be a switching instant such that (4.14) holds, and let $\sigma(\tilde{t}+1)=\overline{\sigma}$. Notice that, since $\tilde{t}$ is a switching instant, we have $\Pi_{\overline{\sigma}}(\tilde{t}) \leq \Pi_i(\tilde{t})\,,\ \forall i \in \overleftarrow{N}$. Consider now a generic time instant $t > \tilde{t}$. Then

$$\begin{aligned}
\Pi_{\overline{\sigma}}(t) &\leq \overline{\Pi}_{\overline{\sigma}} + \frac{\lambda_{\overline{\sigma}} TC_\nu}{\| \nu|_{t_0}^t \|} \\
&\leq \Pi_{\overline{\sigma}}(\tilde{t}) + \frac{\lambda_{\overline{\sigma}} TC_\nu}{\| \nu|_{t_0}^t \|} + \frac{\lambda_{\overline{\sigma}} TC_\nu}{\| \nu|_{t_0}^{\tilde{t}} \|} \\
&\leq \Pi_i(\tilde{t}) + \frac{\lambda_{\overline{\sigma}} TC_\nu}{\| \nu|_{t_0}^t \|} + \frac{\lambda_{\overline{\sigma}} TC_\nu}{\| \nu|_{t_0}^{\tilde{t}} \|} \\
&\leq \overline{\Pi}_i + \frac{\lambda_{\overline{\sigma}} TC_\nu}{\| \nu|_{t_0}^t \|} + \frac{[\lambda_{\overline{\sigma}} + \lambda_i] TC_\nu}{\| \nu|_{t_0}^{\tilde{t}} \|} \\
&\leq \Pi_i(t) + \frac{[\lambda_{\overline{\sigma}} + \lambda_i] TC_\nu}{\| \nu|_{t_0}^t \|} + \frac{[\lambda_{\overline{\sigma}} + \lambda_i] TC_\nu}{\| \nu|_{t_0}^{\tilde{t}} \|} \\
&\leq \Pi_i(t) + \frac{2\overline{\lambda} TC_\nu}{\| \nu|_{t_0}^t \|} + \frac{2\overline{\lambda} TC_\nu}{\| \nu|_{t_0}^{\tilde{t}} \|}.
\end{aligned}$$

In view of (4.14), then both

$$\frac{2\overline{\lambda} TC_\nu}{\| \nu|_{t_0}^{\tilde{t}} \|} < \frac{h}{2} \qquad , \qquad \frac{2\overline{\lambda} TC_\nu}{\| \nu|_{t_0}^t \|} < \frac{h}{2}$$

hold. Consequently $\Pi_{\overline{\sigma}}(t) < \Pi_i(t) + h$ for any $i \in \overleftarrow{N}$ and, according to the HSL, the controller with index $\overline{\sigma}$ will never be removed from the feedback loop after $\tilde{t}$; thus no switching can occur after $\tilde{t}$. □

Proof of Proposition 4.2.1

The bound in (4.15) follows from the stability of $\Sigma_i(d)$. Specifically, the former case coincides with the bound established in (4.10) when a persistent memory is used. As for the case $t \geq t_0 + M_*$, with reference to the cost $\Pi_i(t)$ defined as in (4.7), we recall that $z_i(t)$ is the response of the system $\Sigma_i(d)$ to the input $\varepsilon(t)$. Then, considering $t - M_*$ as the initial time instant, we can decompose $z_i(k)$ at a time $k \geq t - M_*$ as

$$z_i(k) = z_{i,free}(k) + z_{i,forced}(k)\,, \quad \forall k \geq t - M_*$$

where $z_{i,free}(k)$ is the free response of $\Sigma_i(d)$ which depends on the initial conditions at time $t - M_*$, and $z_{i,forced}(k)$ is the forced response of $\Sigma_i(d)$ which depends on the input $\varepsilon(k)$ for

Appendix: Proofs

$k \geq t - M_*$. For the forced response, one has

$$\| z_{i,forced}|_{t-M_*}^{t} \| \leq \|\Sigma_i\|_\infty \| \varepsilon|_{t-M_*}^{t} \|$$

thanks to the stability of $\Sigma_i(d)$. As for the free response, consider any minimal realization of $\Sigma_i(d)$

$$\begin{aligned} x_i(t+1) &= A_i x_i(t) + B_i \varepsilon(t) && (4.34) \\ z_i(t) &= C_i x_i(t) + D_i \varepsilon(t) && (4.35) \end{aligned}$$

and let $x_i(t - M_*)$ be the vector of the initial conditions of $\Sigma_i(d)$ at time $t - M_*$. Then, since $z_{i,free}(k) = C_i A_i^{k-t+M_*} x_i(t - M_*)$ and $\Sigma_i(d)$ is stable, we can derive the bound

$$\| z_{i,free}|_{t-M_*}^{t} \|^2 \leq \bar{\delta}_i^2 \|x_i(t - M_*)\|^2$$

where $\bar{\delta}_i^2$ is a positive scalar which bounds $\|C_i\|^2 \sum_{k=0}^{M_*} \|A_i^k\|^2$. Recalling now that system (4.34)-(4.35) is run from time t_0 with null initial conditions, we can also obtain the bound

$$\|x_i(t - M_*)\| \leq \tilde{\delta}_i C_\nu$$

where C_ν is the peak of the signal $\varepsilon(t) = \nu(t)$ (recall that this equality holds for any $t \geq t_0$) and $\tilde{\delta}_i$ is the input-to-state peak-to-peak gain of system (4.34)-(4.35). Summing up, by defining $\delta_i = \bar{\delta}_i \tilde{\delta}_i$, we can obtain

$$\| z_{i,free}|_{t-M_*}^{t} \| \leq \delta_i C_\nu \tag{4.36}$$

and hence

$$\Pi_i(t) \leq \|\Sigma_i\|_\infty + \frac{\delta_i C_\nu}{\| \varepsilon|_{t-M_*}^{t} \|} .$$

The bound for $t \geq t_0$ in (4.15) then follows thanks to the fact that $\varepsilon(t) = \nu(t)$ for any $t \geq t_0$.

□

Proof of Lemma 4.2.2

Following considerations similar to the ones shown in the proof of Lemma 4.2.1, we can express $z_i|_{t-M_*}^{t}$ as

$$z_i|_{t-M_*}^{t} = z_{i,free}|_{t-M_*}^{t} + z_{i,\Sigma_i}|_{t-M_*}^{t} + z_{i,\nu}|_{t-M_*}^{t} , \tag{4.37}$$

where $z_{i,free}$ is as in the Proof of Proposition 4.2.1, thus obtaining

$$\Pi_i(t) \geq \frac{\| z_{i,\nu}|_{t-M_*}^t \|}{\| \nu|_{t-M_*}^t \|} - \frac{\alpha_i T C_\nu}{\| \nu|_{t-M_*}^t \|} - \frac{\delta_i C_\nu}{\| \nu|_{t-M_*}^t \|} \tag{4.38}$$

and

$$\Pi_i(t) \leq \frac{\| z_{i,\nu}|_{t-M_*}^t \|}{\| \nu|_{t-M_*}^t \|} + \frac{\alpha_i T C_\nu}{\| \nu|_{t-M_*}^t \|} + \frac{\delta_i C_\nu}{\| \nu|_{t-M_*}^t \|}\,, \tag{4.39}$$

with α_i a nonnegative constant as in (4.23), and δ_i a nonnegative constant as in (4.36). Then the proof follows the same reasoning as the one shown in the proof of Lemma 4.2.1. □

Proof of Theorem 4.2.3

Within the proof, we assume that $\lfloor M_*/T \rfloor \geq 1$, otherwise (4.20) obviously does not hold. Let $\overline{\tau} \in [t_1 + M_*\,,\, t_2)$ be a switching instant and let $\sigma(\overline{\tau}+1) = \overline{\sigma}$. Notice that, since $\overline{\tau}$ is a switching instant, then $\Pi_{\overline{\sigma}}(\overline{\tau}) \leq \Pi_i(\overline{\tau})$, $\forall i \in \overleftarrow{N}$. Further, let t be a generic time instant such that $t > \overline{\tau}$ and $t \in (t_1 + M_*\,,\, t_2]$. Then, by applying Lemma 4.2.2, a reasoning very close to the one shown in the proof of Theorem 4.2.2 yields

$$\begin{aligned}\Pi_{\overline{\sigma}}(t) &\leq \Pi_i(t) + \tfrac{2[\overline{\lambda}T+\overline{\delta}]C_\nu}{\| \nu|_{\overline{\tau}-M_*}^{\overline{\tau}} \|} + \tfrac{2[\overline{\lambda}T+\overline{\delta}]C_\nu}{\| \nu|_{t-M_*}^{t} \|} \\ &\leq \Pi_i(t) + \tfrac{2[\overline{\lambda}T+\overline{\delta}]C_\nu}{\lfloor \frac{M_*}{T} \rfloor \| s|_1^T \|} + \tfrac{2[\overline{\lambda}T+\overline{\delta}]C_\nu}{\lfloor \frac{M_*}{T} \rfloor \| s|_1^T \|}\,. \end{aligned} \tag{4.40}$$

Thus, if (4.20) holds, $\Pi_{\overline{\sigma}}(t) < \Pi_i(t) + h$ for any $i \in \overleftarrow{N}$ and, according to the HSL, the controller with index $\overline{\sigma}$ will not be removed from the feedback loop after $\overline{\tau}$ in the interval $[t_1 + M_*, t_2]$; thus no switching can occur after $\overline{\tau}$ in the interval $[t_1 + M_*, t_2]$. □

Chapter 5

Design of a switching controller with guaranteed stability

In the context of ASC techniques, a possible method for dealing with the problem of ensuring stability of the overall closed loop under arbitrary switching is to consider this requirement as one of the specifications within the synthesis of the controller family. In particular, the solution that we propose relies on sufficient conditions which can be expressed in terms of LMI constraints, and thus can be easily integrated in design techniques specifically focusing on the controller performance [18]. Further, the proposed approach allows one to adopt a simple multi-controller architecture by switching directly between the controllers belonging to the family $\mathscr{C}$, making the multi-controller structure independent of the plant model.

5.1 Stability requirement

The idea is based on classical results on the stability of switching systems; specifically, we exploit the well known fact that a sufficient condition ensuring stability of a switching system is the existence of a common quadratic Lyapunov function between the subsystems corresponding to the different possible configurations.

Before stating the main result supporting the proposed approach, it is useful to provide the following definition from [85], where we recall that [88] for a strictly positive

real (SPR) rational transfer matrix $H(d)$ the following properties hold: a) all elements of $H(d)$ are stable; b) $H(e^{-j\omega}) + H^\top(e^{j\omega}) > 0 \ \forall \omega \in [0,\, 2\pi]$.

Definition 5.1.1. Two matrices F and V in $\mathbb{R}^{m\times m}$, with m a positive integer, are called a strictly positive real pair (SPR-pair) if the transfer matrix $H(d)$ defined by the quadruple $(F, I, F-V, I)$, *i.e.*, $H(d) = d(F-V)(I-dF)^{-1} + I$, is SPR.

Then the following proposition can be stated [85], in which the symbol $\bigstar$ is introduced to denote a symmetric block.

Proposition 5.1.1. *Given F and V in $\mathbb{R}^{m\times m}$, if they are a SPR-pair, then they are both stable with a common Lyapunov matrix $Q > 0$ and the following inequalities are equivalent:*

$$\begin{bmatrix} F^\top QF - Q & \bigstar \\ QF - F + V & Q - 2I \end{bmatrix} < 0 \tag{5.1}$$

$$\begin{bmatrix} V^\top QV - Q & \bigstar \\ QV - V + F & Q - 2I \end{bmatrix} < 0\,. \tag{5.2}$$

The equivalence between (5.1) and (5.2) can be derived for example by considering the matrix

$$L = \begin{bmatrix} I & 0 \\ V - F & I \end{bmatrix}.$$

In fact, (5.2) is obtained from (5.1) by pre-multiplying by $L^\top$ and post-multiplying by L (a similar consideration is suggested also in [36]).

Let $(A_{C_i}, B_{C_i}, C_{C_i}, D_{C_i})$ be stabilizable and detectable realizations of $C_i(d)$ having the same order for any $i \in \overleftarrow{N}$ (for example, when all the $C_i(d)$ have the same order, controllable/observable canonical forms can be used). Further, let (A_P, B_P, C_P) be a minimal realization of $P(d)$. Then the i-th closed-loop state matrix is defined as

$$A_{CL,i} = \begin{bmatrix} A_P - B_P D_{C_i} C_P & B_P C_{C_i} \\ -B_{C_i} C_P & A_{C_i} \end{bmatrix}. \tag{5.3}$$

The following result can now be presented.

Theorem 5.1.1. *Let $A_{CL,i}$, $i \in \overleftarrow{N}$, be the closed-loop state matrices, defined as in (5.3). Further, let M_i, $i \in \overleftarrow{N}$, be stable matrices, and T a non-singular matrix, and assume that M_i and $T^{-1}A_{CL,i}T$ are SPR-pair $\forall i \in \overleftarrow{N}$. Finally, let the multi-controller be implemented by means of the shared-state architecture*

$$\begin{aligned} x_C(t+1) &= A_{C_{\sigma(t)}} x_C(t) - B_{C_{\sigma(t)}} y(t) \\ u(t) &= C_{C_{\sigma(t)}} x_C(t) - D_{C_{\sigma(t)}} y(t)\,, \end{aligned} \tag{5.4}$$

with x_C the controller state. Then, if there exists a symmetric positive-definite matrix G such that

$$\left[\begin{array}{cc} M_i^\top G M_i - G & \bigstar \\ G M_i - M_i + T^{-1} A_{CL,i} T & G - 2I \end{array} \right] < 0\,, \quad \forall i \in \overleftarrow{N}\,, \tag{5.5}$$

the overall closed-loop switching system is exponentially stable under arbitrary switching.

Proof: see the Appendix. □

Remark 5.1.1. It it is worth underlining that the matrix T must be the same for all the controllers in $\mathscr{C}$; in fact, this follows clearly from the proof of Theorem 5.1.1 , and specifically from (5.31)-(5.32).

The overall control scheme showing the multi-controller implementation is represented in Fig. 5.1. Consider now a set of linearly-parametrized controllers with transfer functions

$$C_i(d) = \frac{S_i(d)}{R_i(d)} \tag{5.6}$$

expressed in the form

$$C_i(d) = C(d, \rho_i) = \frac{S(d, \rho_i)}{R_i(d)}\,, \quad \forall i \in \overleftarrow{N}\,, \tag{5.7}$$

where the polynomial $S_i(d) := S_i(d, \rho_i)$ is an affine function of an n_ρ-dimensional parameter vector ρ_i, with n_ρ a positive integer, and $R_i(d)$ is a fixed polynomial for each $i \in \overleftarrow{N}$; further, $S_i(d)$ and $R_i(d)$ have strictly Schur g.c.d.

Thanks to the controller parametrization (5.7), if, for example, we realize each $C_i(d)$ in controllable canonical form, then the matrices $C_{C_i} = C_C(\rho_i)$ and $D_{C_i} = D_C(\rho_i)$ are affine functions of the parameter vector ρ_i, while the matrices A_{C_i} and B_{C_i} are constant. This in turn implies that each matrix $A_{CL,i} = A_{CL}(\rho_i)$ depends affinely on ρ_i; thus each inequality (5.5) becomes an LMI with respect to the unknowns G and ρ_i.

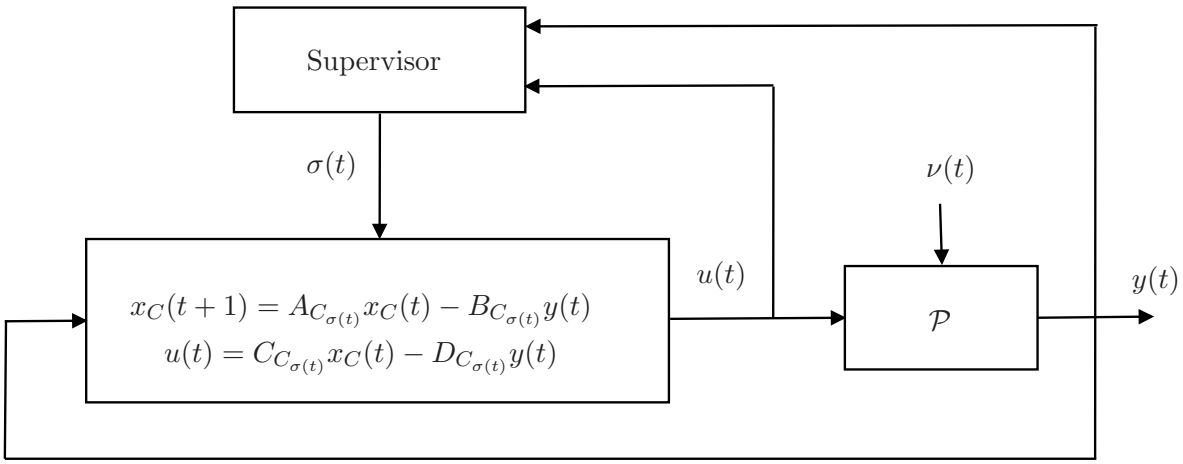

Figure 5.1: Adaptive Switching Control scheme.

5.1.1 Choice of M_i and T

The choice of the matrices M_i and T plays an important role within the proposed method. Following [85], the solution that we adopt relates this choice to the synthesis of a set of N initial fixed-order stabilizing controllers, which we assume to have been synthesized according to any design technique (a possible synthesis approach that can be used is the one described in [55]).

Let $\overline{A}_{CL,i}$ be the closed-loop state matrix related to the i-th controller. Then, the matrices M_i and T can be determined by solving the following feasibility problem

$$\begin{bmatrix} \overline{A}_{CL,i}^{\top} G_{i,T} \overline{A}_{CL,i} - G_{i,T} & \bigstar \\ G_{i,T}\overline{A}_{CL,i} - X\overline{A}_{CL,i} + M_{i,T} & G_{i,T} - 2X \end{bmatrix} < 0\,, \quad \forall i \in \overleftarrow{N} \tag{5.8}$$

$$G_{i,T} = G_{i,T}^{\top} > 0\,, \quad \forall i \in \overleftarrow{N}\,, \tag{5.9}$$

with respect to the unknowns $G_{i,T}$, X, $M_{i,T}$, where $M_{i,T} := T^{-\top} M_i T^{-1}$, $G_{i,T} := T^{-\top} G_i T^{-1}$, $X := T^{-\top} T^{-1}$ (the notation $T^{-\top} := (T^{\top})^{-1}$ is adopted). Thus

$$T = (chol(X))^{-1} \tag{5.10}$$

$$M_i = T^{\top} M_{i,T} T\,, \tag{5.11}$$

where for example the Cholesky factorization, denoted by *chol*, can be used to compute T. In practice, by solving the feasibility problem (5.8)-(5.9), we aim at finding matrices M_i

and T such that M_i and $T^{-1}\overline{A}_{CL,i}T$, $\forall i \in \overleftarrow{N}$, are a SPR-pair, *i.e.*, the SPR-pair property involving M_i and T holds with respect to the initial controllers.

5.2 Performance-oriented design

In this section we will discuss a design technique aiming at providing fixed-order controllers able to attenuate the effects of a disturbance $\nu(t)$ on the output $y(t)$ (recall (4.1)).

The performance criterion, for each $i \in \overleftarrow{N}$, can be defined as

$$\left\| W_{1,i} \frac{R_i}{\chi_i} \right\|_\infty < 1 \,, \tag{5.12}$$

where $W_{1,i}(d)$ is the transfer function of a performance weighting filter for the controller $\mathcal{C}_i$. As pointed out in Chapter 4, $R_i(d)/\chi_i(d)$ represents the disturbance-to-output transfer function of $(\mathcal{P}/\mathcal{C}_i)$, where $\chi_i(d)$ is the characteristic polynomial of $(\mathcal{P}/\mathcal{C}_i)$, with $(\mathcal{P}/\mathcal{C}_i)$ defined as the closed-loop system involving the feedback interconnection of $\mathcal{P}$ with $\mathcal{C}_i$.

Remark 5.2.1. The choice of the weights $W_{1,i}(d)$, $i \in \overleftarrow{N}$, can be related to the a-priori available information on the disturbance characteristics (see for example [54]). For example, let the model related to the disturbance ν depend on an uncertain parameter vector θ, with θ belonging to an uncertainty set Θ. We assume that Θ is such that the task of providing a good level of attenuation of the disturbance cannot be managed by a single robust controller. A possible solution is then to divide the set Θ into N subsets $\Theta_1, \Theta_2, \cdots, \Theta_N$, and to synthesize the controllers $\mathcal{C}_i$, $i \in \overleftarrow{N}$, with each $\mathcal{C}_i$ exhibiting desired attenuation capabilities within a specific subregion Θ_i. If we denote by $\psi(\omega, \theta)$, $\theta \in \Theta_i$, the power spectral density of the disturbance ν in the subregion Θ_i, then $W_i(d)$ could be chosen for example such that

$$\psi(\omega, \theta) \leq |W_{1,i}(e^{-j\omega})|^2 \;\; \forall \theta \in \Theta_i \,. \tag{5.13}$$

Another possible way of defining $W_{1,i}(d)$ is to consider a grid of N values $\theta_1, \theta_2, \cdots, \theta_N$ of θ in Θ, and to address the performance problem expressed by (5.12) only in the correspondence of these values. In this case, we could define $W_{1,i}(d)$ such that $W_{i,1}(e^{-j\omega})$ is a spectral factor of $\psi(\omega, \theta_i)$. Further, if a data series of the disturbance is available for N operating conditions, then each $W_{i,1}(e^{-j\omega})$ can be chosen so as to match, as closely as possible, the frequency profile which can be extracted from the data.

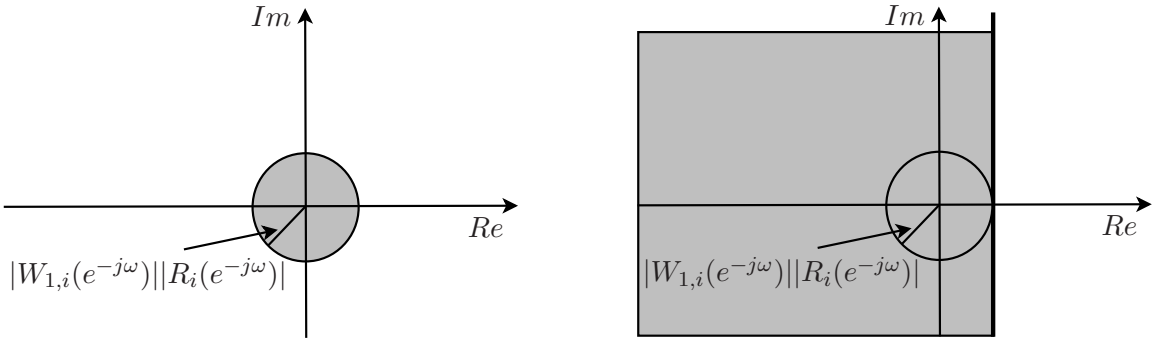

Figure 5.2: Graphical interpretation of condition (5.15) on the left-hand side and its approximation (5.16) on the right-hand side, respectively. In both cases, $\chi_i(e^{-j\omega})$ must lie outside the grey region.

Notice that criterion (5.12) is in general non-convex due to the dependence of χ_i on the parameter vector ρ_i. Nevertheless, it can be linearized by resorting to simple considerations. To this end, let us rewrite (5.12) as

$$\left| W_{1,i}(e^{-j\omega}) \, \frac{R_i(e^{-j\omega})}{\chi_i(e^{-j\omega})} \right| < 1 \,, \quad \forall \omega \,, \tag{5.14}$$

which means

$$\left| W_{1,i}(e^{-j\omega}) \right| \, \left| R_i(e^{-j\omega}) \right| < \left| \chi_i(e^{-j\omega}) \right| \,, \quad \forall \omega \,. \tag{5.15}$$

By recalling that, for a complex number x, $Re\{x\} \leq |x|$, where $|x|$ is the modulus of x, it is possible to assert that if

$$\left| W_{1,i}(e^{-j\omega}) \right| \, \left| R_i(e^{-j\omega}) \right| < Re\{A(e^{-j\omega})R_i(e^{-j\omega}) + B(e^{-j\omega})S(e^{-j\omega}, \rho_i)\} \,, \quad \forall \omega \tag{5.16}$$

holds, then (5.15) is ensured. The graphical interpretation of (5.15) and the approximation (5.16), which is affine in the parameter vector ρ_i, can be explained with reference to Fig. 5.2. If a circle with center at the origin and radius $\left| W_{1,i}(e^{-j\omega}) \right| \, \left| R_i(e^{-j\omega}) \right|$ is considered in the complex plane, then (5.15) requires that $\chi_i(e^{-j\omega})$, for all ω, lies outside that circle. On the other hand, (5.16) imposes that $\chi_i(e^{-j\omega})$, for all ω, lies on the right-hand side with respect to a line which is tangent to the circle and perpendicular to the real positive semi-axis, as depicted in Fig. 5.2.

Further, we underline that the performance criterion expressed by (5.12) can be improved by taking into account an upper bound γ on the H_∞ norm, thus leading to the following optimization problem to be solved:

$$\min_{\gamma,\rho_i} \gamma \tag{5.17}$$

s.t.

$$\left|W_{1,i}(e^{-j\omega})\right| \left|R_i(e^{-j\omega})\right| < \gamma \, Re\{A(e^{-j\omega})R_i(e^{-j\omega}) + B(e^{-j\omega})S(e^{-j\omega},\rho_i)\}\,, \quad \forall\omega\,. \tag{5.18}$$

By adopting the bisection algorithm, thus fixing the value of γ at each step, the problem in (5.17)-(5.18) is a linear programming problem.

A final remark on the synthesis approach described in this section regards the problem of dealing with the infinite number of constraints in (5.18). A practical solution is to impose the constraints only in the correspondence of a finite number of frequencies $\{\omega_1, \omega_2, \cdots, \omega_{\tilde{K}}\}$; accordingly, we define the set $\Omega_{\tilde{K}} := \{\omega_1, \omega_2, \cdots, \omega_{\tilde{K}}\}$. Clearly, the choice of $\tilde{K}$ should be such that both the approximation in the frequency domain is sufficiently accurate, and the problem has a manageable computational burden. Depending on the specific context of application, the $\tilde{K}$ frequencies can be selected by means of either a random or a deterministic approach [55].

5.2.1 The proposed design algorithm

The design algorithm that we propose integrates the constraints introduced in Section 5.1 within the synthesis method described in Section 5.2 and provides a family of controllers guaranteeing the stability of the overall closed-loop switching system and good attenuation capabilities in the presence of a disturbance with unknown and possibly time-varying characteristics.

Algorithm 5.2.1

Step 0 - Initialization. Define the set $\Omega_{\tilde{K}}$. For each $i \in \overleftarrow{N}$, define: the length of the parameter vector ρ_i; the denominator $R_i(d)$ (and compute its frequency response $R_i(e^{-j\omega})$); the weight $W_{1,i}(e^{-j\omega})$ for the sensitivity function.

Step 1. Compute N initial stabilizing controllers accounting for the performance requirement only (for example, by means of the technique proposed in [55]).

Step 2. Compute stabilizable and detectable realizations $(\overline{A}_{C_i}, \overline{B}_{C_i}, \overline{C}_{C_i}, \overline{D}_{C_i})$ having the same order for all the initial controllers (for example, in controllable canonical form); compute a minimal realization of the plant (A_P, B_P, C_P).

Step 3. Compute the state matrix of the closed-loop system on the basis of the state-space realizations of the plant and of the i-th initial controller for all $i \in \overleftarrow{N}$:

$$\overline{A}_{CL,i} = \begin{bmatrix} A_P - B_P \overline{D}_{C_i} C_P & B_P \overline{C}_{C_i} \\ -\overline{B}_{C_i} C_P & \overline{A}_{C_i} \end{bmatrix} . \tag{5.19}$$

Step 4. Solve the feasibility problem

$$\begin{bmatrix} \overline{A}_{CL,i}^\top G_{i,T} \overline{A}_{CL,i} - G_{i,T} & \bigstar \\ G_{i,T} \overline{A}_{CL,i} - X \overline{A}_{CL,i} + M_{i,T} & G_{i,T} - 2X \end{bmatrix} < 0 , \quad \forall i \in \overleftarrow{N} \tag{5.20}$$

$$G_{i,T} = G_{i,T}^\top > 0 , \quad \forall i \in \overleftarrow{N} , \tag{5.21}$$

with respect to the unknowns $M_{i,T}$, $G_{i,T}$, X (defined as in Section 5.1.1), and set

$$T = (chol(X))^{-1} \tag{5.22}$$

$$M_i = T^\top M_{i,T} T . \tag{5.23}$$

Step 5. Consider a set of controllers having transfer functions $C(d, \rho_i), i \in \overleftarrow{N}$, depending on a parameter vector ρ_i, and compute stabilizable and detectable state-space realizations $(A_{C_i}, B_{C_i}, C_{C_i}, D_{C_i})$ having the same order for all of them (for example, in controllable canonical form); compute the corresponding closed-loop state matrices

$$A_{CL}(\rho_i) = \begin{bmatrix} A_P - B_P D_{C_i} C_P & B_P C_{C_i} \\ -B_{C_i} C_P & A_{C_i} \end{bmatrix} . \tag{5.24}$$

Step 6. Solve the optimization problem

$$\min_{\gamma, \rho_i, G} \gamma \tag{5.25}$$

s.t.

$$\left|W_{1,i}(e^{-j\omega})\right| \left|R_i(e^{-j\omega})\right| < \gamma \, Re\{A(e^{-j\omega}) R_i(e^{-j\omega}) + B(e^{-j\omega}) S(e^{-j\omega}, \rho_i)\} , \quad \forall \omega \in \Omega_{\tilde{K}} , \; \forall i \in \overleftarrow{N} ,$$

$$\begin{bmatrix} M_i^\top G M_i - G & \bigstar \\ G M_i - M_i + T^{-1} A_{CL}(\rho_i) T & G - 2I \end{bmatrix} < 0 , \quad \forall i \in \overleftarrow{N} \tag{5.26}$$

$$G = G^\top > 0 . \tag{5.27}$$

Step 7. Compute the set of controllers on the basis of the vectors $\hat{\rho}_i$ as

$$C_i(d) = \frac{S(d, \hat{\rho}_i)}{R_i(d)}\,, \tag{5.28}$$

where $\hat{\rho}_i$ is solution to the problem (5.25)-(5.27).

Remark 5.2.2. The method described in this chapter ensures the stability of the overall closed-loop system under arbitrary switching, provided that a feasible solution can be obtained from **Algorithm 5.2.1**. However, it is to be pointed out that the optimization problem in **Step 6** is not guaranteed to provide a feasible solution. An interesting topic for future research, as indicated within the concluding remarks of this work, could be that of finding a more suitable formulation of the problem accounting for stability within the synthesis step and always ensuring the existence of a feasible solution.

Remark 5.2.3. A design method based on linear or convex constraints expressed in the frequency-domain has been proposed in [55], with the aim of synthesizing a robust fixed-order controller for a SISO LTI plant represented by non-parametric models. This technique, which can be used for the synthesis of the initial stabilizing controllers in **Step 1** of **Algorithm 5.2.1**, has been exploited in [54] in the context of the attenuation of uncertain and time-varying narrow band disturbances by means of a gain-scheduling scheme. In fact, the method of [55] is well suited to dealing with the context of disturbances described by uncertain models (for example, when only empirical estimates of the disturbance spectra are available); further, it addresses the performance problem by means of a convex optimization problem. This technique relies on the idea of linearizing the performance criterion around a desired open-loop transfer function $L_d(d)$, reflecting the open-loop behavior corresponding to a desired controller $C_d(d)$; this turns out to be useful also to provide a stability condition for the closed-loop system. However, in our framework, differently from this approach, the stability of each closed-loop system is ensured by the stability of the overall switching system, addressed by means of the constraints discussed in Section 5.1; this avoids the necessity of relying on desired open-loop transfer functions related to the controllers to be synthesized.

5.A Appendix: Proofs

Proof of Theorem 5.1.1. From classical results on the stability of switching systems it is possible to assert that, if a common quadratic Lyapunov matrix exists for the closed-loop systems with state matrices $A_{CL,i}$ defined in (5.3), this guarantees the stability of the overall closed-loop switching system. The result stated in Theorem 5.1.1 then follows thanks to the fact that M_i and $T^{-1}A_{CL,i}T$ are SPR-pair $\forall i \in \overleftarrow{N}$, and recalling the equivalence between (5.1) and (5.2). This can be proved by following the reasoning explained below.
If

$$\left[\begin{array}{cc} M_i^\top G M_i - G & \bigstar \\ G M_i - M_i + T^{-1}A_{CL,i}T & G - 2I \end{array} \right] < 0\,, \quad \forall i \in \overleftarrow{N}\ , \tag{5.29}$$

holds, then

$$\left[\begin{array}{cc} (T^{-1}A_{CL,i}T)^\top G (T^{-1}A_{CL,i}T) - G & \bigstar \\ G(T^{-1}A_{CL,i}T) - (T^{-1}A_{CL,i}T) + M_i & G - 2I \end{array} \right] < 0\,, \quad \forall i \in \overleftarrow{N}\,, \tag{5.30}$$

holds as well. By multiplying by $diag(T^{-\top}, T^{-\top})$ on the left (with $T^{-\top} := (T^\top)^{-1}$) and by $diag(T^{-1}, T^{-1})$ on the right, from (5.30) one obtains

$$\left[\begin{array}{cc} A_{CL,i}^\top T^{-\top} G T^{-1} A_{CL,i} - T^{-\top} G T^{-1} & \bigstar \\ T^{-\top} G T^{-1} A_{CL,i} + T^{-\top} M_i T^{-1} - T^{-\top} T^{-1} A_{CL,i} & T^{-\top} G T^{-1} - 2T^{-T} T^{-1} \end{array} \right] < 0\,, \quad \forall i \in \overleftarrow{N}\,. \tag{5.31}$$

Thus from (5.31) it is possible to assert that

$$A_{CL,i}^\top (T^{-\top} G T^{-1}) A_{CL,i} - (T^{-\top} G T^{-1}) < 0\,, \quad \forall i \in \overleftarrow{N}\,, \tag{5.32}$$

which means that the matrices $A_{CL,i}$, $i \in \overleftarrow{N}$, have a common Lyapunov matrix $(T^{-\top} G T^{-1})$. Similar considerations are suggested also in [85]. Then, if the multi-controller is implemented as in (5.4), then the closed-loop state matrix of the overall switching system has the form

$$A_{CL,\sigma(t)} = \left[\begin{array}{cc} A_P - B_P D_{C_{\sigma(t)}} C_P & B_P C_{C_{\sigma(t)}} \\ -B_{C_{\sigma(t)}} C_P & A_{C_{\sigma(t)}} \end{array} \right]. \tag{5.33}$$

Thus, thanks to (5.32), it is possible to assert that the overall closed-loop switching system is exponentially stable for any switching signal σ. □

Chapter 6

Switching between the Youla parameters

The approach proposed in Chapter 5 provides a family of controllers to be used within an adaptive switching control scheme and ensuring by construction the stability of the overall switching closed-loop system. While such a method allows the complexity of the multi-controller to be independent of the plant complexity, on the other hand there is not a perfect independence between the synthesis step and the switching mechanism. Further, the design of the N controllers is unavoidably constrained by the necessity of admitting a common quadratic Lyapunov function for all the potential closed-loop systems. In order to recover full modularity of the switching scheme, the stability requirement can be addressed by taking special care on the implementation of the multi-controller [19, 21, 20]. Guidelines for the implementation of a multi-controller able to preserve stability for any arbitrary switching sequence when switching between stabilizing controllers are presented in [47] for the continuous-time case. In this chapter, we will briefly discuss how similar considerations hold also for the discrete-time case, and we will finally focus on a specific implementation which is less general but requires reduced efforts.

6.1 Switching controller implementation

Following the reasoning shown in [47], we adopt the Youla-Kucera parametrization for the controllers in $\mathscr{C}$. For this purpose, consider a controller $\mathcal{C}_0$ with transfer function

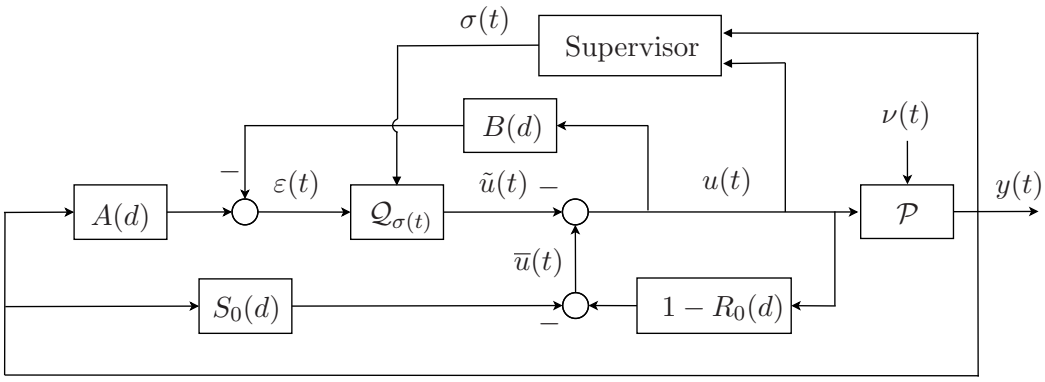

Figure 6.1: Youla-Kucera parametrization: switching between the $\mathcal{Q}_i$.

$C_0(d) = S_0(d)/R_0(d)$ satisfying the Bezout identity

$$A(d)R_0(d) + B(d)S_0(d) = 1\,. \tag{6.1}$$

Then, as well known, each transfer function $C_i(d)$, $i \in \overleftarrow{N}$, can be expressed as

$$C_i(d) = \frac{S_0(d)D_i(d) + A(d)N_i(d)}{R_0(d)D_i(d) - B(d)N_i(d)} \tag{6.2}$$

where

$$Q_i(d) = \frac{N_i(d)}{D_i(d)} \tag{6.3}$$

is the transfer function of the Youla parameter $\mathcal{Q}_i$ corresponding to $\mathcal{C}_i$. Recall also that for any stabilizing controller the corresponding Youla parameter turns out to be stable. Hereafter, we will refer to $\mathscr{Q}$ as the finite family composed of $\{\mathcal{Q}_i,\ i \in \overleftarrow{N}\}$.

Remark 6.1.1. We note that, in terms of the Youla parameter $\mathcal{Q}_i$, the weighted mixed-sensitivity $\Sigma_i(d)$ in (4.4) takes the form

$$\Sigma_i(d) = \frac{1}{D_i(d)} \begin{bmatrix} R_0(d)D_i(d) - B(d)N_i(d) \\ -\eta(S_0(d)D_i(d) + A(d)N_i(d)) \end{bmatrix}.$$

Hence it can be seen that the dependence on the numerator $N_i(d)$ is affine, while the denominator $D_i(d)$ coincides with the closed-loop characteristic polynomial.

The proposed multi-controller implementation is based on the idea of switching between the Youla parameters as depicted in Fig. 6.1. Accordingly the control input $u(t)$

is generated as

$$u(t) = \overline{u}(t) - \tilde{u}(t)\,, \tag{6.4}$$

where $\tilde{u}(t)$ is the output of the switching system $\mathcal{Q}_{\sigma(t)}$ having input $\varepsilon(t)$, and the signals $\overline{u}(t)$ and $\varepsilon(t)$ are obtained as

$$\begin{bmatrix} \overline{u}(t) \\ \varepsilon(t) \end{bmatrix} = \begin{bmatrix} (1 - R_0(d)) & -S_0(d) \\ -B(d) & A(d) \end{bmatrix} \begin{bmatrix} u(t) \\ y(t) \end{bmatrix}. \tag{6.5}$$

As for the switching system $\mathcal{Q}_{\sigma(t)}$, let m be the largest among the orders of the transfer functions of $\mathcal{Q}_i$ in $\mathscr{Q}$ and let us consider, for any $i \in \overleftarrow{N}$, a stabilizable and detectable m-dimensional realization $\{\overline{A}_i, \overline{B}_i, \overline{C}_i, \overline{D}_i\}$ of the transfer function $Q_i(d)$. Then, $\mathcal{Q}_{\sigma(t)}$ takes the form

$$\mathcal{Q}_{\sigma(t)} : \begin{cases} \zeta(t+1) = \overline{A}_{\sigma(t)}\zeta(t) + \overline{B}_{\sigma(t)}\varepsilon(t) \\ \tilde{u}(t) = \overline{C}_{\sigma(t)}\zeta(t) + \overline{D}_{\sigma(t)}\varepsilon(t) \end{cases}. \tag{6.6}$$

Notice that each $\overline{A}_i$ is asymptotically stable since the Youla parameter $Q_i(d)$ is stable by construction.

The following result can now be stated.

Theorem 6.1.1. *Let the multi-controller $\mathcal{C}_{\sigma(t)}$ be implemented as in (6.4)-(6.6). Then, when $\sigma(t) = i$, the frozen-time transfer function between $y(t)$ and $u(t)$ coincides with $-C_i(d)$. If in addition the matrices $\overline{A}_i$, $i \in \overleftarrow{N}$, admit a common quadratic Lyapunov function, i.e., there exists a symmetric positive definite matrix G such that*

$$\overline{A}_i^\top G \overline{A}_i - G < 0, \quad i \in \overleftarrow{N}\,, \tag{6.7}$$

then the switching system $(\mathcal{P}/\mathcal{C}_{\sigma(t)})$, made up of the feedback interconnection of $\mathcal{P}$ and $\mathcal{C}_{\sigma(t)}$, is internally stable for any switching signal σ.

Proof: see the Appendix. □

In the above theorem, by saying that $(\mathcal{P}/\mathcal{C}_{\sigma(t)})$ is internally stable we mean that all the signals in the system remain bounded for any bounded disturbance ν. In view of Theorem 6.1.1, it can be seen that, in order to ensure stability, it is sufficient to choose the realizations $\{\overline{A}_i, \overline{B}_i, \overline{C}_i, \overline{D}_i\}$, $i \in \overleftarrow{N}$, so that condition (6.7) holds. The following lemma shows that this is always possible.

Lemma 6.1.1. *Given any finite set of asymptotically stable transfer functions $Q_i(d)$ related to a family $\mathscr{Q} = \{\mathcal{Q}_i,\, i \in \overleftarrow{N}\}$ and any symmetric positive definite matrix G (whose order m is the largest order of the transfer functions of the systems in $\mathscr{Q}$), there exist stabilizable and detectable m-dimensional realizations $\{\overline{A}_i, \overline{B}_i, \overline{C}_i, \overline{D}_i\}$ for each $Q_i(d)$ such that (6.7) holds.*

Proof: see the Appendix. □

Remark 6.1.2. When the plant to be controlled is stable, *i.e.* $P(d)$ is a stable transfer function, each stabilizing controller in $\mathscr{C}$ can be expressed as:

$$C_i(d) = \frac{A(d)N_i(d)}{A(d)D_i(d) - B(d)N_i(d)}\,, \tag{6.8}$$

and the control input u can be computed as the output of the switching system $\mathcal{Q}_{\sigma(t)}$ having as input a signal $\tilde{e}$ computed as

$$\tilde{e}(t) = \frac{B(d)}{A(d)}u(t) - y(t)\,. \tag{6.9}$$

By following the same line of reasoning as the one shown in the proof of Theorem 6.1.1, stability of the overall feedback system holds provided that the disturbance is bounded and that the multi-controller is implemented so as to satisfy (6.6), (6.7), (6.9).

6.1.1 A simplified implementation

As pointed out in Remark 6.1.1, the weighted mixed-sensitivity $\Sigma_i(d)$ depends affinely on the numerator $N_i(d)$ of the Youla parameter. With this respect, if each $N_i(d)$ is expressed as an affine function of a parameter vector ρ_i, by fixing the denominator $D_i(d)$ of each Youla parameter it is possible to formulate the control design problem as a convex optimization problem. In fact, the choice of a specific structure for the Youla parameter in order to simplify a controller synthesis algorithm or make it enjoy some properties is quite a common practice (see for example [63] or [87] in Section 4.4 and the references therein). Clearly, fixing each $D_i(d)$ can limit the achievable performance; however, it is to be pointed out that, by increasing the number of free parameters in the numerator, it is possible to approximate any finite-order stable transfer function with arbitrary accuracy [49]. Specifically, a convenient choice could be that all the Youla parameters $Q_i(d)$ associated

with the controllers $\mathcal{C}_i \in \mathscr{C}$ share the same denominator, i.e.,

$$Q_i(d) = \frac{N_i(d)}{D(d)} \tag{6.10}$$

with $D(d)$ a given stable polynomial. For example, the characteristic polynomial $D(d)$ can be chosen so as to ensure a desired transient behavior, whereas each numerator $N_i(d)$ can be designed by optimizing a H_2 or H_∞ performance objective defined with respect to a certain disturbance frequency profile (different for each $i \in \overleftarrow{N}$).

The choice of a common denominator $D(d)$ for all the Youla parameters simplifies also the multi-controller architecture and the stability analysis of the closed-loop system.

In fact, in this case it is not necessary to look for realizations $\{\overline{A}_i, \overline{B}_i, \overline{C}_i, \overline{D}_i\}$ satisfying condition (6.7), since $\mathcal{Q}_{\sigma(t)}$ can be simply implemented through the difference equation

$$\mathcal{Q}_{\sigma(t)} : D(d)\tilde{u}(t) = N_{\sigma(t)}(d)\varepsilon(t)\,, \tag{6.11}$$

with $\varepsilon(t)$ defined as in (6.5), from which the stability of the overall switched system follows, as stated in the following result.

Proposition 6.1.1. *Let the multi-controller $\mathcal{C}_{\sigma(t)}$ be implemented as in (6.4), (6.5), (6.11). Then the switching system $(\mathcal{P}/\mathcal{C}_{\sigma(t)})$ is internally stable for any switching signal σ.*

Proof: see the Appendix. □

If the plant transfer function $P(d)$ is stable, the architecture can be further simplified by taking

$$\mathcal{Q}_{\sigma(t)} : D(d)u(t) = N_{\sigma(t)}(d)\tilde{e}(t) \tag{6.12}$$

with $\tilde{e}(t)$ as in (6.9).

In the next sections, we will show simulation results obtained on the active suspension system described in Chapter 2 and the adaptive optics system described in Chapter 1. In both contexts, the multi-controller architecture is implemented as described in Section 6.1.1; since both the plants are stable, $\mathcal{Q}_{\sigma(t)}$ is as in (6.12). Specifically, with respect to the results obtained within the adaptive optics application, a detailed presentation of the synthesis algorithm, involving the employment of the Youla parametrization and the optimization of the Youla parameter, will be provided in Appendix 6.B; controllers synthesized by means of this technique have been tested on an adaptive optics simulator, and very

Controller	Frequency range
$\mathcal{C}_1$	$\Omega_1 = [0,\, 4)\, Hz$
$\mathcal{C}_2$	$\Omega_2 = [4,\, 6.5)\, Hz$
$\mathcal{C}_3$	$\Omega_3 = [6.5,\, 8.5)\, Hz$
$\mathcal{C}_4$	$\Omega_4 = [8.5,\, 10)\, Hz$

Table 6.1: Active suspension system. Frequency ranges Ω_i , $i = 1, 2, 3, 4$.

satisfactory results have been achieved [2] (see also [3] for an extension of the algorithm accounting for robustness with respect to variations of the turbulence and vibration profiles in accordance with the operating conditions of the telescope).

6.2 Disturbance attenuation in an active suspension application

In this section we present simulation tests related to the active suspension system for a quarter-car model, introduced in Chapter 2 and represented in Fig. 2.2. The system is stable and can be described by means of the model (2.7); the aim is that of regulating the displacement y_1 (with respect to its equilibrium point) around zero in the presence of the road excitation n. The discretized model of the system is of the form (4.1), where y is represented by the displacement y_1, u is represented by the force F, and ν is replaced by a moving average of samples of the disturbance n. The considered parameters are summarized in Table 2.1.

We first suppose that the disturbance n is a sinusoidal signal with 0.1 m magnitude and unknown frequency f belonging to the range $\Omega = [0,\, 10]\, Hz$. We subdivide the range Ω into four subsets $\Omega_i \subset \Omega$, $i = 1, 2, 3, 4$, and synthesize four controllers $\mathcal{C}_i$, $i = 1, 2, 3, 4$, with each $\mathcal{C}_i$ exhibiting a satisfactory attenuation level in the subset Ω_i (see Table 6.1). The Youla parameter related to each controller has the form (6.10) and the switching system is implemented as shown in (6.12). The common denominator $D(d)$ is chosen such that all the controllers exhibit a satisfactory transient behavior; each numerator $N_i(d)$ is expressed as an affine function of a parameter vector ρ_i. Specifically, $D(d) = 1 - 0.9\, d$, while $N_i(d) = \varphi^\top(d)\rho_i$, with $\varphi(d) = [1, d, \cdots, d^{10}]^\top$. The design procedure of each controller

involves the solution of an optimization problem, which can be formulated as

$$\min_{\gamma,\rho_i} \gamma \tag{6.13}$$

s.t.

$$|\overline{\Sigma}_{i,1}(e^{-j\omega},\rho_i)|^2 < \gamma\,, \quad \forall\omega\in\Omega_i\,, \tag{6.14}$$

$$|\overline{\Sigma}_{i,2}(e^{-j\omega},\rho_i)|^2 < \delta\,, \quad \forall\omega\in\Omega_i\,, \tag{6.15}$$

where, for each $i \in \overleftarrow{N}$, $\overline{\Sigma}_{i,1}(d,\rho_i)$ is the transfer function from the signal $\overline{n}$, computed as in (2.12), to the output y_1, while $\overline{\Sigma}_{i,2}(d,\rho_i)$ is the transfer function from $\overline{n}$ to the control input F; further, δ is a design parameter. Specifically,

$$\overline{\Sigma}_{i,1}(d,\rho_i) = 1 - P(d)Q_i(d) = 1 - \tfrac{B(d)}{A(d)}\,\tfrac{\varphi^\top(d)\rho_i}{D(d)}\,, \tag{6.16}$$

$$\overline{\Sigma}_{i,2}(d,\rho_i) = Q_i(d) = \tfrac{\varphi^\top(d)\rho_i}{D(d)}\,. \tag{6.17}$$

Since both $\overline{\Sigma}_{i,1}$ and $\overline{\Sigma}_{i,2}$ depend affinely on the parameter vector ρ_i, the problem (6.13)-(6.15) can be recast as an optimization problem with linear objective function and quadratic constraints. In order to overcome the problem of dealing with an infinite number of constraints, a practical solution is to impose (6.14) and (6.15) only in correspondence of a finite number of frequencies; in the proposed setting, a grid with resolution of $0.1\,Hz$ is adopted for each set Ω_i. Figure 6.2 shows the Bode Diagram of the transfer functions from $\overline{n}$ to y_1, obtained when each of the controllers is in feedback with the plant.

We consider a disturbance with time-varying frequency; thus we adopt a finite memory with $M(t)$ defined as in (4.8) and $M_* = 2000$ time samples. As for the switching logic, we set $h = 5\times10^{-3}$. The parameter η is set to zero; as far as sinusoidal disturbances are considered, this choice allows one to immediately identify the best controller to be selected by the supervisory unit as the one corresponding to the maximum attenuation level achieved by the transfer functions in Fig. 6.2 at the frequency f.

In the tests that are shown in this section, we compare the performance achieved by the proposed method with the behavior exhibited by the direct adaptive scheme described in [64, 63], for which a constant forgetting factor with value 0.998 is used in the estimation algorithm.

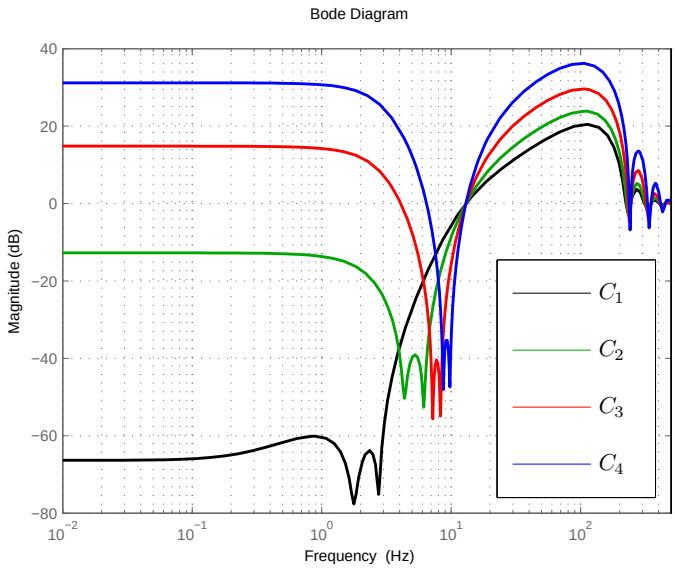

Figure 6.2: Active suspension system. Bode diagram of the transfer functions from $\overline{n}$ to y_1 related to the controllers $\mathcal{C}_i$, $i = 1, 2, 3, 4$.

In Fig. 6.3, the frequency f of the sinusoidal disturbance n is supposed to be defined as follows:

$$f = \begin{cases} 2.6\,Hz\ , & t \in [0, 15)\,s \\ 5.8\,Hz\ , & t \in [15, 30)\,s \\ 7.3\,Hz\ , & t \in [30, 45)\,s \end{cases} . \tag{6.18}$$

When the multi-controller is used, we can notice that the supervisory unit selects, after a short learning time, the controller which provides the best performance level in correspondence to each value of f. The length of the learning time is related to the choice of h and M_*, as discussed in the analysis presented in Chapter 4, but does not depend on any estimation algorithm (as it is the case of the direct adaptive scheme).

Another interesting test is the one shown in Fig. 6.4, where we let the frequency of the sinusoidal disturbance vary continuously with time from 1 Hz to 9.5 Hz, and then back from 9.5 Hz to 1 Hz. The proposed switching scheme achieves a high performance level also in this case.

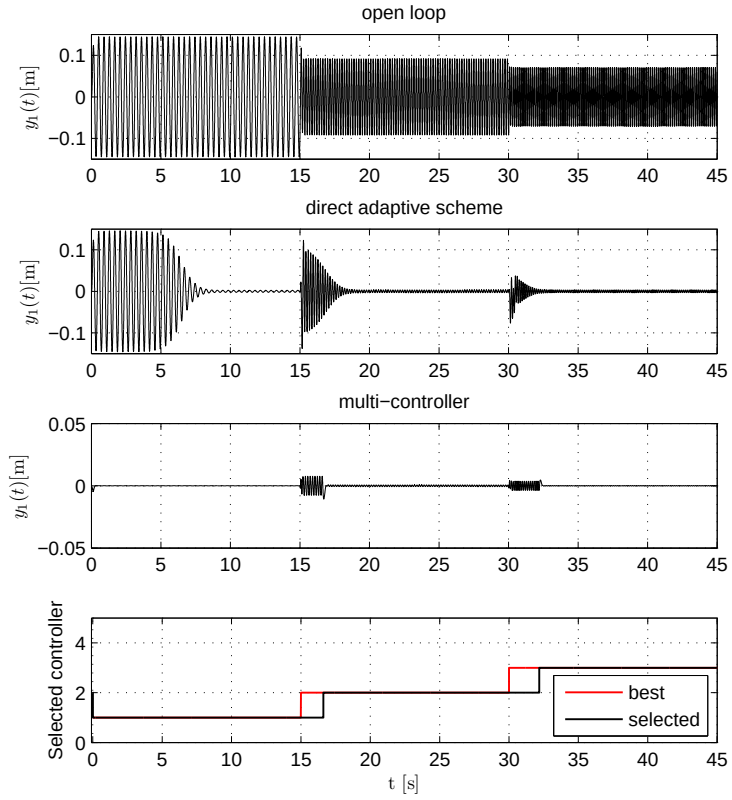

Figure 6.3: Active suspension system. System output in the presence of a sinusoidal road excitation with frequency f as in (6.18): comparison between open-loop, direct adaptive scheme, and multi-controller case.

As a final test, we suppose the disturbance n to be generated as the output of a filter with time-varying characteristics, having a zero-mean white noise as input. We let the characteristics of the filter to be constant over time intervals $TI_1 = [0, 15)\, s$, $TI_2 = [15, 30)\, s$, $TI_3 = [30, 45)\, s$; the Fourier Transforms of the resulting signal n are shown in Fig. 6.5 for $t \in TI_1$, $t \in TI_2$, and $t \in TI_3$, respectively. The results, shown in Fig. 6.6, confirm the ability of the proposed method in providing a high performance level also in the presence of a more general bounded disturbance signal.

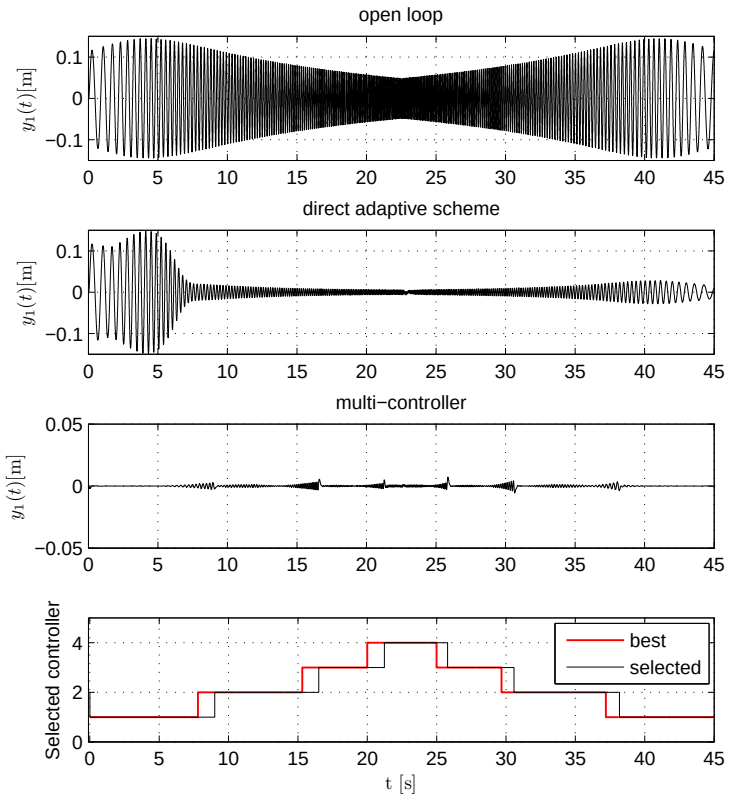

Figure 6.4: Active suspension system. System output in the presence of a sinusoidal road excitation with frequency varying continuously with time: comparison between open-loop, direct adaptive scheme, and multi-controller case.

6.3 Disturbance attenuation in an adaptive optics application

In this section, simulation tests related to an adaptive optics application are shown. We refer to the control scheme depicted in Fig. 1.2, where we consider a family of Dedicated controllers, related to the tip mode, to be used within a switching control architecture as described in Section 6.1. Specifically, the Youla parameter related to each controller has the form (6.10) and the switching system is implemented as shown in (6.12). Each

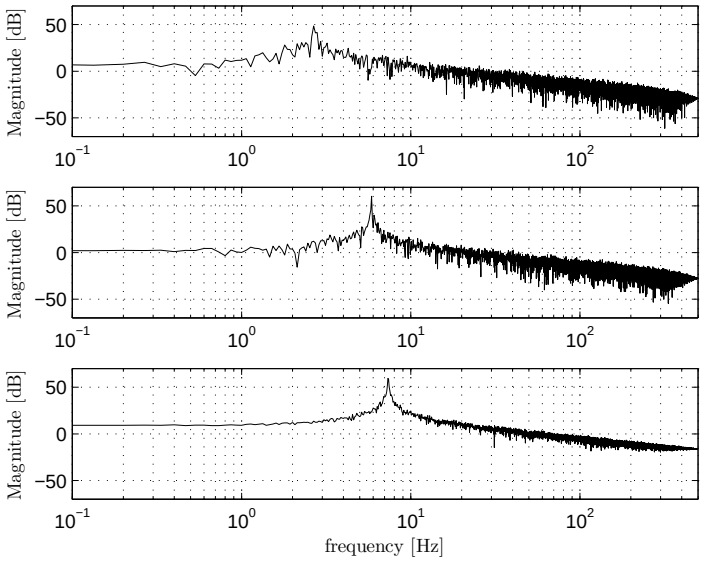

Figure 6.5: Active suspension system. Magnitude of the Fourier Transform of the considered signal, obtained as the output of a filter with time-varying characteristics having a zero-mean white noise as input, for $t \in [0, 15)\ s$, $t \in [15, 30)\ s$ and $t \in [30, 45)\ s$, respectively.

controller belonging to the family is synthesized according to the design algorithm described in Appendix 6.B (where results obtained on an adaptive optics simulator are also presented, with respect to a specific operating condition of the telescope, to show the effectiveness of the proposed synthesis procedure).

In the test that follow, we take into account variations of the variance of the measurement noise w_{tip} (arising in particular situations, *e.g.*, in the case of atmospheric transparency variations due to clouds temporarily "hiding" the object to be observed). Since

$$y_{tip}(t) = H(d)\phi_{tip}^{res}(t) + w_{tip}(t)\,, \tag{6.19}$$

with $H(d)$ behaving as a unit delay, for a measurement noise w_{tip} decorrelated from the residual phase ϕ_{tip}^{res} (we assume that w_{tip} is a zero-mean white noise), we can assert that the part $H(d)\phi_{tip}^{res}(t)$ is decorrelated from the component $w_{tip}(t)$; it follows that minimizing the variance of the residual phase ϕ_{tip}^{res} is equivalent to minimize the variance of the measured output y_{tip}. This line of reasoning is also followed in [31]. The problem can be addressed

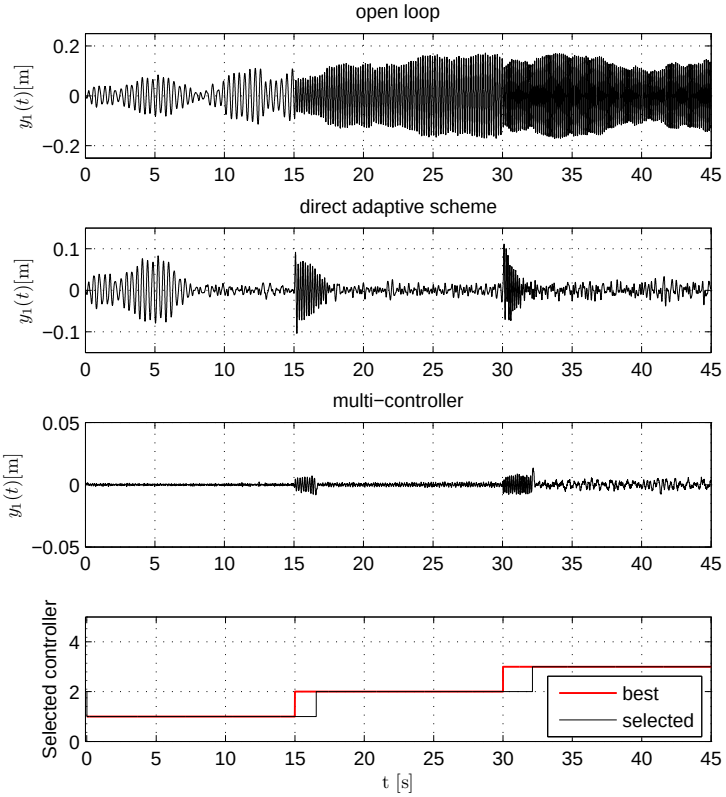

Figure 6.6: Active suspension system. System output in the presence of a disturbance obtained as the output of a filter with time-varying characteristics having a zero-mean white noise as input: comparison between open-loop, direct adaptive scheme, and multi-controller case.

by means of a switching control solution; with respect to the model in (4.1), the output y is represented by y_{tip}, while the disturbance ν is the sum of the measurement noise and the one-step-delayed wavefront distortion.

Within this framework, we synthesize two controllers, by means of the algorithm shown in Section 6.B, related to the following situations: (a) measurement noise having variance of $\approx 10^{-6}$ (almost ideal case, *i.e.*, almost negligible contribution of the measurement

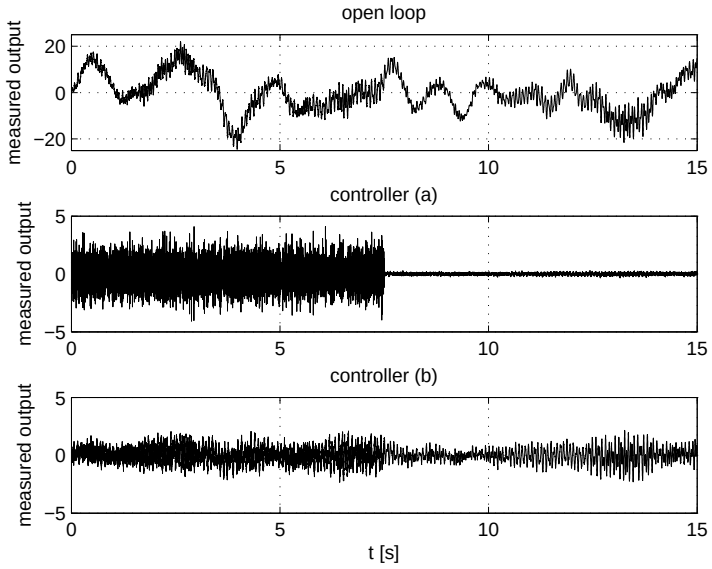

Figure 6.7: Adaptive optics system. Evolution of the measured output in open loop, with the controller (a) in feedback with the plant, and with the controller (b) in feedback with the plant, respectively.

noise); (b) measurement noise having variance $\approx 10^{-2}$ (case accounting for a low signal-to-noise ratio).

The design algorithm is initialized from the starting controller

$$\hat{C}(d) = \frac{0.65}{1 - 0.95\, d}\,; \tag{6.20}$$

the number $\tilde{K}$ of frequencies at which the constraints are imposed within the design algorithm is set to 502, and Γ is set to 18 (the meaning of the "starting controller" and of the parameters $\tilde{K}$ and Γ is explained in Appendix 6.B).

We consider a measurement noise w_t having variance

$$var(w_{tip}) \approx \begin{cases} 10^{-2}\,, & t \in [0,\, 7.5)\, s \\ 10^{-6}\,, & t \in [7.5,\, 15)\, s \end{cases}. \tag{6.21}$$

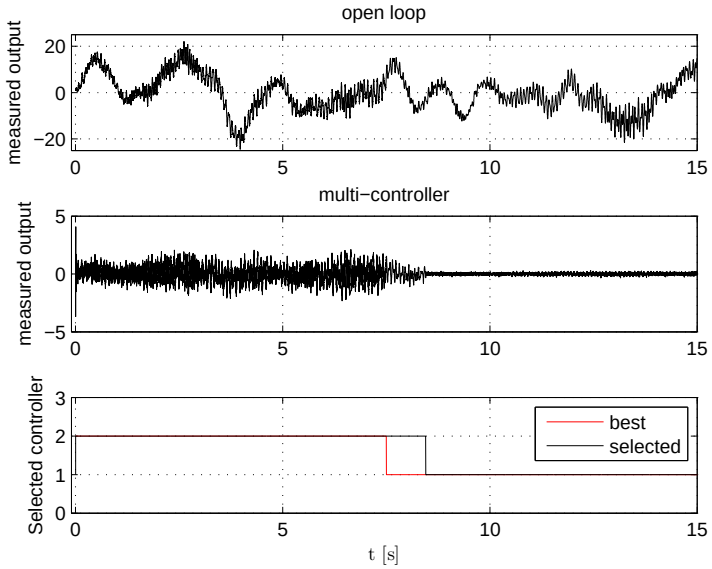

Figure 6.8: Adaptive optics system. Evolution of the measured output: comparison between open loop and multi-controller case.

We first show in Fig. 6.7 the evolution of the signal $y_{tip}(t)$: in open loop; when the controller (a) is in feedback with the plant; when the controller (b) is in feedback with the plant.

Further, we show in Fig. 6.8 a comparison between the evolution of the signal $y_{tip}(t)$ in open-loop and by applying the multi-controller implemented as shown in Section 6.1.1. A fixed memory $M_* = 1000$ time samples, and an hysteresis constant $h = 2 \times 10^{-2}$ are considered. The results underline the validity of the adaptive switching control approach as a solution to the problem.

6.A Appendix: Proofs

Proof of Theorem 6.1.1. The fact that, when $\sigma(t) = i$, the transfer function between $y(t)$ and $u(t)$ coincides with $-C_i(d)$ derives directly from the implementation described in (6.4), (6.5) and (6.6). In the following, we focus on the internal stability of the switching system $(\mathcal{P}/\mathcal{C}_{\sigma(t)})$.

We recall that, for $t \leq t_0$, the switching signal is kept constant (thus one of the stabilizing controllers belonging to $\mathscr{C}$ is continuously in feedback with the plant), and that, for $t > t_0$ the signal $\varepsilon(t)$ coincides with the disturbance $\nu(t)$. This means that $\varepsilon(t)$ is independent of σ and that it is bounded, provided that $\nu(t)$ is bounded. By choosing a stabilizable and detectable realization $\{\overline{A}_i, \overline{B}_i, \overline{C}_i, \overline{D}_i\}$ of each $Q_i(d)$ such that a common Lyapunov function $\mathcal{V}(\zeta) = \zeta^T G \zeta$ exists for the family of linear time-invariant systems $\{\zeta(t+1) = \overline{A}_i \zeta(t),\ i \in \overleftarrow{N}\}$, we can assert that $\mathcal{Q}_{\sigma(t)}$ is exponentially input-to-state stable, and thus its state $\zeta(t)$ and its output $\tilde{u}(t)$ are bounded for all σ. The boundedness of the signal $\tilde{u}(t)$ implies the boundedness of $u(t)$ and $y(t)$. In fact, from (4.1) the following steps hold:

$$\begin{aligned} A(d)y(t) &= B(d)u(t) + \nu(t) \\ &= B(d)\overline{u}(t) - B(d)\tilde{u}(t) + \nu(t) \\ &= B(d)[1 - R_0(d)]u(t) - B(d)\tilde{u}(t) - B(d)S_0(d)y(t) + \nu(t) \\ &= B(d)u(t) - R_0(d)[A(d)y(t) - \nu(t)] - B(d)S_0(d)y(t) - B(d)\tilde{u}(t) + \nu(t)\,. \end{aligned}$$

Thus one obtains

$$[A(d)R_0(d) + B(d)S_0(d)]y(t) = -B(d)\tilde{u}(t) + R_0(d)\nu(t)$$

which, by recalling (6.1), yields $y(t) = -B(d)\tilde{u}(t) + R_0(d)\nu(t)$. Similarly, from (6.4) and thanks to (4.1) and (6.1), one obtains $u(t) = -A(d)\tilde{u}(t) - S_0(d)\nu(t)$. □

Proof of Lemma 6.1.1. This proof follows along the same lines of Appendix A1 of [47]. Let $\{\tilde{A}_i, \tilde{B}_i, \tilde{C}_i, \tilde{D}_i\}$ be any m-dimensional realization of $Q_i(d)$, with $\tilde{A}_i$ asymptotically stable. Thus it is possible to assert that symmetric positive definite solutions G_i to the set of Lyapunov equations

$$\tilde{A}_i^\top G_i \tilde{A}_i - G_i = -I, \quad i \in \overleftarrow{N} \tag{6.22}$$

exist, such that $G_i = \hat{G}_i^\top \hat{G}_i$, with $\hat{G}_i$ nonsingular. Accordingly, we can consider a positive definite matrix $G \in \mathbb{R}^{m\times m}$ such that $G = \hat{G}^\top \hat{G}$, with $\hat{G}$ nonsingular, and define

$$\overline{A}_i := \hat{G}^{-1}\hat{G}_i\tilde{A}_i\hat{G}_i^{-1}\hat{G} \tag{6.23}$$

$$\overline{B}_i := \hat{G}^{-1}\hat{G}_i\tilde{B}_i \tag{6.24}$$

$$\overline{C}_i := \tilde{C}_i\hat{G}_i^{-1}\hat{G} \tag{6.25}$$

$$\overline{D}_i := \tilde{D}_i\,. \tag{6.26}$$

In turn, the set $\{\overline{A}_i, \overline{B}_i, \overline{C}_i, \overline{D}_i\}$ provides a realization of $Q_i(d)$, because it has been obtained from $\{\tilde{A}_i, \tilde{B}_i, \tilde{C}_i, \tilde{D}_i\}$ by means of a similarity transformation.
From (6.23) it is possible to compute $\tilde{A}_i$ as

$$\tilde{A}_i = (\hat{G}^{-1}\hat{G}_i)^{-1}\overline{A}_i(\hat{G}_i^{-1}\hat{G})^{-1}\,. \tag{6.27}$$

Consequently,

$$[(\hat{G}^{-1}\hat{G}_i)^{-1}\overline{A}_i(\hat{G}_i^{-1}\hat{G})^{-1}]^\top\hat{G}_i^\top\hat{G}_i[(\hat{G}^{-1}\hat{G}_i)^{-1}\overline{A}_i(\hat{G}_i^{-1}\hat{G})^{-1}] - \hat{G}_i^\top\hat{G}_i = -I$$

which yields

$$\begin{aligned}&[\hat{G}_i^{-1}\hat{G}\overline{A}_i\hat{G}^{-1}\hat{G}_i]^\top\hat{G}_i^\top\hat{G}_i\hat{G}_i^{-1}\hat{G}\overline{A}_i\hat{G}^{-1}\hat{G}_i - \hat{G}_i^\top\hat{G}_i = -I\\ &\Rightarrow \hat{G}_i^\top(\hat{G}^\top)^{-1}\overline{A}_i^\top\hat{G}^\top\hat{G}\overline{A}_i\hat{G}^{-1}\hat{G}_i - \hat{G}_i^\top\hat{G}_i = -I\,,\end{aligned}$$

from which it is possible to obtain

$$\begin{aligned}&\hat{G}_i^\top(\hat{G}^\top)^{-1}\overline{A}_i^\top\hat{G}^\top\hat{G}\overline{A}_i\hat{G}^{-1}\hat{G}_i - \hat{G}_i^\top(\hat{G}^\top)^{-1}\hat{G}^\top\hat{G}\hat{G}^{-1}\hat{G}_i = -I\\ &\Rightarrow \hat{G}_i^\top(\hat{G}^\top)^{-1}[\overline{A}_i^\top G\overline{A}_i - G]\hat{G}^{-1}\hat{G}_i = -I\,.\end{aligned}$$

Thus

$$\overline{A}_i^\top G\overline{A}_i - G = -(\hat{G}_i^{-1}\hat{G})^\top\hat{G}_i^{-1}\hat{G} < 0\,, \tag{6.28}$$

which concludes the proof. □

Proof of Proposition 6.1.1. As shown in the proof of Theorem 6.1.1, in order to prove stability it is sufficient to verify that $\tilde{u}$ remains bounded for any σ when ν is bounded. This readily follows from the fact that $D(d)$ is stable and $N_{\sigma(t)}(d)\varepsilon(t)$ is bounded, since it is a moving average, with bounded coefficients, of a bounded signal. □

6.B Appendix: Modal control design in adaptive optics applications

In this section, we show a frequency-based design algorithm, proposed in [2] within a "Modal-Control" framework in the context of adaptive optics systems for ground-based telescopes; this method builds upon an optimization procedure performed on the Youla parameter of a given modal controller with respect to a relevant adaptive optics performance criterion defined on a "sampled" frequency domain. The algorithm is initialized with a starting controller, which can be either a model-based controller (synthesized on the grounds of disturbance models of low complexity), or a non-model-based one. Controllers synthesized by means of this technique have been tested on an adaptive optics simulator, and some results are shown at the end of this section.

6.B.1 A frequency based approach

With reference to Fig. 1.2, we consider the transfer function $C(d, \rho)$ of an arbitrary controller with fixed structure depending on a parameter vector ρ which has to be tuned so as to achieve desired performances. We recall that the plant, with transfer function $P(d)$, is composed of the cascade of the blocks $M(d)$ and $H(d)$, representing the dynamics of the ASM and WFS, respectively, each one assumed to behave as a unit delay (*i.e.* $M(d) \approx H(d) \approx d$). In fact, the internal position control acting on the mirror shell works with a sampling time much lower than the one of the external AO loop.

The main objective of the AO system is to regulate the residual phase about zero by rejecting the disturbances acting on the system. To this end, a typical AO performance criterion to be minimized is the sampled-valued variance of the residual phase, defined as (see [30])

$$f(\rho) = \lim_{h\to\infty} \frac{1}{h+1} \sum_{k=0}^{h} |\phi_{tip}^{res}(k)|^2 \tag{6.29}$$

In fact, minimizing $f(\rho)$ amounts to maximizing the Strehl-ratio (SR), which is the ratio of the maximum of the Point Spread Function (PSF) of the distorted image and the maximum of the theoretical diffraction limited image PSF [44]. Let now $\Upsilon_\phi(\omega)$ and $\Upsilon_w(\omega)$ denote the PSDs of the signals $\phi_{tip}^{tot}(t)$ and $w_{tip}(t)$, respectively. Supposing $\phi_{tip}^{tot}(t)$ and $w_{tip}(t)$ mutually uncorrelated, by virtue of the Parseval's relationship, one can rewrite $f(\rho)$ in the frequency

domain as follows

$$f(\rho) = \frac{1}{2\pi} \int_{-\pi}^{\pi} (\, |S(e^{-j\omega}, \rho)|^2 \, \Upsilon_\phi(\omega) + \, |T(e^{-j\omega}, \rho)|^2 \, \Upsilon_w(\omega) \,) d\omega \, , \tag{6.30}$$

where $S(d, \rho)$ is the transfer function mapping the phase aberration $\phi_{tip}^{tot}(t)$ into the residual phase $\phi_{tip}^{res}(t)$, whereas $T(d, \rho)$ is the transfer function mapping the measurement noise $w_{tip}(t)$ into the residual phase $\phi_{tip}^{res}(t)$. With reference to Fig. 1.2, it is immediate to see that $S(d, \rho) = (1 + C(d, \rho) \, P(d))^{-1}$ and $T(d, \rho) = -M(d) \, C(d, \rho) \, (1 + C(d, \rho) \, P(d))^{-1}$.

In practice, it is convenient to approximate the integral in (6.30) with a finite sum by considering the samples at certain frequencies $\omega_1, \omega_2, \ldots, \omega_{\tilde{K}}$ of the PSDs of $\phi_{tip}^{tot}(t)$ and $w_{tip}(t)$. These samples can be obtained either from a model, possibly infinite-dimensional and non parametric, or directly from collected data series. Accordingly, we redefine the performance criterion in (6.30) as

$$f(\rho) = \frac{1}{\tilde{K}} \sum_{k=1}^{\tilde{K}} (|S(e^{-j\omega_k}, \rho)|^2 \, \hat{\Upsilon}_\phi(\omega_k) + |T(e^{-j\omega_k}, \rho)|^2 \, \hat{\Upsilon}_w(\omega_k)) \, , \tag{6.31}$$

where $\hat{\Upsilon}_\phi(\omega_k)$ and $\hat{\Upsilon}_w(\omega_k)$ denote estimates of the PSDs $\Upsilon_\phi(\omega_k)$ and $\Upsilon_w(\omega_k)$, respectively, at the frequency ω_k.

In order to derive a controller $C(d, \rho)$ with optimized performance with respect to the objective function $f(\rho)$, we resort to the Youla parametrization, implemented as in (6.8) since the plant is stable. In particular, in the framework proposed in this context, we can resort to the following expression for the family $\mathcal{C}(P)$ of all the stabilizing controllers described by means of the Youla parametrization [33]:

$$\mathcal{C}(P) = \left\{ C(d) = \frac{Q(d)}{1 - P(d) \, Q(d)}, \qquad Q(d) \in \mathcal{S} \right\} \, , \tag{6.32}$$

where $Q(d)$ is an arbitrary transfer function belonging to $\mathcal{S}$, with $\mathcal{S}$ the family of all stable proper transfer functions. Thus, the transfer function $Q(d)$ has to be regarded as a free parameter which can be tuned so as to achieve the desired control performance. To this end, we give $Q(d)$ a fixed structure depending on a parameter vector ρ, i.e., $Q(d) = Q(d, \rho)$, thus considering controllers of the form

$$C(d, \rho) = \frac{Q(d, \rho)}{1 - P(d) \, Q(d, \rho)} \, . \tag{6.33}$$

Thanks to the adopted Youla parametrization, it is possible to express both $S(d,\rho)$ and $T(d,\rho)$ in a form which is affine in the Youla parameter $Q(d,\rho)$:

$$S(d,\rho) = 1 - P(d)Q(d,\rho)\,, \tag{6.34}$$

$$T(d,\rho) = -M(d)Q(d,\rho)\,. \tag{6.35}$$

Hence, by expressing $Q(d)$ as a linear combination of functions $\psi_i(d)$, each one weighted by a parameter ρ_i, *i.e.*

$$Q(d,\rho) = \psi^\top(d)\rho, \tag{6.36}$$

where $\psi(d) = \left[\psi_1(d)\,\psi_2(d)\,\cdots\,\psi_{n_\rho}(d)\right]^\top$ and $\rho = \left[\rho_1\,\rho_2\,\cdots\,\rho_{n_\rho}\right]^\top$, it is possible to make both $S(d,\rho)$ and $T(d,\rho)$ affine functions of the parameter vector ρ:

$$S(d,\rho) = 1 - P(d)\psi^\top(d)\rho\,, \tag{6.37}$$

$$T(d,\rho) = -M(d)\psi^\top(d)\rho\,. \tag{6.38}$$

With respect to the choice of the vector $\psi(d)$, many alternatives are possible (for instance, one can choose $\psi(d)$ as a collection of basis functions, through which it is possible to approximate any finite-order stable transfer function with arbitrary accuracy by increasing the value of n_ρ [55]). In this framework, we consider

$$\psi(d) = \frac{1}{D(d)}[1\;\; d\,\cdots\, d^{n_\rho-1}]^\top\,, \tag{6.39}$$

where the denominator $D(d)$ is a fixed polynomial. As it can be seen from (6.37) and (6.38), the polynomial $D(d)$ determines the closed-loop poles of the considered modal control loop. Accordingly, the choice of $D(d)$ allows to a priori fix an adequate stability margin. As will be discussed in detail in Section 6.B.2, in practice $D(d)$ can be chosen on the basis of a given reference controller which represents the starting point of the proposed control design procedure.

The parameter vector ρ plays a fundamental role, in that it is used as the decision variable of the optimization problem. In fact, the objective function in (6.31) can be equivalently written as a quadratic function of ρ:

$$f(\rho) = \frac{1}{\tilde{K}}\sum_{k=1}^{\tilde{K}}\Big\{|(1 - P(e^{-j\omega_k})\psi^\top(e^{-j\omega_k})\rho)|^2\,\hat{\Upsilon}_\phi(\omega_k) + |M(e^{-j\omega_k})\psi^\top(e^{-j\omega_k})\rho|^2\,\hat{\Upsilon}_w(\omega_k)\Big\}.$$

Thanks to the form of the function $f(\rho)$, it would now be immediate to compute the parameter vector, say ρ°, which minimizes $f(\rho)$. The resulting controller $C(d, \rho^\circ)$ would provide optimized performance in the sense of the minimum sampled-valued variance.

Nevertheless, in many situations a controller should fulfill additional requirements beyond stabilization and performance. For instance, while observing an astronomical object, several circumstances may cause the command signal $u(t)$ to be interrupted for a few time steps: actuators may be required to perform an action that is not compatible with their stroke or with the force they can bear (this phenomenon can be frequent, up to some events per second, in seeing conditions ≥ 1.2"); also, slopes may not be delivered for a frame or two, producing the same effects of command interruptions (though the latter is an extremely rare event).

With this respect, common practice suggests that it is not advisable to make use of unstable controllers, especially if the plant itself is stable, as it is within our setting. In fact, if the feedback loop opens (generalizing, this could happen due to a sensor or actuator failing, or deliberately being turned off during start-up or shutdown), overall stability is maintained if both plant and controller *individually* are stable [33].

Clearly, the Youla parametrization does not ensure by itself that a generic controller of the form shown in (6.33) is stable, thus unconstrained minimization of $f(\rho)$ can result in an unstable (albeit stabilizing) controller $C(d, \rho^\circ)$. A possible way of overcoming such a drawback consists in solving a *constrained* optimization problem (COP), defined such that $f(\rho)$ is the objective function and the controller stability requirement characterizes the feasibility domain

$$\min_{\rho} f(\rho)\,, \tag{6.40}$$

s.t.

$$C(d, \rho) \in \mathcal{S}. \tag{6.41}$$

6.B.2 Algorithm details

Solving an optimization problem is not a trivial numerical task, and requires that the constraints, as well as the objective function, are expressed in the simplest possible form. Unfortunately, the feasibility domain embodied by (6.41) is in general non convex and thus it is advisable to consider some kind of convex approximation. This can be done provided that a reference parameter vector $\hat{\rho}$ is available corresponding to a stable controller

$C(d,\hat{\rho})$ (in practice $\hat{\rho}$ can be computed from a given stable and stabilizing controller as will be detailed in the following). In fact, a sufficient condition for the stability of a controller $C(d,\rho)$ is that

$$Re\left\{(1-P(e^{j\omega})Q(e^{j\omega},\hat{\rho}))(1-P(e^{-j\omega})Q(e^{-j\omega},\rho))\right\}>0\,,\qquad\forall\omega\,,\tag{6.42}$$

where $Re\{\cdot\}$ denotes the real part. Indeed, condition (6.42) ensures that the number of counterclockwise encirclements around the origin of the Nyquist plot of $1-P(d)Q(d,\rho)$ equals that of the Nyquist plot of $1-P(d)Q(d,\hat{\rho})$. In view of the Nyquist stability criterion [41], this ensures that $C(d,\rho)$ and $C(d,\hat{\rho})$ have the same stability property (recall (6.33)).

The condition given above is defined for all ω, *i.e.* over a continuum, thus of no practical use. One possible solution in order to avoid this drawback is to impose that (6.42) is satisfied only in the sampled-frequency domain $\{\omega_1,\omega_2,...\omega_{\tilde{K}}\}$. As recalled in Chapter 5, the problem of dealing with an infinite number of frequency constraints via a finite number of frequencies has been addressed for example in [55], wherein guidelines on the choice of the sampled-frequency domain can be found. The resulting condition can be written in the form of linear constraints

$$A(\hat{\rho})\,\rho+b(\hat{\rho})<0\tag{6.43}$$

by conveniently defining matrix A and vector b. Specifically, matrix A takes the form

$$A(\hat{\rho})=\begin{bmatrix}a_{11}(\hat{\rho}) & \cdots & a_{1n_\rho}(\hat{\rho})\\ \vdots & \ddots & \vdots\\ a_{\tilde{K}1}(\hat{\rho}) & \cdots & a_{\tilde{K}n_\rho}(\hat{\rho})\end{bmatrix}\tag{6.44}$$

with elements $a_{ki}(\hat{\rho})$, $k=1,...,\tilde{K}$, $i=1,...,n_\rho$, computed as

$$a_{ki}(\hat{\rho})=Re\left\{(1-P(e^{j\omega_k})Q(e^{j\omega_k},\hat{\rho}))P(e^{-j\omega_k})\psi_i(e^{-j\omega_k})\right\},\tag{6.45}$$

and vector $b(\hat{\rho})$ is defined as

$$b(\hat{\rho})=\left[b_1(\hat{\rho})\cdots b_{\tilde{K}}(\hat{\rho})\right]^\top\tag{6.46}$$

with elements $b_k(\hat{\rho})$, $k=1,...,\tilde{K}$, computed as

$$b_k(\hat{\rho})=-Re\left\{1-P(e^{j\omega_k})Q(e^{j\omega_k},\hat{\rho})\right\}.\tag{6.47}$$

Summing up, by replacing the original stability constraint in (6.41) with the linear constraints in (6.43), we obtain a quadratic programming problem which can be solved

efficiently by means of several numerical tools. Typical algorithms for solving such a kind of problems are based on Active-Set, Sequential Quadratic Programming (SQM) or Interior-Point methods. In the proposed implementation, the Active-Set method is adopted.

Hereafter, we write the proposed synthesis procedure step by step and provide a schematic summary of the algorithm. As previously mentioned, the procedure starts with a pre-existing stable and stabilizing controller $\hat{C}(d)$ which can be synthesized either by means of a simple non-model based technique or of some model-based design procedure. Then we compute the Youla parameter

$$\hat{Q}(d) = \frac{\hat{C}(d)}{1 + P(d)\hat{C}(d)} = \frac{\hat{N}(d)}{D(d)}\,, \tag{6.48}$$

where $\hat{N}(d) = \hat{n}_0 + \hat{n}_1\, d + \cdots + \hat{n}_{\partial\hat{N}}\, d^{\partial\hat{N}}$ is a polynomial of degree $\partial\hat{N}$. In order to increase the degrees of freedom of our optimization problem, n_ρ can be set as $n_\rho = \partial\hat{N} + 1 + \Gamma$, with Γ a nonnegative integer; then the reference parameter vector $\hat{\rho}$ is defined as

$$\hat{\rho} = [\hat{n}_0\ \hat{n}_1\ \cdots\ \hat{n}_{\partial\hat{N}}\ \underbrace{0\ \ldots\ 0}_{\Gamma}]^\top\,. \tag{6.49}$$

Then it is possible to minimize the performance criterion $f(\rho)$ under the constraints in (6.43). In addition, in order to improve the controller performance, one can construct an iterative procedure by using, at every step, the solution of the optimization problem as a novel reference parameter vector. This idea gives rise to the following iterative procedure.

Iterative design procedure

Step 1: given an initial controller $\hat{C}(d)$ and a nonnegative integer Γ, compute $\hat{Q}(d)$, n_ρ, and $\hat{\rho}$ as described above;
Step 2: set $i := 0$ and $\rho^{(0)} := \hat{\rho}$;
Step 3: compute the matrix $A(\rho^{(i)})$ and the vector $b(\rho^{(i)})$;
Step 4: compute the parameter vector $\rho^{(i+1)}$ as the solution of the quadratic programming problem

$$\min_{\rho} f(\rho) \tag{6.50}$$

s.t.

$$A(\rho^{(i)})\,\rho + b(\rho^{(i)}) < 0; \tag{6.51}$$

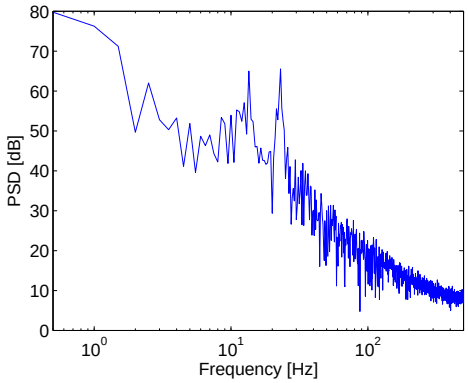

Figure 6.9: Turbulence and vibration PSD related to tip.

Step 5: if the termination criterion is met, then return $\rho^{(i+1)}$; otherwise set $i := i + 1$ and go back to **Step 3**.

As for the termination criterion, an upper bound on the difference between the value functions corresponding to subsequent iterations is imposed, thus terminating the algorithm when $|f(\rho^{(i+1)}) - f(\rho^{(i)})| < \epsilon$, with ϵ a given threshold. With this respect, notice that by construction the sequence $f(\rho^{(i)})$ is monotonically non-increasing with i. In fact, it can be easily verified that $\rho^{(i)}$ always satisfies the constraint in (6.51) so that $f(\rho^{(i+1)}) \leq f(\rho^{(i)})$. Since $f(\rho)$ is bounded from below, this ensures that the sequence $f(\rho^{(i)})$ converges to some finite limit and, hence, that the termination criterion is always eventually met.

6.B.3 Simulation results

In this section we provide the results obtained from simulation studies. The simulation results rely on an End-to-End simulator of the First Light Adaptive Optics system of the LBT.

Appendix: Modal control design in adaptive optics applications

We adopt the residual phase variance and the Strehl ratio (computed at 1.65 μm) as performance parameters. Specifically, the SR is defined as

$$SR = \frac{PSF_{res}(\underline{o})}{PSF_{Airy}(\underline{o})}, \tag{6.52}$$

where PSF_{res} denotes the intensity value at the center $\underline{o}$ of the AO-corrected PSF and PSF_{Airy} denotes the intensity value at the center $\underline{o}$ of the diffraction-limited PSF of the telescope. The PSF_{res} is determined as the Fourier transform of the residual phase at the telescope pupil, while PSF_{Airy} is the Fourier transform of a uniform phase over the telescope pupil. The pyramid WFS [82] with tilt modulation is simulated with a full Fourier-optics code developed at the Arcetri Astrophysical Observatory. In the simulator the image on the detector is obtained by two Fourier Transforms. The first one converts, for each step of modulation, the complex amplitude of the tilted incoming wavefront into the electrical field on the pyramid; the second one converts the electrical field on the pyramid multiplied by the phase mask of the pyramid into the image on the detector. Finally the signal is computed as in [90]. The atmospheric turbulence is simulated in order to emulate a typical LBT operating environment. Specifically, the turbulent phase is represented by a set of turbulent layers, where each layer corresponds to a phase screen. In the simulations presented in this section, a set of two layers is considered. The phase screens are generated following the McGlamery method [72]. They have altitude of 0 and 6000 m over the telescope and their relative intensity is 60% and 40%, respectively (they produce a seeing of 0.8"). The temporal evolution of the turbulence is simulated, based on the Taylor's hypothesis, by displacing the phase screens in front of the telescope pupil according to the specified speed of 15 and 18 m/s respectively (the considered mean wind speed is 16.5 m/s). The considered telescope structural vibrations have frequencies at 13 and 22 Hz, with a standard deviation of 20 mas and a damping ratio of 0.01. Figure 6.9 shows the PSD of turbulence and vibrations, related to tip. The ASM spatial response was modeled by using the influence functions determined via the FEA (Finite Elements Analysis) model of the LBT ASM, while the temporal one is considered as a delay of 1 ms. Specifically, the ASM is characterized by 672 Karhunen-Loève modes projected onto the ASM influence functions.

The simulation results reported hereafter consider two scenarios: in the first one, the proposed procedure is initialized from a non-model-based controller, *i.e.*, from a controller synthesized without identifying mathematical models of turbulence and vibrations; in the second scenario, the proposed procedure is initialized from a H_2-controller synthesized

	$C_a(d)$	$C_b(d)$	$C_c(d)$	$C_d(d)$	$C_e(d)$	$C_f(d)$
SR %	58.51	86.22	86.49	79.20	84.02	86.61

Table 6.2: Performance exhibited by the controllers considered in the simulation tests.

using mathematical models of turbulence and vibrations of reduced complexity, namely a second-order autoregressive (AR) model for the turbulence and two second-order autoregressive moving-average (ARMA) models for the vibrations.

In both scenarios, the optimization procedure is carried out by sampling the PSDs of the phase aberration related to tip/tilt modes, as reported in Fig. 6.9, and the PSD of the measurement noise (assumed having variance of $\approx 10^{-4}$). As for the sampling of the PSDs in (6.31), we select $\tilde{K} = 2000$ samples with linear gridding (simulation results, not reported here, indicate that $\tilde{K} > 500$ samples are sufficient for achieving satisfactory closed-loop performance). The termination criterion of the optimization algorithm is defined on the basis of the threshold $\epsilon = 10^{-3}$ on the difference between the value functions corresponding to two successive iterations. The closed-loop performance (in terms of Strehl ratio) is evaluated over the last 2000 samples of the residual phase (in the steady state). Finally, all the modes except for tip and tilt are controlled by means of integrators with optimized gains selected via the Optimized Modal Gain Integrator (OMGI) approach as described in [31]. Finally, also the constraint on the controller stability are considered.

First scenario: Let

$$\hat{C}(d) = \frac{g}{1 - 0.95\, d}\,, \tag{6.53}$$

with g such that the closed-loop is stable. By following the procedure described in Section 6.B.2, $\hat{Q}(d)$ takes the form

$$\hat{Q}(d) = \frac{g}{1 - 0.95\, d + g\, d^2} = \frac{\hat{N}(d)}{D(d)}\,. \tag{6.54}$$

Accordingly,

$$\psi(d) = \frac{1}{D(d)}\,[1 \;\; d \cdots d^{n_\rho - 1}]^\top \;=\; \frac{1}{1 - 0.95\, d + g\, d^2}\,[1 \;\; d \cdots d^{n_\rho - 1}]^\top\,. \tag{6.55}$$

Then, the algorithm is initialized by letting

$$\rho^{(0)} = \hat{\rho} = [\, g \;\; \underbrace{0 \;\; \ldots \;\; 0}_{\Gamma}\,]\,. \tag{6.56}$$

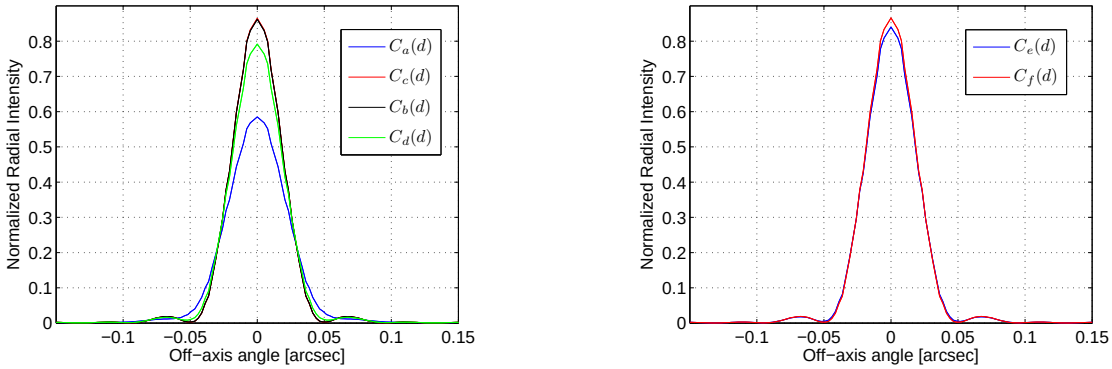

Figure 6.10: PSF profiles resulting from the use of the controllers in the control loop.

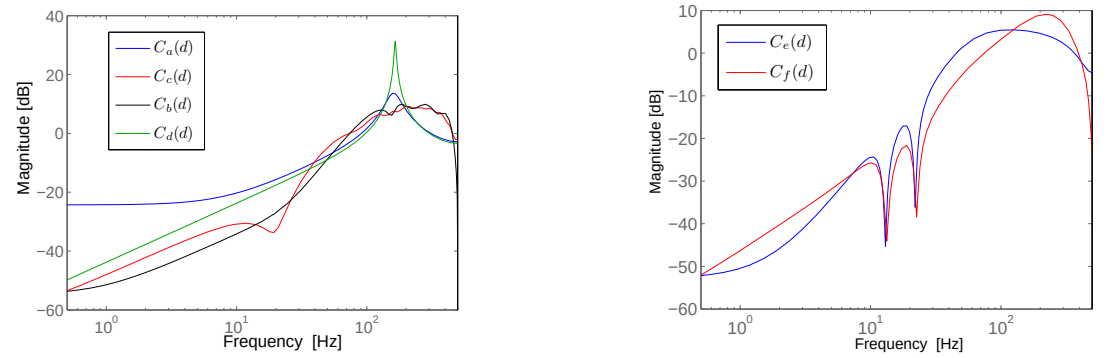

Figure 6.11: Bode diagram of the sensitivity function related to the controllers.

As for the simulation, we set $g = 0.77$. Compared with $\hat{C}(d)$, which achieves a residual phase variance (VAR) $VAR = 0.2528$ ($SR = 58.51\%$), controllers provided by the proposed procedure show a significant performance improvement; in particular, for $\Gamma \geq 9$ we obtain $VAR < 0.0209$ ($SR > 86.22\%$).

Second scenario: As the initial controller, we now consider a H_2-controller synthesized by using mathematical models of turbulence and vibrations of reduced complexity. Specifically, we adopt the design procedure described in [5], with the following choices: the model of the turbulence is taken as a second-order AR model having input $\overline{\eta}$ and output ξ,

and described by the difference equation

$$\xi(t) = 1.9774\,\xi(t-1) - 0.9776\,\xi(t-2) + \overline{\eta}(t)\,, \tag{6.57}$$

where $\overline{\eta}$ is a white-noise process. As for the structural vibrations, we consider two second-order ARMA models having input μ_i and output ζ_i, $i = 1, 2$. They are described by the difference equations

$$\zeta_1(t) = 1.9917\,\zeta_1(t-1) - 0.9984\,\zeta_1(t-2) + 1.8431\,\mu_1(t-1) - 0.8493\,\mu_1(t-2)\,, \tag{6.58}$$

for the model having a vibration peak around 13Hz, and

$$\zeta_2(t) = 1.9782\,\zeta_2(t-1) - 0.9972\,\zeta_2(t-2) + 1.7418\,\mu_2(t-1) - 0.7585\,\mu_2(t-2)\,, \tag{6.59}$$

for the model having a vibration peak around 22Hz, where μ_1 and μ_2 are both white-noise processes.

With respect to the H_2-controller, the corresponding $\partial\hat{N} = 9$, and we set $\Gamma = 2$. In this case, the simulation results show a performance improvement from $VAR = 0.0393$ ($SR = 84.02\%$) to $VAR = 0.0152$ ($SR = 86.61\%$). The performance obtained for larger values of Γ is very similar to the one obtained for $\Gamma = 2$.

Figures 6.10, 6.12 and 6.11, along with Table 6.2, provide a summary of the obtained results, also compared with the optimized modal gain integrator (OMGI) controller of [31], applied to all modes (including tip/tilt). For simplicity, we adopt the following notation: $C_a(d)$ initial controller in the first scenario; $C_b(d)$ final controller in the first scenario with $\Gamma = 9$; $C_c(d)$ final controller in the first scenario with $\Gamma = 18$; $C_d(d)$ OMGI controller; $C_e(d)$ initial controller in the second scenario; $C_f(d)$ final controller in the second scenario with $\Gamma = 2$. The results are very close to what one could expect: $C_c(d)$, $C_e(d)$ and $C_f(d)$ are those exhibiting lower residual phase both at low frequencies as well as in correspondence of the vibration peaks (Fig. 6.12). This is also evident from Fig. 6.11. In particular, the sensitivity functions related to $C_e(d)$ and $C_f(d)$ both exhibit the two anti-resonance peaks at the frequencies characterizing the vibration models.

It is worth mentioning that, as shown in Table 6.2, the best performance is achieved when starting from a model-based controller synthesized in accordance with models of reduced complexity. Such a result, obtained without identifying mathematical turbulence and vibration models of increased complexity, underlines that the proposed approach is best viewed as cooperative with (rather than as alternative to) classical AO control design approaches.

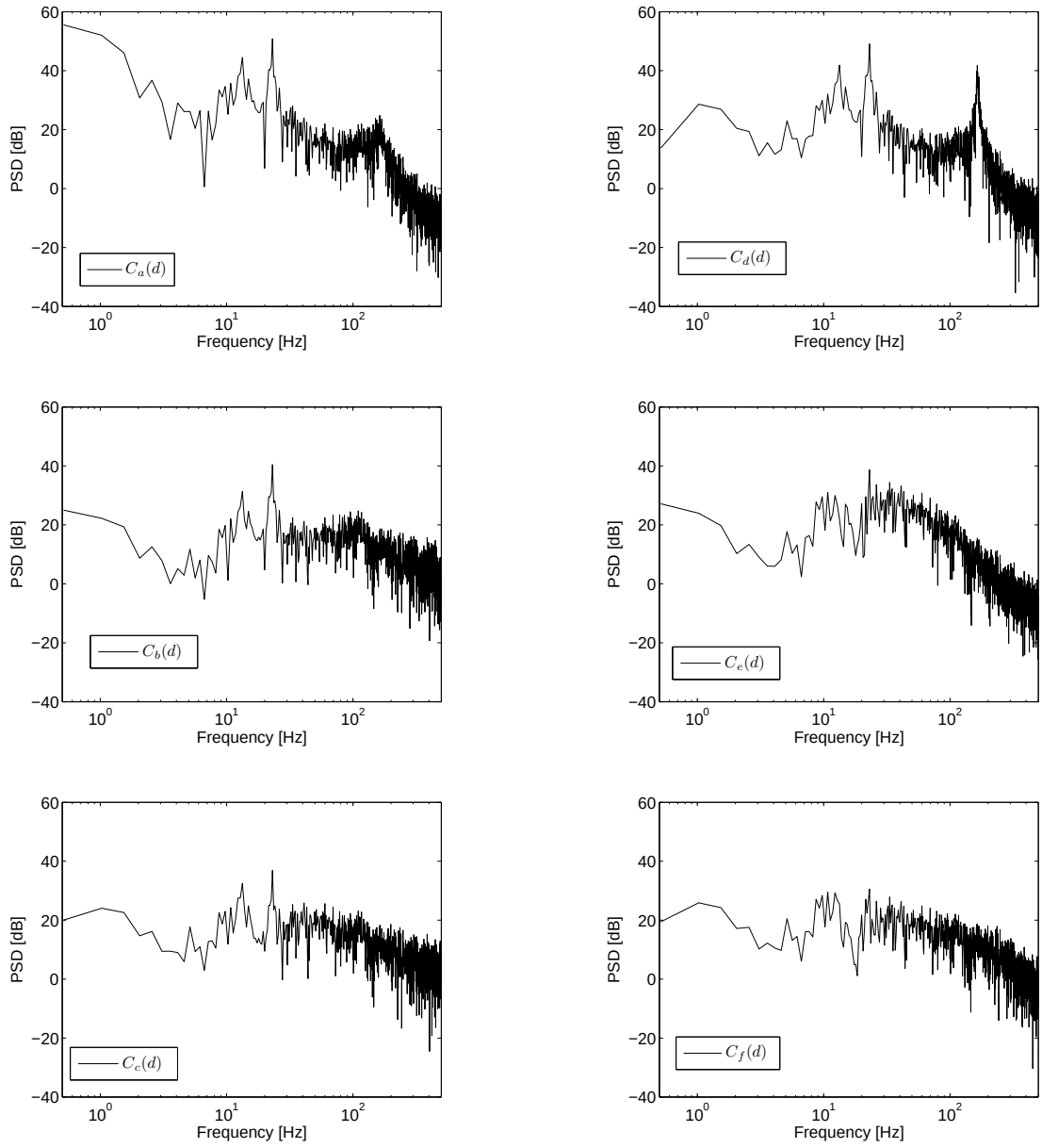

Figure 6.12: PSDs of the residual phase (related to tip/tilt).

PART III
Combining switching and tuning

Chapter 7

A hierarchical approach: combining switching and tuning

In the previous chapters, we have shown the performance level that can be achieved by applying the ASC paradigm to the context of active disturbance attenuation. Particular attention has been focused on the choice of the test functionals that the supervisory unit has to compute and compare, in order to select, at each time instant, the (potentially) best controller within the finite family $\mathscr{C}$; it is worth recalling that each test functional is computable in real-time from the plant input/output data, and reflects the potential performance of the related controller. Another crucial issue which has been taken into account within an ASC structure is that of the stability of the overall closed loop under arbitrary switching, and different possible solutions have been proposed.

It has been underlined (for example with reference to the simulation results shown in Section 6.2) that the switching approach, if compared to classical adaptive techniques based on parameter tuning strategies, is in general more suitable to quickly achieve satisfactory performance and to deal with abrupt changes of the unknown characteristics, provided that the supervisor is able to select in a short time the controller providing the more desirable behavior. However, the attenuation level achievable by the pre-synthesized controllers in the finite set determines the performance that can be achieved by the overall control scheme. On the other hand, classical Adaptive Control techniques can usually achieve better performance levels as a final result, but the tuning procedure of the controller parameters

can require in general a non-negligible time interval before leading the closed-loop system to a satisfactory behavior.

This brief overview suggests that a technique integrating switching and tuning appears to be suitable to combine the advantages of the two different approaches, while possibly overcoming the aforementioned drawbacks. This idea has been exploited in the past in the context of adaptive control of uncertain plants, usually within multi-model architectures (see for example [76, 56, 14] and the references therein). The aim of this chapter is that of proposing an algorithm combining switching and tuning in the context of active disturbance attenuation, and of providing an analysis of the properties that the proposed scheme is able to ensure [20].

7.1 Problem setting

With reference to the problem defined in Section 4.1, the aim is that of obtaining an arbitrary level of attenuation in the presence of a bounded disturbance ν having uncertain and possibly time-varying characteristics. Following the ASC paradigm, a controller is selected by a supervisory unit among a finite set of stabilizing controllers, by resorting to the computation in real-time of test functionals evaluating their potential performance; then, a local refinement of the selected controller is performed, providing a new controller which can be put in feedback with the plant in accordance to a switching rule, possibly different from the logic adopted for the controller selection applied to the finite family. We recall that $\mathscr{C} := \{\mathcal{C}_i,\, i \in \overleftarrow{N}\}$ denotes the finite family of pre-designed candidate controllers. The i-th controller has transfer function $C_i^*(d) = S_i^*(d)/R_i^*(d)$ with the polynomials $R_i^*(d)$ and $S_i^*(d)$ having strictly Schur g.c.d.; $R_i^*(0) = 1$. We denote by $\mathscr{C}_\ell$ the augmented family of controllers composed of $\mathscr{C}$ and the controller $\mathcal{C}_\ell^\circ$ obtained by means of the tuning procedure. The transfer function of the optimized controller $\mathcal{C}_\ell^\circ$ is denoted by $C_\ell^\circ(d)$. Since the refinement of the controller selected from $\mathscr{C}$ will be performed iteratively in general, as will be explained in the next section, we use the subscript $\ell = 1, 2, \cdots$, to refer to the sequence of solutions of the tuning problems. Clearly, the set $\mathscr{C}_\ell$ has cardinality $N + 1$ for any ℓ.

In the proposed framework, the switching signal σ is the signal that identifies which of the candidate controllers belonging to the augmented family $\mathscr{C}_\ell$ is in feedback with the plant at each time instant, thus $\sigma(\cdot) : \mathbb{Z}_+ \to \overleftarrow{N+1}$. The notation $\mathcal{C}_{\sigma(t)}$ for the multi-controller means that, on all the time intervals on which $\sigma(t)$ is constant and equal

to a certain j, the multi-controller takes the form of a LTI system having transfer function equal to $C_j^*(d)$ if $j \in \overleftarrow{N}$ or equal to $C_\ell^\circ(d)$ if $j = N+1$.

7.1.1 Combining switching and tuning

With the aim of addressing the problem of disturbance attenuation with arbitrary attenuation level, we propose an algorithm based on a hierarchical structure. First, a high-level switching logic SL_1 is applied to the controllers belonging to the set $\mathscr{C}$ in order to select the controller, say $\mathcal{C}_j$, guaranteeing the best attenuation capabilities within $\mathscr{C}$; then an optimization criterion is adopted to find a local refinement of $\mathcal{C}_j$, and a switching logic SL_2, possibly different from SL_1, is used to decide whether to substitute $\mathcal{C}_j$ with its refinement or not.

The output of the first switching logic SL_1 is a switching signal $\overline{\sigma}(t)$ taking value in $\overleftarrow{N}$. Then, at any time t, the true controller switching signal $\sigma(t)$ will be equal either to $\overline{\sigma}(t)$ or to $N+1$ in case the optimized controller is selected.

The potential performance of each candidate controller in $\mathscr{C}$ is evaluated in terms of test functionals $\Pi(t) := \{\Pi_i(t),\, i \in \overleftarrow{N}\}$, which are computed in real-time on the basis of the plant input/output data. As in Chapter 4, the well-known *hysteresis switching logic* [73] is adopted as SL_1 by the supervisory unit to generate the switching signal $\overline{\sigma}(t)$ which selects the controller $\mathcal{C}_j$ within $\mathscr{C}$. We denote by t^*, with $t^* \leq t$ being t the current time, the most recent time instant in which the index j has been changed by the SL_1.

If the index $\overline{\sigma}(t)$ remains constant and equal to a certain j for a pre-defined time interval T_L, then an optimization procedure is applied in order to find a local refinement of $\mathcal{C}_j$. To this end, a parametric set of controller transfer functions $\{C_j(d,\rho_j), \rho_j \in \mathcal{R}_j\}$ is considered depending on a parameter vector ρ_j belonging to a given set $\mathcal{R}_j \subseteq \mathbb{R}^{n_{\rho_j}}$. We denote by $\rho_j^* \in \mathcal{R}_j$ the parameter vector of the pre-designed controller $\mathcal{C}_j$, i.e., $C_j^*(d) = C_j(d,\rho_j^*)$. The refinement aims at optimizing a functional $J_\ell(\rho_j)$ starting from ρ_j^*. Some constraints in the optimization problem could be imposed in order to match specific requirements; this will be discussed in Section 7.2. We denote by t_ℓ and t_ℓ^* the time instants at which the ℓ-th optimization starts and, respectively, terminates. Thus at each time t_ℓ^* a new controller $\mathcal{C}_\ell^\circ$ with transfer function $C_\ell^\circ(d) = C_j(d,\rho_{j,\ell}^o)$ is available, where $\rho_{j,\ell}^o$ is the optimal parameter vector obtained from the ℓ-th optimization, and the controller family is updated accordingly.

$\mathscr{C} := \{\mathcal{C}_i,\, i \in \overleftarrow{N}\}$	finite family of stabilizing controllers
$C_i^*(d) = S_i^*(d)/R_i^*(d)$	transfer function of the i-th controller $\mathcal{C}_i$ belonging to $\mathscr{C}$
$\ell = 1, 2, \cdots$	index related to the solutions of the iterative tuning procedure
$\mathcal{C}_\ell^\circ$	controller obtained by means of the tuning procedure when the ℓ-th optimization terminates
$\mathscr{C}_\ell := \mathscr{C} \cup \{\mathcal{C}_\ell^\circ\}$	augmented family of stabilizing controllers
$\overline{\sigma}(\cdot) : \mathbb{Z}_+ \to \overleftarrow{N}$	output of the SL_1
$\sigma(\cdot) : \mathbb{Z}_+ \to \overleftarrow{N+1}$	output of the SL_2
t^*	the most recent time instant in which the index j has been changed by the SL_1
t_ℓ	time instant in which the ℓ-th optimization starts
t_ℓ^*	time instant in which the ℓ-th optimization terminates
ρ_j^*	the parameter vector of the controller $\mathcal{C}_j$ selected by SL_1, *i.e.*, $C_j^*(d) = C_j(d, \rho_j^*)$
$\rho_{j,\ell}^o$	the optimal parameter vector obtained from the ℓ-th optimization

Table 7.1: Summary of the adopted notation.

After an optimization has terminated, a novel one is performed until a controller achieving a pre-specified performance level γ is found.

Table 7.1 provides a brief summary of the notation adopted for the technique outlined above.

Remark 7.1.1. The selection of the controller $\mathcal{C}_j \in \mathscr{C}$ is performed at each time instant. Thus, it could happen that the selected controller within $\mathscr{C}$ changes (*i.e.*, the index j changes) while the ℓ-th optimization is running. In this case, the optimization routine is stopped, and a local refinement of the novel $\mathcal{C}_j$ will be performed once $\overline{\sigma}(t)$ remains constant and equal to the novel j for at least T_L instants (obviously if this will actually happen).

For the optimized controller $\mathcal{C}_\ell^\circ$, a test functional $\Pi_{N+1}(t)$ is computed having the same form of the test functionals in $\Pi(t)$. Then the test functionals $\Pi_j(t)$ and $\Pi_{N+1}(t)$ are compared in accordance with the switching logic SL_2. Again, a hysteresis switching logic is adopted possibly with a different hysteresis constant. The SL_2 is active only if there is a valid optimized controller. We use a binary variable $f(t)$ to indicate this fact.

The outline of the algorithm can be presented as follows.

Algorithm 7.1.1

Step 0. (initialization)

Select an initial controller $\mathcal{C}_{i_0}$ to be put in feedback with the plant until a starting time t_0. Set $\sigma(t_0) = \overline{\sigma}(t_0) = i_0$, $\ell = 0$, $f(t_0) = 0$ and $t^* = t_0$.

For $t = t_0 + 1, t_0 + 2, \ldots$

Step 1. (SL_1)

Select the candidate controller achieving the best (potential) attenuation performance within the finite set $\mathscr{C}$ as follows

$$\overline{\sigma}(t+1) = \arg\min_{i \in \overleftarrow{N}} \left\{ \Pi_i(t) - \overline{h}\, \delta_{i\overline{\sigma}(t)} \right\} \tag{7.1}$$

where δ_{ij} is the Kronecker delta and $\overline{h} > 0$ is the hysteresis constant for the SL_1.

Step 2. (SL_2)

If $\overline{\sigma}(t+1) \neq \overline{\sigma}(t)$

Set $\sigma(t+1) = \overline{\sigma}(t+1)$ and $t^* = t$; stop the optimization routine and set $f(t) = 0$;

Else

Perform the following operations:

- check if the $(\ell+1)$-th optimization has successfully terminated. In this case, construct the novel set $\mathscr{C}_{\ell+1}$, and set $f(t) = 1$, $t^*_{\ell+1} = t$, and $\ell = \ell + 1$; otherwise set $f(t) = f(t-1)$;

- in case no optimization is running and $t - t^* \geq T_L$, check if there is a valid optimized controller whose potential performance is below the prescribed level γ, i.e., such that

$$\max_{\tau \in [t^*_\ell, t]} \Pi_{N+1}(\tau) \leq \gamma\,. \tag{7.2}$$

  In the negative, then start a novel optimization and set $t_{\ell+1} = t$;

- if $f(t) = 0$ then set $\sigma(t+1) = \overline{\sigma}(t+1)$. Otherwise select between the starting and the optimized controller as follows

$$\sigma(t+1) = \arg \min_{i \in \{\overline{\sigma}(t), N+1\}} \left\{ \Pi_i(t) - h\, \delta_{i\sigma(t)} \right\} \tag{7.3}$$

  where $h > 0$ is the hysteresis constant for the SL_2.

End if
End for

The time instant t_0 from which Algorithm 7.1.1 is initialized is the time instant at which the switching logic is activated, as discussed in Section 4.1. We note that Algorithm 7.1.1 has a hierarchical structure, since the low-level switching logic SL_2 does not interfere with the high-level one. Hence the proposed approach turns out to be modular, in the sense that the behavior of the signal $\overline{\sigma}(t)$ can be analyzed without worrying of what happens at the lower level. This means that the results presented in Chapter 4 still hold, provided that the same choice for the test functionals is adopted. As previously noticed, the hysteresis constants in SL_1 and SL_2 will be different in general. For instance, $\overline{h}$ in SL_1 has to be chosen large enough so as to avoid spurious switching and ensure a more rapid selection of the index j (recall Chapter 4). On the other hand, as will be clarified in Section 7.3.1, by taking h suitably small one can improve the attenuation performance.

7.2 Controller implementation and stability analysis

The implementation of the multi-controller adopted in this framework is the one discussed in Chapter 6. Specifically, each controller belonging to $\mathscr{C}_\ell$ is realized by means of the Youla-Kucera parametrization of all the stabilizing controllers, then the switching occurs between the controller Youla parameters.

Hereafter, $Q_j^*(d) = N_j^*(d)/D_j^*(d)$ will denote the transfer function of the Youla parameter of the j-th predesigned controller $\mathcal{C}_j$. As for the optimized controller $\mathcal{C}_\ell^\circ$, it is supposed that only the Youla parameter numerator depends on the parameter vector ρ_j whereas the denominator is kept constant in the optimization and equal to $D_j^*(d)$. Accordingly, whenever $\overline{\sigma}(t) = j$, the Youla parameter of the optimized controller $\mathcal{C}_\ell^\circ$ takes the form $Q_\ell^\circ(d) = N_j(d, \rho_{j,\ell}^\circ)/D_j^*(d)$. For the pre-designed controller $\mathcal{C}_j$, we let $N_j^*(d) = N_j(d, \rho_j^*)$.

We recall from Chapter 6 that the control input is computed as

$$u(t) = \overline{u}(t) - \tilde{u}(t)\,, \tag{7.4}$$

where $\tilde{u}(t)$ is the output of a switching system $\mathcal{Q}_{\sigma(t)}$ having input $\varepsilon(t)$, which represents the prediction error at time t; the signals $\overline{u}(t)$ and $\varepsilon(t)$ are obtained as

$$\begin{bmatrix} \overline{u}(t) \\ \varepsilon(t) \end{bmatrix} = \begin{bmatrix} (1 - R_0(d)) & -S_0(d) \\ -B(d) & A(d) \end{bmatrix} \begin{bmatrix} u(t) \\ y(t) \end{bmatrix}. \tag{7.5}$$

With respect to the specific implementation of the switching system $\mathcal{Q}_{\sigma(t)}$, we compute, for any $i \in \overleftarrow{N}$, the filtered prediction error $\varepsilon_{f,i}(t)$ by solving the difference equation

$$D_i^*(d)\,\varepsilon_{f,i}(t) = \varepsilon(t)\,. \tag{7.6}$$

Then, supposing that at time t the switching signal $\overline{\sigma}(t)$ takes on value j, we let

$$\tilde{u}(t) = \begin{cases} N_j^*(d)\,\varepsilon_{f,j}(t) & \text{if } \sigma(t) = j \\ N_j(d, \rho_{j,\ell}^\circ)\,\varepsilon_{f,j}(t) & \text{if } \sigma(t) = N+1 \end{cases}. \tag{7.7}$$

The following results state that such an implementation ensures internal stability, provided that the parameter vector $\rho_{j,\ell}^\circ$ is bounded. We recall from Chapter 6 that the internal stability of the feedback interconnection $(\mathcal{P}/\mathcal{C}_{\sigma(t)})$ means that all the signals in the system remain bounded for any bounded disturbance ν.

Theorem 7.2.1. *Let the multi-controller $\mathcal{C}_{\sigma(t)}$ be implemented as in (7.4)-(7.7). Then, when $\overline{\sigma}(t) = j$, the frozen-time transfer function between $y(t)$ and $u(t)$ coincides either with $-C_j^*(d)$ if $\sigma(t) = j$ or with $-C_\ell^\circ(d)$ if $\sigma(t) = N+1$.*
Further, if for any $i \in \overleftarrow{N}$ the set $\mathcal{R}_i$ is bounded, then the switching system $(\mathcal{P}/\mathcal{C}_{\sigma(t)})$ is internally stable for any switching signal σ.

Proof: see the Appendix. □

Since each set $\mathcal{R}_i$, to which the parameter vector ρ_i belongs, can be freely chosen by the designer, the conditions of Theorem 7.2.1 can be easily satisfied in practice. For instance, if we denote by $\|\cdot\|$ the Euclidean norm, one can simply let $\mathcal{R}_i = \{\rho_i \in \mathbb{R}^{n_{\rho_i}} : \|\rho_i\|^2 \leq K\}$, where the bound K has to be chosen large enough so that the controllers belonging to the

resulting parametric family can ensure a satisfactory performance level in response to the class of disturbances of interest. Further, instead of imposing a common bound K, a different bound K_i can be chosen with respect to each $\mathcal{R}_i$, that is, $\mathcal{R}_i = \{\rho_i \in \mathbb{R}^{n_{\rho_i}} : \|\rho_i\|^2 \leq K_i\}$.

Remark 7.2.1. We underline that the same implementation for the switching system $\mathcal{Q}_{\sigma(t)}$ as in Chapter 6 could be adopted in principle; however, the use of the one described in terms of (7.6)-(7.7) avoids the necessity of computing an appropriate realization for the Youla parameter related to the controller $\mathcal{C}_\ell^o$ such that a common Lyapunov function exists (recall Theorem 6.1.1), thus reducing the computational burden of the proposed algorithm. Further, this specific implementation allows the proposed scheme to achieve an arbitrary attenuation level in the presence of particular classes of disturbances (see the results of Section 7.3.1 and specifically Corollary 7.3.1).

7.3 Choice of the functionals and attenuation properties

The test functionals $\Pi_i(t)$, $i \in \overleftarrow{N}$, are computed in order to evaluate the potential performance related to each controller $\mathcal{C}_i$. A possible definition for $\Pi_i(t)$, $i \in \overleftarrow{N}$, is the one provided in Chapter 4. Specifically, in the proposed framework, we adopt the same definition with the particular choice of the value zero for the parameter η, which appears in (4.5), in order to derive the results shown in Section 7.3.1 and thus to ensure an arbitrary attenuation level in the presence of particular classes of disturbances; thus in practice

$$\Pi_i(t) := \begin{cases} \dfrac{\| y_i|_{t-M(t)}^t \|}{\| \varepsilon|_{t-M(t)}^t \|}, & \text{if } \| \varepsilon|_{t-M(t)}^t \| > 0 \\ \\ 0\,, & \text{if } \| \varepsilon|_{t-M(t)}^t \| = 0 \end{cases} . \tag{7.8}$$

Similarly to the line of reasoning followed in Chapter 4, by computing $\Pi_i(t)$ as defined in (7.8), we aim at evaluating the potential performance associated with each controller $\mathcal{C}_i$, $i \in \overleftarrow{N}$, in terms of the plant output hypothetical response y_i to the disturbance ν by means of the i-th disturbance-to-output transfer function

$$\Sigma_i(d) = \frac{R_i^*(d)}{\chi_i(d)}\,. \tag{7.9}$$

Notice that, in terms of the adopted Youla-Kucera parametrization of the controllers, $\Sigma_i(d)$ can be expressed as

$$\Sigma_i(d) = \frac{1}{D_i^*(d)} \left[R_0(d) D_i^*(d) - B(d) N_i^*(d) \right] . \tag{7.10}$$

We recall that the prediction error ε computed as in (7.5) is such that $\varepsilon(t) \equiv \nu(t)$ for any $t \geq n = \max\{n_a, n_b\}$. Hence, y_i can be obtained as

$$y_i(t) = \frac{1}{D_i^*(d)} \left[R_0(d) D_i^*(d) - B(d) N_i^*(d) \right] \varepsilon(t) . \tag{7.11}$$

In practice, we can exploit the filtered prediction error defined in (7.6) and compute y_i as

$$y_i(t) = R_0(d)\varepsilon(t) - B(d) N_i^*(d) \varepsilon_{f,i}(t) , \tag{7.12}$$

starting from the time instant $t_0 \geq n$ at which the switching logic is activated.

As regards the tuning procedure, the aim is that of computing a local refinement of the controller $\mathcal{C}_j$ which has been selected by the switching rule SL_1. In view of the definitions in (7.10)-(7.12), a possible choice for the optimization criterion at time t_ℓ is as follows:

$$J_\ell(\rho_j) = \| R_0(d)\varepsilon|_{t_\ell - I}^{t_\ell} - B(d) N_j(d, \rho_j) \varepsilon_{f,j}|_{t_\ell - I}^{t_\ell} \|^2 , \tag{7.13}$$

with I a specified time interval and $\varepsilon_{f,j}$ the filtered prediction error related to the controller $\mathcal{C}_j$. Notice that J_ℓ in (7.13) is defined in terms of the norm, computed on the time interval $[t_\ell - I, t_\ell]$, of the hypothetical output signal $y_j(t, \rho_j)$ depending on ρ_j and defined as

$$y_j(t, \rho_j) = R_0(d)\varepsilon(t) - B(d) N_j(d, \rho_j) \varepsilon_{f,j}(t) . \tag{7.14}$$

For $\rho_j = \rho_j^*$, it turns out that $y_j(t, \rho_j^*)$ coincides with the signal $y_j(t)$ defined in (7.12); the understanding is that, even though the time intervals involved in (7.8) and (7.13) are different, in both the performance evaluation (by means of the test functional Π_i) and the tuning procedure (by means of the optimization of J_ℓ) the aim is that of determining the control configuration which minimizes the effects of the disturbance ν on the system output. Further we can notice that, if we let $N_j(d, \rho_j)$ depend linearly on ρ_j, i.e. $N_j(d, \rho_j) = \varphi_j(d)^\top \rho_j$, where $\varphi_j := [1,\, d,\, \cdots, d^{n_{\rho_j}-1}]^\top$, then the functional $J_\ell(\rho_j)$ is quadratic.

The test functional $\Pi_{N+1}(t)$ for the optimized controller $\mathcal{C}_\ell^\circ$ is defined as in (7.8) with $y_i(t)$ replaced by $y_j(t, \rho_{j,\ell}^\circ)$ for any $t \in [t_\ell^* - M(t), t_{\ell+1}^* - 1]$.

Remark 7.3.1. As discussed in Section 4.1.1, several choices for the memory $M(t)$ are possible. Specifically, in the proposed framework we refer to a finite memory defined as in (4.8).

7.3.1 Analysis of the attenuation properties

For the results presented in this section, we will refer to the following assumptions.

A1. There exists a finite time $\overline{t}_f$ after which $\overline{\sigma}(t)$ remains constant, *i.e.*, $\overline{\sigma}(t) = j$ for any $t \geq \overline{t}_f$.

A2. The disturbance $\nu(t)$ in (4.1) can be expressed as the output of an autoregressive model

$$\Delta(d)\nu(t) = 0\,, \tag{7.15}$$

with $\Delta(d)$ having all simple roots on the unit circle.

A3. For any $i \in \overleftarrow{N}$, there exists a parameter vector $\hat{\rho}_i \in \mathcal{R}_i$ such that the controller with transfer function $C_i(d, \hat{\rho}_i)$ perfectly rejects the disturbance $\nu(t)$.

Sufficient conditions for assumption **A1** to hold, depending on the disturbance characteristics and on the choice of the parameters M_* and $\overline{h}$, can be found in Chapter 4.

Under assumptions **A1**-**A3**, we can show that the proposed algorithm is able to attenuate the effects of the disturbance $\nu(t)$ expressed as the output of the model (7.15) with a desired attenuation level.

Lemma 7.3.1. *Let assumptions **A1**-**A3** hold and suppose that an infinite number of optimizations is performed. Then*

$$J_\ell(\rho^o_{j,\ell}) \xrightarrow[\ell\to\infty]{} 0\,. \tag{7.16}$$

Proof: see the Appendix. □

In the results that follow we denote by ∂p the degree of a generic polynomial $p(d)$.

Lemma 7.3.2. *Let assumptions **A1**-**A3** hold and suppose that an infinite number of optimizations is performed. If $I \geq M_* + \partial\Delta + \partial D^*_j$ and $M_* > \partial\Delta$, then*

$$\Pi_{N+1}(t) \xrightarrow[t\to\infty]{} 0\,. \tag{7.17}$$

Proof: see the Appendix. □

The results shown in Lemma 7.3.1 and in Lemma 7.3.2 are useful to prove the following theorem.

Theorem 7.3.1. *Let assumptions **A1**-**A3** hold; further, suppose that* $I \geq M_* + \partial\Delta + \partial D_j^*$, $M_* > \partial\Delta$, *and* $h > \gamma$. *Then the following facts hold.*

i) Only a finite number $\overline{\ell}$ *of optimizations is performed and the final optimized controller with transfer function* $C_j(d, \rho^o_{j,\overline{\ell}})$ *is such that* $\Pi_{N+1}(t) \leq \gamma$ *for any* $t > t^*_{\overline{\ell}}$.

ii) There exists a finite time t_f *after which* $\sigma(t)$ *remains constant, i.e.,* $\sigma(t) = \mu$ *for any* $t \geq t_f$. *In addition,*

$$\Pi_\mu(t) \leq h + \gamma \tag{7.18}$$

for any $t \geq t_f$.

Proof: see the Appendix. □

Notice that the attenuation level in (7.18) can be made arbitrarily small by suitably decreasing the parameters h and γ. While $\Pi_\mu(t)$ is designed to measure the potential performance, when the same controller is kept in the loop for a sufficiently long time then $\Pi_\mu(t)$ will also reflect the true performance of the feedback loop.

Corollary 7.3.1. Let the same assumptions as in Theorem 7.3.1 hold. Then, for $t \geq t_f + M_* + \partial B$,

$$\|y|^t_{t-M_*}\| \leq (h+\gamma)\|\nu|^t_{t-M_*}\| \tag{7.19}$$

holds.

Proof: see the Appendix. □

7.4 Simulation results

The simulation results provided in this section refer to the quarter-car model introduced in Chapter 2, with the parameters shown in Table 2.1.

Controller	Frequency range
$\mathcal{C}_1$	$\Omega_1 = [0,\, 5)\, Hz$
$\mathcal{C}_2$	$\Omega_2 = [5,\, 8)\, Hz$
$\mathcal{C}_3$	$\Omega_3 = [8,\, 10)\, Hz$

Table 7.2: Frequency ranges Ω_i , $i = 1, 2, 3$.

We assume that the disturbance power spectral density is in the frequency range $\Omega = [0,\, 10]\, Hz$; as for the finite set $\mathscr{C}$, we synthesize three controllers $\mathcal{C}_i$, $i = 1, 2, 3$, each one designed so as to guarantee a desired attenuation level in a subset $\Omega_i \subset \Omega$ (see Table 7.2). Specifically, the transfer function of each controller $\mathcal{C}_i$ is parametrized in terms of (6.2), with $N_i(d) = N_i^*(d)$ an affine function of a parameter vector ρ_i, *i.e.*, $N_i^*(d) = \varphi^\top(d)\rho_i^*$ and $D_i(d) = D_i^*(d)$ a fixed polynomial (different for each $i \in \overleftarrow{N}$), chosen so that a satisfactory transient behavior is ensured. The controller $\mathcal{C}_0$ with transfer function $C_0(d) = S_0(d)/R_0(d)$ is obtained by solving the Bezout identity (6.1), imposing that both $S_0(d)$ and $R_0(d)$ are polynomials of degree 3. Then, the following optimization problem is solved

$$\min_{\gamma,\rho_i} \gamma \tag{7.20}$$

s.t.

$$|\overline{\Sigma}_{i,1}(e^{-j\omega}, \rho_i)|^2 < \gamma \quad \forall \omega \in \Omega_i \tag{7.21}$$

$$|\overline{\Sigma}_{i,2}(e^{-j\omega}, \rho_i)|^2 < \delta \quad \forall \omega \in \Omega_i\,, \tag{7.22}$$

where

$$\overline{\Sigma}_{i,1}(d, \rho_i) = A(d)[R_0(d)D_i^*(d) - B(d)\varphi^\top(d)\rho_i]/D_i^*(d) \tag{7.23}$$

$$\overline{\Sigma}_{i,2}(d, \rho_i) = A(d)[S_0(d)D_i^*(d) + A(d)\varphi^\top(d)\rho_i]/D_i^*(d)\,. \tag{7.24}$$

Fig. 7.1 shows the transfer functions from $\overline{n}$ to y_1, related to each of the controllers.

We set $\overline{h} = 7 \times 10^{-3}$ in (7.1); $M_* = 2000$ time samples in (4.8); $I = 2500$ time samples in (7.13). The time interval T_L is set equal to M_*.

We first consider a disturbance n made up of the superposition of two sinusoidal signals having frequency $3\, Hz$ and $6.4\, Hz$, respectively, and magnitude $0.1\, m$ and $0.05\, m$,

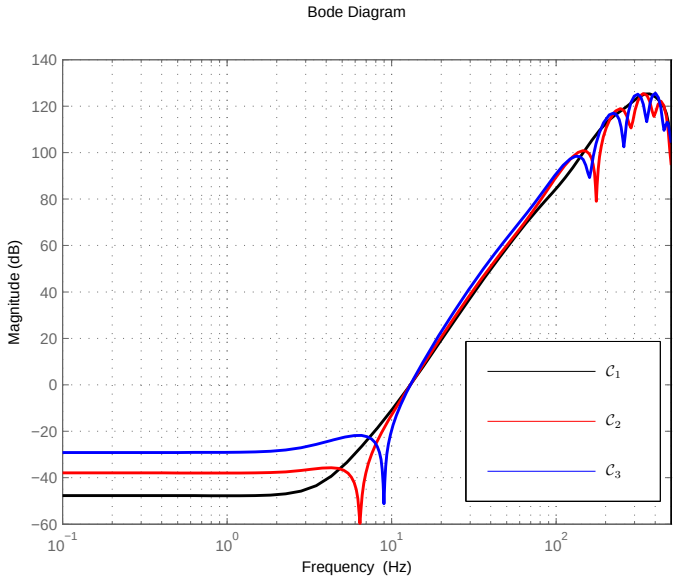

Figure 7.1: Bode diagram of the the transfer functions from $\overline{n}$ to y_1 related to the controllers $\mathcal{C}_i$, $i = 1, 2, 3$.

respectively. In Fig. 7.2 we can notice that the controller $\mathcal{C}_j$ in $\mathscr{C}$ achieving the best potential performance is quickly selected by the supervisory unit in accordance with SL_1; then, a local refinement of $\mathcal{C}_j$ is iteratively computed and selected by the supervisor according to SL_2, thus improving the achieved attenuation level.

Further, we consider a signal generated as the output of a filter having a zero-mean white noise as input (the Fourier Transform of the resulting signal is shown in Fig. 7.3); the disturbance n is now generated by adding this signal to the disturbance considered in the previous test. The results obtained from this simulation are shown in Fig. 7.4. As can be noticed, after selecting the controller C_j, the proposed method is able to further improve the achieved performance level even in this case.

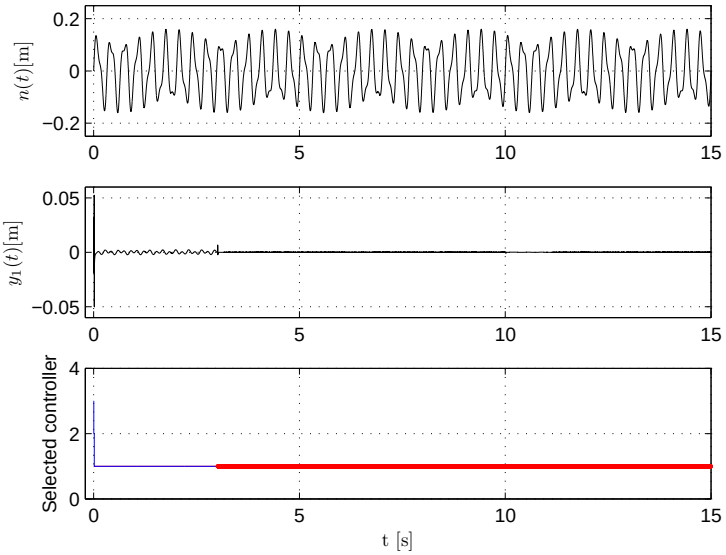

Figure 7.2: Response $y_1(t)$ to a road excitation $n(t)$ composed of the sum of two sinusoidal signals. With respect to the selected controller, the blue thin line represents $\overline{\sigma}(t)$, while the superimposed red thick line indicates the time instants in which the optimized controller is selected by the SL_2.

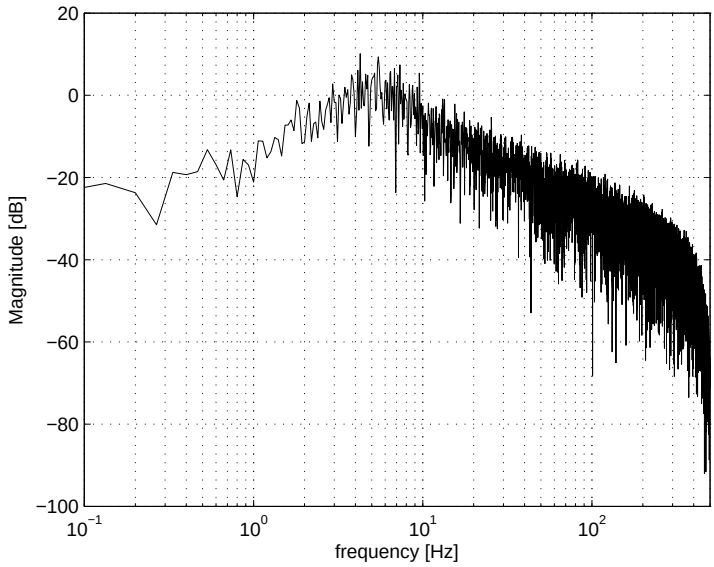

Figure 7.3: Magnitude of the Fourier Transform of the signal obtained as the output of a filter having a zero-mean white noise as input.

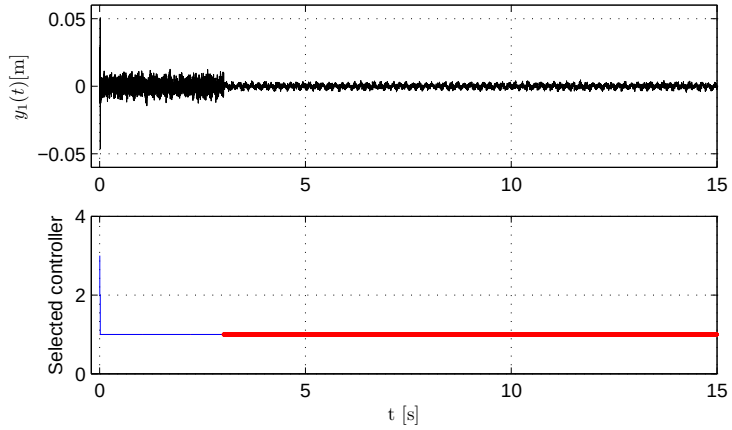

Figure 7.4: Response $y_1(t)$ to a road excitation $n(t)$ composed of the sum of two sinusoidal signals and a filtered white noise. With respect to the selected controller, the blue thin line represents $\overline{\sigma}(t)$, while the superimposed red thick line indicates the time instants in which the optimized controller is selected by the SL_2.

7.A Appendix: Proofs

Proof of Theorem 7.2.1. The fact that, when $\overline{\sigma}(t) = j$, the transfer function between $y(t)$ and $u(t)$ coincides either with $-C_j^*(d)$ if $\sigma(t) = j$ or with $-C_j(d, \rho_{j,\ell}^\circ)$ if $\sigma(t) = N+1$ follows directly from the implementation described in (7.4), (7.5), (7.6) and (7.7).
The proof of the internal stability of the switching system $(\mathcal{P}/\mathcal{C}_{\sigma(t)})$ is shown in the following steps. We can compute $y(t)$ and $u(t)$ from (4.1), (6.1), (7.4) and (7.5). In fact

$$\begin{aligned} A(d)y(t) &= B(d)u(t) + \nu(t) \\ &= B(d)\overline{u}(t) - B(d)\tilde{u}(t) + \nu(t) \\ &= B(d)[1 - R_0(d)]u(t) - B(d)\tilde{u}(t) - B(d)S_0(d)y(t) + \nu(t) \\ &= B(d)u(t) - R_0(d)[A(d)y(t) - \nu(t)] - B(d)S_0(d)y(t) - B(d)\tilde{u}(t) + \nu(t)\,. \end{aligned}$$

Thus one obtains

$$[A(d)R_0(d) + B(d)S_0(d)]y(t) = -B(d)\tilde{u}(t) + R_0(d)\nu(t)$$

which, by recalling (6.1), yields

$$y(t) = -B(d)\tilde{u}(t) + R_0(d)\nu(t)\,. \tag{7.25}$$

Similarly,

$$u(t) = -A(d)\tilde{u}(t) - S_0(d)\nu(t)\,. \tag{7.26}$$

Thus the signals $u(t)$ and $y(t)$ are bounded, provided that $\tilde{u}(t)$ is bounded (recall that $\nu(t)$ is bounded). The boundedness of $\tilde{u}(t)$ follows from (7.6) and (7.7). In fact, each filtered prediction error $\varepsilon_{f,i}(t)$ is bounded, since it is computed by filtering the bounded signal $\varepsilon(t)$ by means of a stable filter $1/D_i^*(d)$; further, $\tilde{u}(t)$ is a moving average of $\varepsilon_{f,i}(t)$ as shown in (7.7). Thus $\tilde{u}(t)$ is bounded, provided that the coefficients of both $N_j^*(d)$ (if $\sigma(t) = j$) and $N_j(d, \rho_{j,\ell}^\circ)$ (if $\sigma(t) = N+1$) are bounded. The former case is related to the synthesis of the controllers within the finite family $\mathscr{C}$, while the latter is ensured provided that the set $\mathcal{R}_i$ is bounded for any $i \in \overleftarrow{N}$. □

Proof of Lemma 7.3.1. With respect to the parameter vector $\hat{\rho}_j$ defined in assumption **A3**, by letting $\ell \to \infty$ it is possible to assert that

$$J_\ell(\hat{\rho}_j) \xrightarrow[\ell\to\infty]{} 0\,. \tag{7.27}$$

Further, thanks to the optimality of $\rho^o_{j,\ell}$, the following holds:

$$0 \leq J_\ell(\rho^o_{j,\ell}) \leq J_\ell(\hat{\rho}_j)\,, \tag{7.28}$$

from which (7.16) follows straightforwardly. □

Proof of Lemma 7.3.2. By assumption **A2**, when $M_* > \partial\Delta$ and ν is not identically null, the denominator of $\Pi_{N+1}(t)$ can be bounded from below. As for the numerator, the signal $y_j(k, \rho^o_{j,\ell})$ is computed as

$$y_j(k, \rho^o_{j,\ell}) = R_0(d)\varepsilon(k) - B(d)N_j(d, \rho^o_{j,\ell})\varepsilon_{f,j}(k)\,. \tag{7.29}$$

Multiplying both sides of (7.29) by the polynomial $\Delta(d)D^*_j(d)$ and recalling (7.6), the following identities hold:

$$\begin{aligned}
&\Delta(d)D^*_j(d)y_j(k, \rho^o_{j,\ell}) = \\
&\Delta(d)D^*_j(d)[R_0(d)\varepsilon(k) - B(d)N_j(d, \rho^o_{j,\ell})\varepsilon_{f,j}(k)] = \\
&D^*_j(d)R_0(d)\Delta(d)\varepsilon(k) - B(d)N_j(d, \rho^o_{j,\ell})\Delta(d)D^*_j(d)\varepsilon_{f,j}(k) = \\
&D^*_j(d)R_0(d)\Delta(d)\varepsilon(k) - B(d)N_j(d, \rho^o_{j,\ell})\Delta(d)\varepsilon(k)\,,
\end{aligned} \tag{7.30}$$

from which, for $k \geq t_0$ and recalling (7.15), one obtains

$$\begin{aligned}
&\Delta(d)D^*_j(d)y_j(k, \rho^o_{j,\ell}) = \\
&D^*_j(d)R_0(d)\Delta(d)\nu(k) - B(d)N_j(d, \rho^o_{j,\ell})\Delta(d)\nu(k) = 0\,.
\end{aligned} \tag{7.31}$$

Thus, it can be seen from the previous steps that the signal $y_j(k, \rho^o_{j,\ell})$ satisfies the following autoregressive model

$$\Delta(d)D^*_j(d)y_j(k, \rho^o_{j,\ell}) = 0\,, \tag{7.32}$$

whose state is defined as $x(k) := [y_j(k-1, \rho^o_{j,\ell})\ y_j(k-2, \rho^o_{j,\ell})\ \cdots\ y_j(k - \partial\Delta D^*_j, \rho^o_{j,\ell})]^\top$, with $\partial\Delta D^*_j$ the degree of the polynomial $\Delta(d)D^*_j(d)$. The recursion in (7.32) can be initialized at time t_ℓ. Recall that $\Delta(d)$ has all the roots on the unit circle and $D^*_j(d)$ is stable by construction. Thus the following holds:

$$|y_j(k, \rho^o_{j,\ell})|^2 \leq \xi \|x(t_\ell)\|^2\,, \tag{7.33}$$

with ξ a nonnegative constant and

$$\|x(t_\ell)\|^2 = \sum_{h=t_\ell - \partial\Delta D^*_j}^{t_\ell - 1} |y_j(h, \rho^o_{j,\ell})|^2\,. \tag{7.34}$$

Appendix: Proofs

If $I \geq M_* + \partial\Delta + \partial D_j^*$, then for any $k \in [t_\ell^* - M(t), t_{\ell+1}^* - 1]$

$$|y_j(k, \rho_{j,\ell}^o)|^2 \leq \xi J_\ell(\rho_{j,\ell}^o)\,, \tag{7.35}$$

with $J_\ell(\rho_{j,\ell}^o) \to 0$ as $\ell \to \infty$ (recall Lemma 7.3.1), which means, equivalently, that $J_\ell(\rho_{j,\ell}^o) \to 0$ as $t \to \infty$. Thus the validity of (7.17) is proved. □

Proof of Theorem 7.3.1. Fact i) follows straightforwardly from (7.17) and from the fact that no novel optimization is run if condition (7.2) is satisfied, as shown in the outline of the Algorithm 7.1.1 in Section 7.1.1.

With respect to Fact ii), suppose first that $\sigma(t) = \overline{\sigma}(t)$ holds true for any $t \geq \tilde{t}$, with $\tilde{t} > t_{\overline{\ell}}^*$. This means that

$$\Pi_{\overline{\sigma}(t)}(t) - h \leq \Pi_{N+1}(t) \tag{7.36}$$

with $\Pi_{N+1}(t) \leq \gamma$ as shown in Fact i). Thus, according to (7.3), $\sigma(t+1) = \overline{\sigma}(t)$ for any $t \geq \tilde{t}$, and (7.18) holds with $\mu = \overline{\sigma}(t)$.

On the contrary, suppose that there exists a time instant $\hat{t} > t_{\overline{\ell}}^*$ such that $\sigma(\hat{t}) = N+1$. Since $h > \gamma$ and $\Pi_{N+1}(\hat{t}) \leq \gamma$, it follows that $\Pi_{N+1}(\hat{t}) - h < 0$. We recall that $\Pi_{\sigma(\hat{t})} \geq 0$ by construction; then, according to (7.3),

$$\sigma(\hat{t}+1) = N+1\,, \tag{7.37}$$

thus proving that, for any $t \geq \hat{t}$, $\sigma(t) = N+1$; in addition, (7.18) holds with $\mu = N+1$.

In both cases, t_f can be identified as the final switching instant. □

Proof of Corollary 7.3.1. The proof follows by comparing the expressions of $y(t)$ and $y_j(t, \rho_j)$

$$\begin{aligned} y(t) &= -B(d)\tilde{u}(t) + R_0(d)\nu(t) \\ &= -B(d)\tilde{u}(t) + R_0(d)\varepsilon(t) \\ &= -B(d)N_j(d, \rho_j)\varepsilon_{f,j}(t) + R_0(d)\varepsilon(t) \quad \text{for } t \geq t_f + \partial B\,, \qquad (7.38) \\ y_j(t, \rho_j) &= -B(d)N_j(d, \rho_j)\varepsilon_{f,j}(t) + R_0(d)\varepsilon(t)\,, \qquad (7.39) \end{aligned}$$

where ρ_j can be either the parameter vector ρ_j^* if $\sigma(t) = j$ or $\rho_{j,\ell}^\circ$ if $\sigma(t) = N+1$. Thus, recalling (7.7), once ∂B time instants have elapsed after t_f we have that $y(t)$ and $y_j(t, \rho_j)$ coincide. Finally, (7.19) follows from Theorem 7.3.1 after additional M_* time instants have elapsed. □

Conclusions and future work

In this work, the problem of active disturbance attenuation has been addressed, and solutions have been proposed with specific focus on the performance of the control system, as well as on stability under arbitrary switching.

In particular, the aim of providing a control scheme able to *reconfigure* its action in real-time has been addressed by means of an Adaptive Switching Control (ASC) approach. In ASC, a finite family of candidate controllers is pre-synthesized off-line, and a supervisory logic has to select the potentially best one to be put in feedback with the plant. This mechanism relies on the use of test functionals which are computable in real-time and reflect the potential behavior of the candidate controllers. A detailed analysis of the properties of the test functionals is provided in Chapter 4. Further, the problem of stability of the overall closed-loop system has been addressed, and two different solutions have been proposed in Chapters 5 and 6. Specifically, the method described in Chapter 5 accounts for the stability requirement directly within the synthesis of the controller family. It has been pointed out that this allows the complexity of the multi-controller architecture to be independent of the plant order, but the inclusion in the synthesis step of a constraint related to the switching mechanism affects the modularity which is typical of the ASC paradigm. On the other hand, the method described in Chapter 6 relies on a specific implementation of the multi-controller based on a switching mechanism between the Youla parameters related to the candidate controllers. This solution completely preserves the modularity of the switching control approach, even if the complexity of the adopted architecture is unavoidably influenced by the plant order.

The ASC paradigm has emerged as an alternative solution to classical Adaptive Control. The ASC approach is more suitable to quickly achieve satisfactory performance and to deal with abrupt changes in the uncertain disturbance characteristics, provided that

the supervisor is able to select in a short time the potentially best controller; however, the attenuation level achievable by the pre-synthesized controllers in the finite set determines the performance that can be achieved by the overall control scheme. On the other hand, classical adaptive techniques based on parameter tuning can usually achieve better performance levels in the long run, but it is possible that the tuning procedure requires a non-negligible time interval before achieving a satisfactory behavior. With this respect, as an extension of the proposed solution to the problem of active disturbance attenuation based on the ASC paradigm, an algorithm has been proposed (and described in Chapter 7) combining both switching and tuning, aiming at preserving the beneficial features of the two different approaches, while possibly overcoming the mentioned drawbacks.

The effectiveness of the proposed solutions is validated by means of simulation tests performed in the contexts of two case studies, namely an active suspension system and an adaptive optics system.

A final remark is devoted to possible future perspectives arising from this work. First of all, since in our framework it has been assumed that the plant model is known, an interesting extension would be to account for plant model uncertainty within the proposed control solutions.
Further, it has been pointed out that the technique described in Chapter 5 is not guaranteed to provide a feasible solution to the optimization problem to be solved in order to find a common quadratic Lyapunov function for the closed-loop systems. Thus, it would be interesting to find a suitable formulation of the problem accounting for stability within the synthesis step and always ensuring the existence of a feasible solution.

Bibliography

[1] G. Agapito, S. Baldi, G. Battistelli, D. Mari, E. Mosca, and A. Riccardi. Automatic tuning of the internal position control of an adaptive secondary mirror. *European Journal of Control*, 17(3):273–289, 2011.

[2] G. Agapito, G. Battistelli, D. Mari, D. Selvi, A. Tesi, and P. Tesi. Frequency based design of modal controllers for adaptive optics systems. *Optics Express*, 20(24):27108–27122, 2012.

[3] G. Agapito, G. Battistelli, D. Mari, D. Selvi, A. Tesi, and P. Tesi. Frequency-based design of Adaptive Optics Systems. *Proceedings of the Third AO4ELT Conference - Adaptive Optics for Extremely Large Telescopes, Florence, Italy*, pages 1–8, 2013.

[4] G. Agapito, F. Quiros-Pacheco, P. Tesi, S. Esposito, and M. Xompero. Optimal control techniques for the adaptive optics system of the LBT. *Proc. SPIE*, 7015:70153G, 2008.

[5] G. Agapito, F. Quiros-Pacheco, P. Tesi, A. Riccardi, and S. Esposito. Observer-based control techniques for the LBT adaptive optics under telescope vibrations. *European Journal of Control*, 17(3):316–326, 2011.

[6] T. B. Airimitoaie, A. Castellanos Silva, and I. D. Landau. Indirect adaptive regulation strategy for the attenuation of time varying narrow-band disturbances applied to a benchmark problem. *European Journal of Control*, 19(4):313–325, 2013.

[7] T. B. Airimitoaie and I. D. Landau. Indirect adaptive attenuation of multiple narrow-band disturbances applied to active vibration control. *IEEE Transactions on Control Systems Technology*, 22(2):761–769, 2014.

[8] T. B. Airimitoaie and I.D. Landau. Improving adaptive feedforward vibration compensation by using "Integral + Proportional" adaptation. *Automatica*, 49(5):1501–1505, 2013.

[9] F. B. Amara, P. T. Kabamba, and A. G. Ulsoy. Adaptive sinusoidal disturbance rejection in linear discrete-time systems–Part I: Theory. *Journal of Dynamic Systems, Measurement, and Control*, 121:648–654, 1999.

[10] F. B. Amara, P. T. Kabamba, and A. G. Ulsoy. Adaptive sinusoidal disturbance rejection in linear discrete-time systems–Part II: Experiments. *Journal of Dynamic Systems, Measurement, and Control*, 121:655–659, 1999.

[11] F. A. Ansari and R. Taparia. Modeling, analysis and control of active suspension system using sliding mode control and disturbance observer. *International Journal of Scientific and Research Publications*, 3(1):1–6, 2013.

[12] P. Arcara, S. Bittanti, and M. Lovera. Periodic control of helicopter rotors for attenuation of vibrations in forward flight. *IEEE Transactions on Control Systems Technology*, 8:883–894, 2000.

[13] K.J. Aström and B. Wittenmark. *Adaptive Control*. Addison-Wesley Publishing Cokmpany, 1995.

[14] S. Baldi, G. Battistelli, D. Mari, E. Mosca, and P. Tesi. Multi-model adaptive switching control with fine controller tuning. *Proceedings of the 18th IFAC World Congress*, 2011.

[15] S. Baldi, G. Battistelli, E. Mosca, and P. Tesi. Multi-model unfalsified adaptive switching supervisory control. *Automatica*, 46(2):249–259, 2010.

[16] G. Battistelli, J. P. Hespanha, E. Mosca, and P. Tesi. Model-free adaptive switching control of time-varying plants. *IEEE Transactions on Automatic Control*, 58(5):1208–1220, 2013.

[17] G. Battistelli, J. P. Hespanha, and P. Tesi. Supervisory control of switched nonlinear systems. *International Journal of Adaptive Control and Signal Processing*, 26(8):723–738, 2012.

[18] G. Battistelli, A. Karimi, D. Selvi, and A. Tesi. Design of a switching controller for adaptive disturbance attenuation with guaranteed stability. *submitted*, 2014.

[19] G. Battistelli, D. Mari, D. Selvi, A. Tesi, and P. Tesi. Adaptive disturbance attenuation via logic-based switching. *Systems & Control Letters*, 73:48–57, 2014.

[20] G. Battistelli, D. Mari, D. Selvi, A. Tesi, and P. Tesi. A Hierarchical Approach to Adaptive Disturbance Attenuation Combining Switching and Tuning. *Proceedings of the 53rd IEEE Conference on Decision and Control, Los Angeles, California, USA*, pages 6254–6259, 2014.

[21] G. Battistelli, D. Mari, D. Selvi, A. Tesi, and P. Tesi. Switching Control for Adaptive Disturbance Attenuation. *Proceedings of the 19th IFAC World Congress*, pages 1483–1488, 2014.

[22] G. Battistelli, E. Mosca, and P. Tesi. Adaptive memory in multi-model switching control of uncertain plants. *Automatica*, 50:874–882, 2014.

[23] L. Beranek and I. Ver. *Noise and vibration control engineering: Principles and applications*. NewYork: Wiley, 1992.

[24] M. Bodson and S. C. Douglas. Adaptive algorithms for the rejection of sinusoidal disturbances with unknown frequency. *Automatica*, 33:2213–2221, 1997.

[25] M. Born and E. Wolf. *Principles of Optics*. Cambridge University Press, Cambridge, U.K., 1980.

[26] C. Canudas de Wit and L. Praly. Adaptive eccentricity compensation. *IEEE Transactions on Control Systems Technology*, 8:757–766, 2000.

[27] A. Castellanos Silva, I. D. Landau, and T. B. Airimitoaie. Direct adaptive rejection of unknown time-varying narrow band disturbances applied to a benchmark problem. *European Journal of Control*, 19(4):326–336, 2013.

[28] L. Close, V. Gasho, D. Kopon, J. Males, K.B. Follette, K. Brutlag, A. Uomoto, and T. Hare. The Magellan telescope adaptive secondary AO system: a visible and mid-IR AO facility. *Proc. SPIE*, 7736:773605, 2010.

[29] J.-M. Conan, C. Kulcsár, and H.-F. Raynaud. Adaptive optics control for ground based telescopes. *European Journal of Control (Special Issue, Lavoisier)*, 17(3):219–334, 2011.

[30] C. Correia, H.F. Raynaud, and C. Kulcsar, and J.M. Conan. Minimum-variance control for astronomical adaptive optics with resonant deformable mirrors. *Eur. J. Control*, 17(3):222–236, 2011.

[31] C. Dessenne, P.-Y. Madec, and G. Rousset. Optimization of a predictive controller for closed-loop adaptive optics. *Applied Optics*, 37(21):4623–4633, 1998.

[32] Z. Ding. Global stabilization and disturbance suppression of a class of nonlinear systems with uncertain internal model. *Automatica*, 39:471–479, 2003.

[33] J. Doyle, B. Francis, and A. Tannenbaum. *Feedback Control Theory*. Macmillan Publishing Company, 1992.

[34] S. J. Elliot and P. A. Nelson. Active noise control. *Noise/NewsInternational*, 2(2), 1994.

[35] S. J. Elliot and T. J. Sutton. Performance of feedforward and feedback systems for active control. *IEEE Transactions on Speech and Audio Processing*, 4(3), 1996.

[36] Z. Emedi and A. Karimi. Robust fixed-order disctrete-time LPV controller design. *Proceedings of the 19th IFAC World Congress*, 2014.

[37] S. Esposito, E. Pinna, F. Quirós-Pacheco, A. Puglisi, L. Carbonaro, M. Bonaglia, V. Biliotti, R. Briguglio, G. Agapito, C. Arcidiacono, L. Busoni, M. Xompero, A. Riccardi, L. Fini, and A. Bouchez. Wavefront sensor design for the GMT natural guide star ao system. *Proc. SPIE*, 8447:84471L, 2012.

[38] S. M. Fayyad. Constructing control system for active suspension system. *Contemporary Engineering Sciences*, 5(4), 2012.

[39] R. Fedrigo, E. Muradore and D. Zillo. High performance adaptive optics system with fine tip/tilt control. *Control Eng. Pract*, 17(1):122–135, 2009.

[40] C. R. Fuller, S. J. Elliot, and P. A. Nelson. *Active control of vibration*. NewYork: Academic Press, 1995.

[41] S.F. Graebe G.C. Goodwin and M.E. Salgado. *Control system design*. Prentice Hall, 2001.

[42] E. Gendron and P. Lena. Modal control optimization. *Astron. Astrophys.*, 291:337–347, 1994.

[43] J. C. Geromel and P. Colaneri. Stability and stabilization of discrete time switched systems. *International Journal of Control*, 79(7):719–728, 2006.

[44] J. Herrmann. Phase variance and strehl ratio in adaptive optics. *J. Opt. Soc. Am. A*, 9:2257–2258, 1992.

[45] J. P. Hespanha, D. Liberzon, and A. S. Morse. Hysteresis-based switching algorithms for supervisory control of uncertain systems. *Automatica*, 39:263–272, 2003.

[46] J. P. Hespanha, D. Liberzon, and A. S. Morse. Overcoming the limitations of adaptive control by means of logic-based switching. *Systems & Control Letters*, 49:49–65, 2003.

[47] J.P. Hespanha and A.S. Morse. Switching between stabilizing controllers. *Automatica*, 38:1905–1917, 2002.

[48] K. Hinnen, M. Verhaegen, and N. Doelman. A data-driven H_2-optimal control approach for adaptive optics. *IEEE Trans. Control Syst. Technol*, 16(3):381–395, 2008.

[49] K. Hoffman. *Banach Spaces of Analytic Functions*. Englewood Cliffs, NJ: Prentice-Hall, 1962.

[50] P. A. Ioannou and B. Fidan. *Adaptive Control Tutorial*. SIAM, 2006.

[51] P.A. Ioannou and J. Sun. *Robust Adaptive Control*. Prentice-Hall, Upper Saddle River, NJ, 1996.

[52] S. Jafari, P. Ioannou, B. Fitzpatrick, and Y. Wang. Robust stability and performance of adaptive jitter supression in laser beam pointing. *Proceedings of 52nd IEEE Conference on Decision and Control, Florence, Italy*, pages 6916–6921, 2013.

[53] H. Jin and M. G. Safonov. Unfalsified adaptive control: Controller switching algorithms for nonmonotone cost functions. *International Journal of Adaptive Control and Signal Processing*, 26(8):692–704, 2012.

[54] A. Karimi and Z. Emedi. H_∞ gain-scheduled controller design for rejection of time-varying narrow-band disturbances applied to a benchmark problem. *European Journal of Control*, 19(4):279–288, 2013.

[55] A. Karimi and G. Galdos. Fixed-order H_∞ controller design for nonparametric models by convex optimization. *Automatica*, 46:1388–1394, 2010.

[56] A. Karimi and I.D. Landau. Robust adaptive control of a flexible transmission system using multiple models. *IEEE Transactions on Control Systems Technology*, 8:321–331, 2000.

[57] C. Kulcsár, H.-F. Raynaud, C. Petit, J.-M. Conan, and P. Viaris de Lesegno. Optimal control, observers and integrators in adaptive optics. *Opt. Express*, 14(17):7464–7476, 2006.

[58] S.M. Kuo and D.R. Morgan. Active noise control: a tutorial review. *Proceedings of the IEEE*, 87:943–973, 1999.

[59] I. D. Landau, M. Alma, and T. B. Airimitoaie. Adaptive feedforward compensation algorithms for active vibration control with mechanical coupling. *Automatica*, 47:2185–2196, 2011.

[60] I. D. Landau, A. Castellanos Silva, T. B. Airimitoaie, G. Buche, and M. Noë. Benchmark on adaptive regulation – rejection of unknown/time-varying multiple narrow band disturbances. *European Journal of Control*, 19(4):237–252, 2013.

[61] I.D. Landau, T. B. Airimitoaie, and M. Alma. A youla–kucera parametrized adaptive feedforward compensator for active vibration control with mechanical coupling. *Automatica*, 48(9):2152–2158, 2012.

[62] I.D. Landau, T. B. Airimitoaie, and M. Alma. IIR youla-kucera parameterized adaptive feedforward compensators for active vibration control with mechanical coupling. *IEEE Transactions on Control Systems Technology*, 21(3):765–779, 2013.

[63] I.D. Landau, M. Alma, A. Constantinescu, J.J. Martinez, and M. Noë. Adaptive regulation – rejection of unknown multiple narrowband disturbances (a review on algorithms and applications). *Control Engineering Practice*, 19:1168–1181, 2011.

[64] I.D. Landau, A. Constantinescu, and D. Rey. Adaptive narrow band disturbance rejection applied to an active suspension – an internal model principle approach. *Automatica*, 41:563–574, 2005.

[65] D. Liberzon. *Switching in Systems and Control*. Birkhauser, 2003.

[66] E. Marchetti, M. Le Louarn, C. Soenke, E. Fedrigo, P.-Y. Madec, and N. Hubin. ERIS adaptive optics system design. *Proc. SPIE*, 8447:84473M, 2012.

[67] R. Marino, G. Santosuosso, and P. Tomei. Robust adaptive compensation of biased sinusoidal disturbances with unknown frequency. *Automatica*, 39:1755–1761, 2003.

[68] R. Marino and G. L. Santosuosso. Regulation of linear systems with unknown exosystems of uncertain order. *IEEE Transactions on Automatic Control*, 52:352–359, 2007.

[69] R. Marino and P. Tomei. Output regulation for linear systems via adaptive internal model. *IEEE Transactions on Automatic Control*, 48:2199–2202, 2003.

[70] R. Marino and P. Tomei. An adaptive learning regulator for uncertain minimum phase systems with undermodeled unknown exosystems. *Automatica*, 47:739–747, 2011.

[71] R. Marino and P. Tomei. Disturbance cancellation for linear systems by adaptive internal models. *Automatica*, 49(5):1494–1500, 2013.

[72] B. L. McGlamery. Computer simulation studies of compensation of turbulence degraded images. *Proc. SPIE*, 74(9):225–233, 1976.

[73] A. S. Morse, D. Q. Mayne, and G. C. Goodwin. Applications of hysteresis switching in parameter adaptive control. *IEEE Trans. on Automatic Control*, 37:1343–1354, 1992.

[74] E. Mosca. *Optimal, Predictive, and Adaptive Control*. Prentice Hall, 1995.

[75] K. S. Narendra and J. Balakrishnan. Adaptive control using multiple models. *IEEE Transactions on Automatic Control*, 42:171–187, 1997.

[76] K.S. Narendra and C. Xiang. Adaptive control of discrete-time systems using multiple models. *IEEE Transactions on Automatic Control*, 45:1669–1686, 2000.

[77] R. J. Noll. Zernike polynomials and atmospheric turbulence. *Journal of the Optical Society of America*, 66(3):207–211, 1976.

[78] C. Petit, J.-M. Conan, C. Kulcsár, H.-F. Raynaud, and T. Fusco. First laboratory validation of vibration filtering with LQG control law for adaptive optics. *Opt. Express*, 16(1):87–97, 2008.

[79] C. Petit, F. Quiros-Pacheco, J.-M. Conan, C. Kulcsár, H.-F. Raynaud, T. Fusco, and G. Rousset. Kalman filter based control for adaptive optics. *Proc. SPIE*, 5490:1414–1425, 2004.

[80] L.A. Poyneer, B.A. Macintosh, and J.-P. Véran. Fourier transform wavefront control with adaptive prediction of the atmosphere. *J. Opt. Soc. Am. A*, 24(9):2645–2660, 2007.

[81] W. Qian, S. K. Panda, and J.-X. Xu. Torque ripple minimization in PM synchronous motors using iterative learning control. *IEEE Transactions on Power Electronics*, 19:272–279, 2004.

[82] R. Ragazzoni. Pupil plane wavefront sensing with an oscillating prism. *J. Mod. Optic.*, 43:289–293, 1996.

[83] A. Riccardi, G. Brusa, P. Salinari, D. Gallieni, R. Biasi, M. Andrighettoni, and H.M. Martin. Adaptive secondary mirrors for the Large Binocular Telescope. *Proc. SPIE*, 4839:721–732, 2003.

[84] F. Roddier. *Adaptive Optics in Astronomy*. Cambridge University Press, 1999.

[85] M. S. Sadabadi and A. Karimi. An LMI formulation of fixed-order H_∞ and H_2 controller design for discrete-time systems with polytopic uncertainty. *Proceedings of the 52nd IEEE Conference on Decision and Control*, 2013.

[86] S. M. Savaresi, C. Poussot-Vassal, C. Spelta, O. Sename, and L. Dugard. *Semi-Active Suspension Control Design for Vehicles*. Butterworth-Heinemann (Elsevier), 2010.

[87] C. Scherer and S. Weiland. Linear matrix inequalities in control. *DISC course lecture notes*, 1999.

[88] G. Tao and P. A. Ioannou. Necessary and sufficient conditions for strictly positive real matrices. *Circuits, Devices and Systems, IEE Proceedings G*, 137(5):360–366, 1990.

[89] S. Valentinotti, B. Srinivasan, U. Holmberg, D. Bonvin, C. Cannizzaro, M. Rhiel, and U. von Stockar. Optimal operation of fed-batch fermentations via adaptive control of overflow metabolite. *Control Engineering Practice*, 11:665–674, 2003.

[90] C. Vérinaud. On the nature of the measurements provided by a pyramid wave-front sensor. *Opt. Commun.*, 233(1–3):27–38, 2004.

[91] B. Widrow and S. D. Stearns. *Adaptive signal processing.* EnglewoodCliffs, NJ: Prentice-Hall, 1985.

[92] K. Zhou, J. C. Doyle, and K. Glover. *Robust and Optimal Control.* Prentice Hall, 1995.